Chapter 10
Sensor Design

Jacqueline Gölz and Christian Hatzfeld

Abstract Multiple sensors are applied in haptic devices designs. Even if they are not closed-loop controlled in a narrow sense of force or torque generation, they are used to detect movement ranges and limits or the detection of the presence of a user and its type of interaction with an object or human-machine-interface (HMI). Almost any type of technical sensor had been applied in the context of haptic devices. The emerging market of gesture based user interaction and integration of haptics due to ergonomic reasons extends the range of sensors potentially relevant for haptic devices. However, what exactly is a sensor? Which is the *right one* for your purpose and is there a systematic way to choose it? To support you answering these fundamental questions, classification of sensors is helpful. This chapter starts with a definition and classifications according to measurand and sensing principles. Constraints, you will have to focus on, are discussed and selection criteria are deduced. An introduction in technologies and design principles for mechanical sensors serves as an overview for your selection process. Common types of force/torque, positioning, velocity and acceleration sensors are presented. Furthermore, imaging and temperature sensors are addressed briefly in this section.

Christian Hatzfeld deceased before the publication of this book.

J. Gölz (✉)
Technische Hochschule Ulm, Ulm, Germany

Fakultät Elektrotechnik und Informationstechnik, Institut für Automatisierungssysteme (IAS), Albert-Einstein-Allee 53, 89081 Ulm, Germany
e-mail: jacqueline.goelz@thu.de; j.goelz@hapticdevices.eu

C. Hatzfeld
Technische Universität Darmstadt, Darmstadt, Germany

© The Author(s) 2023

T. A. Kern et al. (eds.), *Engineering Haptic Devices*, Springer Series on Touch and Haptic Systems, https://doi.org/10.1007/978-3-031-04536-3_10

10.1 What is a Sensor?—A Definition

What is a sensor and why is it crucial for every technical system? Let me give you an example: Grasping an object is a very complex task. You need information about position and dimension as well as elasto-mechanic properties, weight and texture of the object to be able to grasp and to avoid slipping. Your brain is processing information about object location (detected with your eyes) and object properties (detected with small cells in your skin, joints and muscles) to plan and realize the mentioned task. These organs of perception are nothing more than transducers, linking non-electric parameters with electric pulses containing the necessary information for controlling the task of grasping. The transformation into an electric signal is needed, so that the information can be processed by our brain.

In haptic systems different physical domains are interacting too. A transducer (sensor) connecting different physical domains is needed, so that information can be processed in electric control units to control system behavior. You can interpret a sensor as a black box providing a certain transmission behaviour (Fig. 10.1). Correlation of electrical signal and associated measurand can be derived from measurement data and resulting characteristic curves. A mathematical description models the ideal functional dependence of measurand (input signal x) and sensor response (output signal $y = f(x)$). The characteristic curve usually is measured under controlled reference conditions (e.g. constant environmental conditions, defined measuring procedure). Due to imperfections of every sensor (e.g. cross-sensitivity to temperature, noise or drift) and varying environmental conditions measurement data is deviating from the reference characteristics and thus from the true value. These deviations of the ideal transmission behavior are indicated in errors and are usually listed in the data sheets

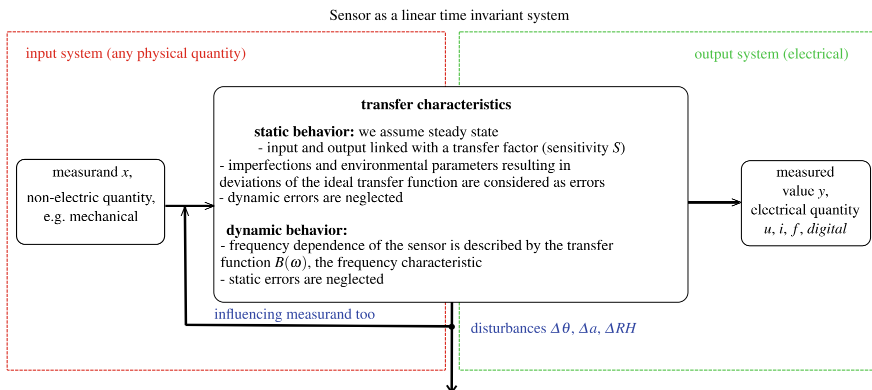

Fig. 10.1 Sensor as a black box linking input values x (measurands) to electrical output values $y = f(x)$ (measured value). Depending on the analysis of static or dynamic behavior we distinguish a (constant) transfer factor B_0 (equivalent to sensitivity S) or a frequency dependent transfer function $B(\omega)$ displaying the frequency characteristic. Environmental influences like temperature, vibration or humidity etc. are disturbances, which do influence transfer characteristics

of the sensor manufacturer. To describe sensor performance, we distinguish between the analysis of:

- **Static characteristics**, describing the output signal due to very slow changes of the measurand: Offset and sensor sensitivity as well as errors due to intrinsic aspects (e.g. noise) and influence of environmental conditions like temperature-induced effects are identified. Offset, nonlinearity, hysteresis, noise and thus resolution characterize the real sensor behavior (Fig. 10.2). The accuracy of the sensor can be estimated.
- **Dynamic characteristics**, describing the sensor response due to fast changes of the measurand: Analyzing the step response and/or performing a frequency analysis, transient behavior und frequency-dependent effects on transmission behavior are identified. The sensor is stated as a linear time invariant transmission system. Time constants, response time, resonant frequency and dynamic errors like drift are the main outputs of the dynamic sensor analysis. Hereby, nonlinearity and statistic errors are usually neglected (Fig. 10.3).

Based on the analysis of static and dynamic transmission behavior, characteristics of sensors are determined and listed for example in the manufacturers' datasheet as characteristics of the actual sensor. Your measurement task dictates the scale of these parameters. If you are choosing sensors for your haptic system, you need to take specifications like dimensions, measuring range, sensitivity, resolution, frequency range and thus accuracy of sensors into account, regardless of measurand. Following Regtien [1] important universal sensor specifications are put together (Fig. 10.4):

- **Sensitivity**: Ratio between the change in the output signal y due to a change of input signal x. To reduce computing effort, a linear transmission behavior is preferred, thus the sensitivity is expected to be a constant transfer factor B_0. In reality, a sensor has a nonlinear transfer function $y = f(x)$, thus $S(x) = \frac{\Delta y}{\Delta x}$ is varying too. In case of slight nonlinearity, an approximation by using a straight line can be done. Common characteristic errors like nonlinearity and hysteresis can be determined. They quantize the maximum deviation of real transfer characteristics according to the chosen straight line. It is crucial to know the specification of the approximation, because it is influencing the amount of the calculated deviation. Several definitions for the straight line are in use [1]; in this book the end-point line connecting calibrated end-points of the range after calibration zero and scale is used.
- **Nonlinearity**: The maximum deviation of the idealized transfer function is specified by the linearity error: $\Delta v_{i,max} = max\,\{v_i - v_{si}\}$, where v_i represents the actual measured value, v_{si} the actual nominal value.
- **Hysteresis**: Are both increase and decrease of the measurand in the measurement range analyzed, the maximum deviation of the increasing curve and the decreasing curve has to be derived to get the hysteresis error: $\Delta v_{h,max} = max\,\left\{v_{i,dec} - v_{i,inc}\right\}$, where $v_{i,dec}$ and $v_{i,inc}$ represent increasing and decreasing actual value.
- **Offset and Zero drift**: Even if the measurand is zero, you get an output signal. This offset mainly arises from component tolerances and can be adjusted in a calibration process. However, temperature-induced drift of the sensor can lead to

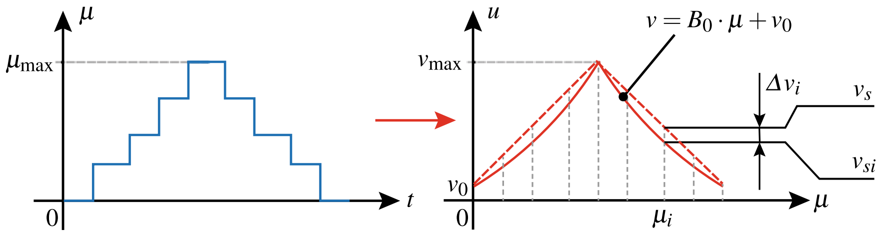

Fig. 10.2 Static transfer factor is determined under steady state and reference condition by (equidistantly) in- and decreasing the measurand. v_i refers to the measured values and v_{is} to the nominal characteristic curve. Environmental parameters are tracked and kept constant. Imperfections of the sensor and the measurement setup lead to deviations of the ideal (linear) transfer function (nominal characteristic curve). Beside transfer factor B_0, nonlinearity and hysteresis error as main systematic errors can be estimated

a variation of the offset during measurement. This very slow change of the offset is called zero drift and has be taken into account.

- **Resolution**: Smallest detectable increment of the input quantity.
- **Electrical Noise**: Fluctuations in current and voltage lead to a random variation of the sensor output relative to the value of the measurand. This kind of deviation is limiting the resolution of the sensor.
- **Dynamic transfer behavior**: Response time is associated with the speed of change in the output according to a stepwise change of measurand. It is crucial for designing the control of a haptic system. A second important parameter is the bandwidth of the sensor. The lower limit may be quasi-static, thus zero. The upper limit that is determined by the resonant frequency of the sensor itself. Designing haptic systems, the resonance frequency of the sensor should be at minimum four times the upper limit of the systems bandwidth to guarantee a proper transmission behavior of the sensor.

Nonlinearity and hysteresis are systematic errors that can be compensated. Noise and other random deviations can be reduced e.g. using filtering, but cannot be compensated and do limit the resolution of the sensor. Five basic error reduction methods are in use: compensation, feedback, filtering, modulation and correction. [1] gives a short overview about the mentioned five. All methods do influence the topology of the internal signal processing. For further reading [2, 3] are recommended. Until now, we had a universal look at sensors as a transmission system with an unknown internal life, a black box. We described the transmission behavior considering responses $y = f(x)$ on input signals x. If it comes to quantification, it is crucial to analyze our measurement chain in detail: measurand, its input into the measuring system, physical operating principle and its imperfections as well as signal processing and sensor electronics.

In the following, we want to focus on measurand and sensing principle to perform a helpful classification of sensors. You may ask yourself: *whatsoever does classification of sensors help me developing haptic systems?*

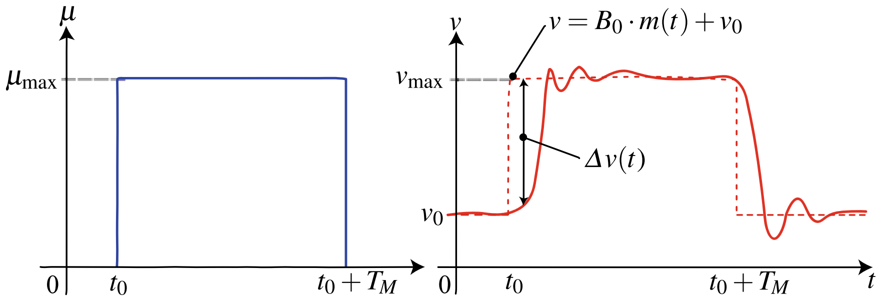

Fig. 10.3 Measuring the step response due to a step of the measurand leads us to the frequency dependent transfer function. We assume a linear and time invariant system and we are neglecting static and random errors

Let us recap: You learned about haptic perception (Sect. 2.1), did your conscious choice in actuation technology (Chap. 9) and want to implement a control system (Chap. 7). You understood now (Sect. 10.1) what a sensor is. Let us assume you have to pick the appropriate sensor to measure forces up to 50 N at a handle. Prescreening the market, you find dozens of sensors. Which one would you choose? In our book, we narrow down the selection to three different sensors. The table above lists heir key parameters. From a dynamics perspective of course the piezoelectric sensor would be great, from a building-space consideration, the resistive sensor is fantastic. However,

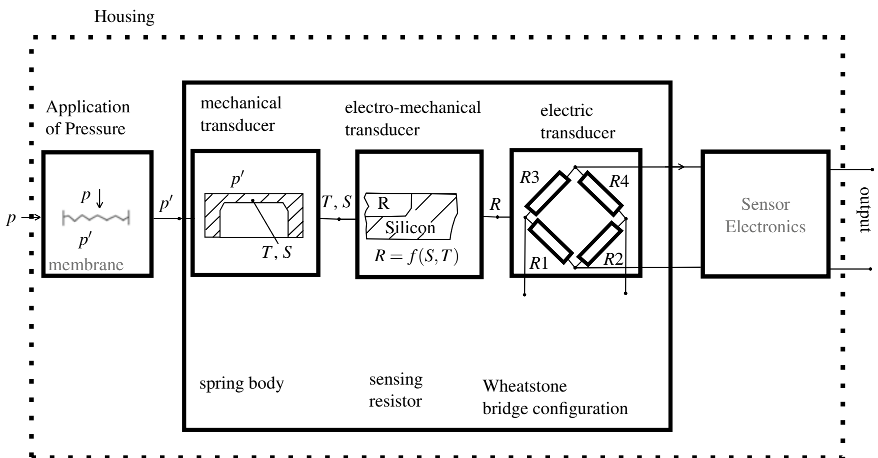

Fig. 10.4 The internal structure of a sensor depends on considered input values, function blocks and thus its signal processing. We distinguish chain structure, parallel structure (open-loop) and closed-loop structure (see also [1] © Elsevier, all rights reserved.). The most common one is the chain structure, consisting of several function blocks transforming or converting the measurand. Representatively, the structure of a piezoresistive pressure sensor is presented to show typical function blocks

Table 10.1 Selection of Force Sensors: piezoelectric load cell 9217A1, *Kistler*, strain gage Micro-Force, *Forsentek*, and piezoresistive load cell TAL220, *HTC-Sensor*

Parameter	Piezoelectric	Resistive	Piezoresistive
Nominal Load	50 N	50 N	50 N
Span (typical)		20 mV/V	2 mV/V
Accuracy in %(Span)	±1%	0.1%	0.05%
Dynamic Range	Quasi-static to several kHz	Static to 500 Hz	Static to 1 kHz
Dimensions	Diam. 8.5 mm×46 mm	$2 \times 2 \times 2\,\text{mm}^3$	$12.7 \times 12.7 \times 80\,\text{mm}^3$

in most cases the piezoresistive sensors are chosen. Why is this? Well, because of dynamic range they can cover (from static to several hundred Hz) and because of their high accuracy. What does this example tell you? It is important to know more about sensors and their functions to make an educated decision because rash and unfounded sensor choice may impair the overall performance of the haptic system. The following chapters will introduce typical sensing principles to you to enable you to understand the pros and cons of each of those sensors for your haptic and tactile application (Table 10.1).

10.2 Classification According to Sensing Principles

About 5,000 physical and chemical effects are known which could be used as sensing principles. About 150 are already in use for sensors [4]. The principles differ in basic parameters like sensitivity, resolution, error rate and dynamics. Classifying can help you to narrow down the plenty of principles according to your measuring task. One way is to cluster these principles in three groups depending on interaction of measuring object and sensing system:

- **Tactile measurement**: measuring object is interacting via direct physical contact or a mechanical linking interface. All active transformers (e.g. resistive one like strain gage based sensors or also optic sensors like encoders) belong to that group, but also passive transformers like piezoelectric or electrostatic ones
- **Contactless or proximity based measurement**: depending on the distance between object and sensor field components of electric, magnetic or electromagnetic field are modulated (e.g. triangulation sensors, inductive ore capacitive proximity sensors)
- **Image processing system**: distance between measuring object and sensor are secondary, images or videos of measuring objects (also users and their gestures) are evaluated using usually AI or other analysis algorithms like Dynamic Time Warping or Hidden Markov Modelling [5, 6])

Quite helpful in terms of assessing dynamic behavior and power consumption is the classification depending whether or not external energy is necessary. Most sensors used in industrial environment are active transformers based on the so-called deflection method. The measurand is converted in an intermediate non-electric quantity

like stress, strain or intensity, which serves as actual input for the sensing element. They are called active ones, because the measurand is modulating an external electric power or energy; even if the measurand is state and does not vary, an output signal is generated. Thus, active sensors are suitable for state measurands. Sensors belonging to the group of active transducers are resistive, capacitive, inductive, optic and magnetic ones. Active transformers can be clustered in five groups:

1. Parameter variation of passive components: Resistor $R = \rho \cdot \frac{l}{A}$, where A means area and l means length of the element (potentiometric sensors, strain gages based sensors, piezo-resistive silicon sensors, magneto-resistive sensors like AMR, GMR or TMR, textile sensors etc.), inductor $L = \mu \cdot N \cdot \frac{A}{l}$ (proximity sensors, linear differential transformers, chokes or magneto-elastic sensors) and capacitor $C = \varepsilon \cdot \frac{A}{l}$ (single or differential capacitors, silicon sensors for measurement of (angular) acceleration and rotation rate etc. are most common).
2. Magnetic sensors: Measurement of current or electric potential difference (voltage) using hall or magneto-resistive sensors.
3. Resonant sensors: Evaluation of bulk or surface acoustic waves in solid objects.
4. Wave propagation: Evaluation of ultrasound, microwave signals (e.g. RADAR, LIDAR used in automotive context) and all time-of-flight sensors.
5. Opto-electronic sensors: Varying intensity of light via geometric optics and transmission properties e.g. reflexion, diffraction and absorption (light barriers, proximity switches (reflexion-based), triangulation sensors, interferometry, fiber-optic and light section sensors).

The upper cut-off frequency is influenced by the resonance frequency of the mechanical linking system transforming the measurand into the intermediate quantity. Modelling of frequency characteristics of the linking system is crucial to rate the upper cut-off frequency of the sensor. Miniaturization can shift the resonance frequency and thus enlarge the bandwidth of the sensor. Resonant sensors have the highest resonant frequency of all active transducers.

For high dynamics and less power consumption, passive transducers, especially piezoelectric sensors are recommended. Beside piezoelectric, electro-dynamic or electro-static sensors are passive transducers. Energy is taken from interaction process itself, for example deformation of piezo-electric material. They are called passive, because only in case of a variation on the measurand, an output signal will be generated. For state measurands, passive transformers are unsuitable. Table 10.2 links sensing principles to common physical measurands.

10.3 Classification According to Measurand and Application Field

As we stated, a sensor is performing an exchange of information or energy from one subsystem to another, it is an interface between different physical domains and the electric subsystem. Physical quantities can be classified according to different

Table 10.2 Mechanical measurands and common sensing principles in process measuring. *X* marks industrial application, $\otimes$ major application, (*X*) rare application. Beside resistive strain gages, differential pressure sensors and sensors based on Coriolis-force are used for flow (mark 1) and level detection (mark 2) too. Within piezoelectric transducers, position and velocity are derived from integration of acceleration signal (mark 3)

Sensing principle		Mechanical quantities								
		Distance + Angle	Velocity	Acceleration	Mass + Force	Torque	Pressure	Flow	Level	Strain
Active trans-ducers	Change of passive parameters resistive (Strain gage)	X			$\otimes$	$\otimes$	X	1)	2)	$\otimes$
	Piezoresistive			X	(X)		$\otimes$			
	Capacitive			$\otimes$		X	X			
	Inductive	X				X	(X)			
	Magnetic sensors (Hall-Sensors, Magneto-resistive Sensors (XMR))	$\otimes$	X							
	Resonant sensors (SAW- und BAW-Sensors)			(X)	(X)	(X)	X			
	Ultrasound and Microwave Sensors		$\otimes$					X	(X)	
	Opto-electronic Sensors (Reflexive Principles, Inter-ferometry, Fiberoptic Sensors)	$\otimes$			(X)	X	(X)	(X)	(X)	X
Passive	Sensors using Electro-static transducer	X		X			$\otimes$ Microphone			
	Sensors using piezo-electric transducer	$X^{3)}$	$X^{3)}$	$\otimes$	X		X			
	Sensors using electro-dynamic transducer		X		X			X (MID)		
	Sensors using piezo-magnetic transducer				(X)		(X)			

Table 10.3 List of physical quantities according to [7]

Mechanical, solids	*Mechanical, fluids*	*Nuclear radiation*	*Acoustic*
Acceleration	density	Ionization degree	Sound frequency
Angle	Flow direction	Mass absorption	Sound intensity
Angular velocity	Flow velocity	Radiation dose	Sound polarization
Area	Level	Radiation energy	Sound pressure
Diameter	Pressure	Radiation flux	Sound velocity
Distance	Rate of flow	Radiation type	Time of flight
Elasticity	Viscosity		
Expansion	Volume	*Chemical*	*Magnetic, electrical*
Filling level		Cloudiness	Capacity
Force	*Thermal*	Composition	Charge
Gradient	Enthalpy	Concentration	Current
Hardness	Entropy	Electrical conductivity	Dielectric constant
Height	Temperature	Humidity	Electric field strength
Length	Thermal capacity	Impurity	Electric power
Mass	Thermal conduction	Ionization degree	Electric resistance
Moment	Thermal expansion	Moisture	Frequency
Movement	Thermal radiation	Molar weight	Inductivity
Orientation		Particle form	Magnetic field strength
Pitch	*Optical*	Particle size	Phase
Position	Colour	pH	Pulse duration
Pressure	Light polarization	Polymerization degree	Signal distortion
Proximity	Light wavelength	Reaction rate	
Rotation	Luminance	Redox potential	*Time*
Roughness	Luminous intensity	Thermal conductivity	Time
Shape	Reflection	Water content	Frequency
Tension	Refractive index		Duty cycle
Torque			
Torsion			
Velocity			
Vibration			
Weight			

characteristics and a comprehensive classification is for example given in [1, 7]: We will focus on the following and do a classification in association with...

- Physicals domain: acoustic, chemical, electric, magnetic, mechanical, nuclear radiation, optical, thermal and time. Table 10.3 shows many possible measurands. For each of the mentioned quantities severals sensing principles are known.

Table 10.4 Summary of relations between measurands in haptic systems

Domain	State variable	Rate variable	Effort	Energy/J	Power/W
Mechanical (transition)	Position x/m	v = dx/dt = $\dot{X}$/m/s $q = dv/dt = d^2x/dt^2 =$ $\ddot{X}$/m/s^2	Force F/N	F.dx	F.v
Mechanical (rotation)	Angle φ/rad	$w = d\varphi/dt =$ $\dot{\varphi}$/rad/s $\dot{w} = d^2\varphi/dt^2 =$ $\ddot{\varphi}$/m/s^2	Torque M/Nm	T.dφ	T.φ
Electrical	Charge Q/C	I = dQ/dt	Voltage v/V	v.dQ	V.I
Magnetic	Flux ϕ	V = ϕ	Current I/A	I.dϕ	I.V
Thermal	Entropy $\sigma/J/k/m^2$	σ	Temperature θ/°C	$\theta.d\sigma$	$\theta.\dot{\sigma}$

- Time behavior: We distinguish between state variables describing a static property and rate variables describing a dynamic property. For example in mechanical domain: distance or length x is state, velocity $v = dx/dt$ is rate.
- Dependency of direction: a quantity having a direction is a so called *vector* like velocity or force. Does the quantity not have a direction it is a *scalar* like temperature, time or pressure (Table 10.3).
- Measurement method: is the measurand compared to a solid measure, e.g. weighing using standard weights it is called a *direct* measurement method. If the measurand has to be converted to a proportional intermediate quantity, which is then compared to a solid measure, we talk about *indirect* measurement method. Sensors using a compensation principle (closed-loop sensor systems) or are based on deflection method belong to indirect methods, e.g. a strain gage based force sensor, where the intermediate quantity strain occurring at the surface of a spring body is detected (Sect. 10.5.1.1). Most sensors use the indirect measurement method.

Our field of application limits the amount of direct mechanical measurands to only a fistful ones related to user movement and interaction with objects. Force plays a major role in haptic system control followed by the movement related (translational and rotatory) quantities acceleration, velocity, displacement and position. As temperature is both the major disturbance and important parameter while interacting with objects, it should be observed too. In addition, current and voltage sensors can also be useful in haptic systems. Table 10.4 summarizes measurands and their relationship. To understand, where they come from, let us take a closer look to the constraints resulting from our field of application.

10.4 Constraints in Haptic Systems

The topology of haptic systems significantly influences our sensor design. The application of the haptic device itself has an extraordinary relevance. All systems have in common that an user mechanically contacts objects. It has to be clarified, which use of the device is intended, e.g. if it is going to be a telemanipulator for medical purposes, or a CAD tool with force feedback. The mechanical properties of the user itself and in case of telemanipulation systems the mechanical properties of manipulating objects have to be analyzed for sensor development or selection. Beside constraints resulting from mechanical contacts, interaction and movement have to be tracked. Thus, position, acceleration and velocity (both rotation and translation) of interactions are relevant measurands too. Directions in space (according to active DoF) and sensor specifications like measuring range, resolution and bandwidth depend on the topology of the haptic device itself and the intended kind of interaction (kinesthetic or tactile). All these factors will be discussed within this section.

10.4.1 Topology of the Device

The application itself appoints the topology of the haptic device. Taking control engineering aspects into account haptic systems can be classified into four types, which are discussed in Chap. 6. In the following, these topologies are analyzed referring to the measured values:

- Open-loop control of impedance: Measurement of user movements (velocity or displacement or acceleration), feedback of a force
- Closed-loop control of impedance: Measurement of both user movements and interaction, feedback of a force
- Open-loop control of admittance: Optional measurement of user force, feedback of a position
- Closed-loop control of admittance: Measurement of both user force and movements, feedback of a position.

In case of open-loop control, only mechanical properties of objects have to be taken into account for sensor design, irrespective of whether objects are physical or virtual ones. In case of haptic simulators like flight simulators virtual objects are acting. Mechanical properties are often stored in look-up tables and force sensors are dispensable. In case of telemanipulation systems, the end effector of the haptic system interacts with physical objects. Their mechanical properties have to be detected with capable force sensors.

Most telemanipulation systems are impedance controlled. In case of closed-loop control the mechanical impedance of both user and manipulating object are considered. Designing closed-loop impedance controlled systems force sensors have to be integrated into the device detecting the user force. Designing closed-loop admittance

controlled systems the output movements of the haptic interface have to be measured using e.g. a velocity sensor (Chap. 6, Sect. 10.7)

Consequently, the measuring object can be both the user itself and a real, physical object. Beside its mechanical properties the modality of the interaction with haptic systems has to be analyzed to identify fundamental sensor requirements like dynamic bandwidth, nominal load and resolution. The main factors influencing the sensor design are both contact situation and objects' mechanical properties. In the following, they are analyzed by examining mechanical properties and texture of the objects' surface separately.

10.4.2 Contact Situation

It is necessary to distinguish between the user of the haptic system and the physical object due to different interaction modalities identifying mechanical properties. If the user is the "measuring object", interaction forces have to be measured. Universally valid conclusions concerning amplitude, direction and frequency of the acting force cannot be done. Mechanical impedance depends on the manner of grasping the device, age and gender of the user itself (Chap. 3). In Sect. 3.1.3 manners of grasping are classified: power-grasps, precision-grasps and touch-grasps. In case of power- and precision-grasps finger or palm are used as counter bearing, which results in a high absolute value of force up to 100 N [8, 9] and a stiffer contact.

Additionally, the direction of the force vector has to be taken into account. Depending on application of the haptic device and manner of grasping up to six degrees of freedom result–three force components and sometimes three torques. Neglecting torques between user and device three components of force have to be measured. If the user is in static contact with the handheld device, measuring normal force components with respect to orientation of the contact plane is sufficient. If the user is exerting relative movements to the device, also, shear forces occur and three components have to be measured.

Considering the frequency dependence of humans' haptic perception, both static and dynamic signal components have to be considered equally. The lower cut-off frequency of haptic devices tends to quasi-static action at almost zero Hertz, which may happen when a device is held without movement in free space. If the force signal is subject to noise or even the slightest drift, the haptic impression will be disturbed soon (compare perception thresholds in Sect. 2.1). Manner and pre-load of grasping affect the upper cut-off frequency of the sensor. In case of power- and precision-grasps, the absolute value of force achieves higher values which results in an upper cut-off frequency being $\ll$ 10,000 Hz. Values of about 300 Hz are sufficient (Sect. 2.1). Within contact grasps pre-load is much lower than before enabling high frequency components to be transmitted directly to the skin up to a range of approximately 1,000 Hz.

In case of telemanipulation systems, the end effector interacts with a real, physical object. Assumptions made for the measuring object "'user"' can partially be

transferred to this situation. Following NEWTON's law *actio et reactio*, the absolute value of force depends on intensity and way of interaction. Possible examples are compression and lift of objects with a gripper, or exploration with a stick. For telemanipulation systems in minimally invasive surgery, the absolute value of force ranges from 1 to 60 N (comp. e.g. [10]). The most promising approach is given by analyzing the intended application within preliminary tests and derivation of a model. The mechanical impedance of the object itself, which will be described within the following section, dominates the dynamics of the interaction, especially of the upper cut-off frequency.

10.4.3 Mechanical Properties of Measuring Objects

As stated for the user in Chap. 3, the mechanical impedance of objects can be subdivided into three physical actions: elastic compliance n, damping d and mass m. In case of rigid objects made of e.g. metal or ceramics, the property of elasticity is dominant. Interaction between haptic systems and objects can be considered as a rigid contact. Consequently, the force signal includes high-frequency components. The upper cut-off frequency should take a value of at minimum 1,000 Hz, to make sure to cover all dynamics responsible for haptic perception. Soft objects, such as silicone or viscera have a viscoelastic material performance. Following KELVIN viscoelastic behavior can be simulated by a network made of elastic compliances n_i and damping elements d_i, such as masses m_i. Using such an equivalent network, dynamic effects like relaxation and creeping can be modeled (Figs. 10.5 and 10.6).

First of all the elasticity of measuring objects has to be investigated for designing a haptic sensor. An arithmetic example in Sect. 2.4.2 compares the different cut-off

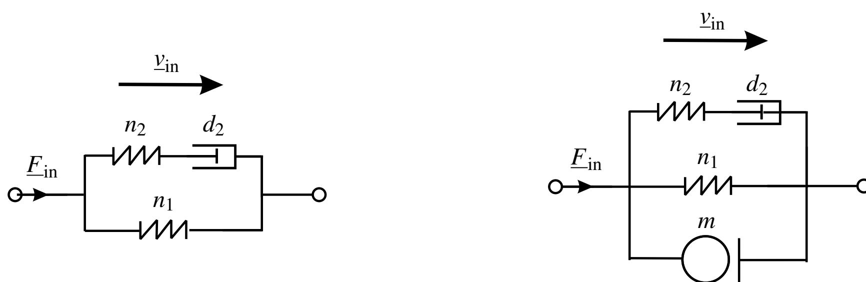

(a) Kelvin model modeling dynamically effects

(b) Kelvin model extended by objets weight for calculating the resonance frequency

Fig. 10.5 Kelvin model (standard linear solid) modeling viscoelastic behavior of objects. For calculating the resonance frequency a mass element has to be added. By adding further damping and spring elements dynamic behavior of every object material can be modeled

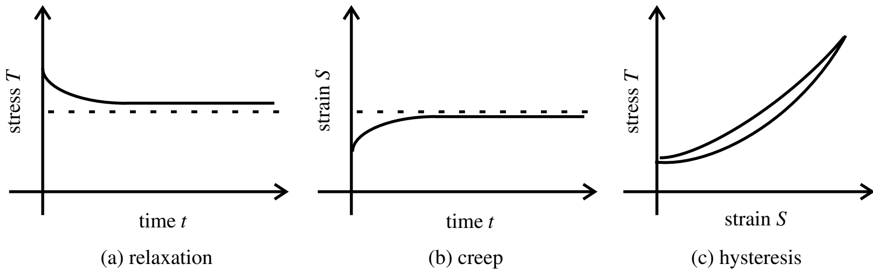

Fig. 10.6 Visualization of visco-elastic phenomena relaxation, creep and hysteresis

frequencies of materials. For soft materials such as rubber, upper cut-off frequency takes values below 10 Hz. During interaction with soft materials mainly low frequency components appear. The upper cut-off frequency is defined by the interaction frequency of 10 Hz at maximum [11–13]. If the measuring object is a soft one with embedded rigid objects, like for example tumors in soft body tissue, an upper cut-off frequency of about 1,000 Hz should be realized. To get a more precise information about frequency requirements, it can hardly be done without an analysis of the interaction object. For a first rule of thumb calculated cut-off frequency as derived in Sect. 2.4.2 are sufficient. In case of doubt, the frequency range of the sensor should always be oversized, not to already loose relevant haptic information already at this very first point in the processing chain.

Beside dynamics, the required force resolution depends on a physiological value too. The ↪ JND lies in the range between 5 and 10% of the absolute force value (Sect. 2.1). From the JND the sensor characteristics of measurement uncertainty can be derived. If realized as a constant value—which is common to many technical sensor solutions—5% of the lowest appearing value of force should be chosen to prevent distortion of the haptic impression of the object. Nevertheless, there is no actual requirement for haptic applications to have a constant or even linear sensor resolution. With telemanipulation systems, the interaction of the haptic system and real, physical objects is the main application. Depending on the type of interaction, frequently the surface structure of objects, the so-called texture become equally or even more important than the object's elastic compliance. Helpful literature for modeling dynamics of mechanical or electromechanical systems are [14, 15]. The resulting challenges for sensor development are discussed within the following subsection.

10.4.4 Texture of Measuring Objects

Properties, which are relevant for the human perception of texture, are geometrical surface structure on the one hand (e.g. the wood grain), on the other hand some kind of "frequency image" generated by the geometrical structure in the (vibro-)tactile receptors when being touched by skin. To detect the surface structure of an object,

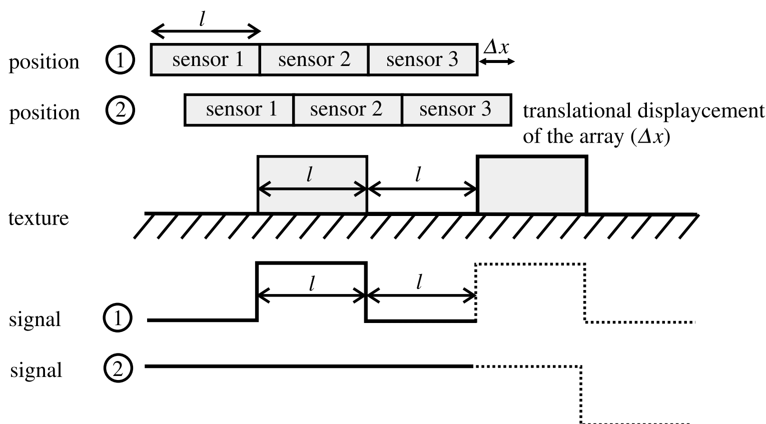

Fig. 10.7 Illustration of static and spatially resolved force measurement using as 3xn array. One sensing element has the same dimension like a texture element. At position 1 the array is optimally placed. If the array is shifted about Δx to position 2 the texture is incorrectly detected

variation of force against the contact area can be derived. For **static measurement** sensor arrays of single-component force or pressure sensors are a common technical solution. These arrays are placed onto the object. The objects structure generates different values of contact forces, providing a force distribution on the sensor surface. Size of both array and individual array element cannot be defined in general, but it depends on the smallest detectable structure on the measurement object itself. In case of static measurement sketched above, number and size of the sensor, array elements should be dimensioned slightly smaller than the minimum structure of the measuring object. The size of each element should be less than half of the size of the smallest structure to be measured. However, even fulfilling this requirement aberration will appear. Figure 10.7 shows that in case of the width of the sensor element being larger or identical to the smallest structure the distance between the elements is detected smaller than in reality. With n sensor elements the width of the structure element is replayed to $\frac{n+1}{n}$ and the distance to $\frac{n-1}{n}$. If the number of sensor elements per surface area increase, the aberration is diminishing and the structure is approximated more realistic (Fig. 10.8). However, with the number of elements the effort of signal conditioning and analysis is increasing.

Beside the described aberration, an additional disadvantage of static measurements is given by the fact, that the knowledge of the texture is not sufficient to get information about the object's material. The complete haptic impression needs frequency information depending on the elastic properties of texture and surface friction too. To gain these data, a relative movement between object and haptic system should be performed, to measure the texture **dynamically and spatially**. Depending on velocity of the relative movement and speed of the signal detection algorithms, the spatial resolution can be multiplied using the same number of sensor elements as in the example shown before. Even the use of sensor array with a simultaneous detec-

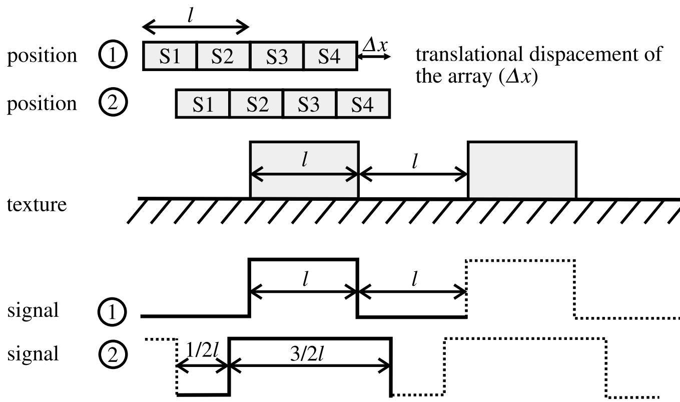

Fig. 10.8 Illustration of static and spatially resolved force measurement using as 6xn array. Size of one sensing element is half of a texture element. At position 1 the array is optimally placed. In case of any other position an aberration occurs. Aberration decreases with increasing number of sensing elements in an appropriate array

tion of multiple points becomes unnecessary. With knowledge about the exploration velocity and its direction, the information can be put into relation to each other. For texture analysis, multi-component force sensors should be used, as especially the combined forces in the direction of movement and normal to the surface contribute to haptic perception [16]. This dynamic measurement principle is comparable with the intuitive exploration made by humans: To gain the texture of an object humans gently touch and stroke over its surface. The surface structure excites the fingerprint to oscillate and the vibrotactile sensors acquire the frequency image. The absolute value of normal forces reached during such explorations are in a range of 0.3–4.5 N [17]. As stated earlier, force resolution is defined by the ↪ JND. Haptic information about texture is included into the high-frequency components of the signal. For haptic applications the maximum frequency should be located at 1,000 Hz. The absolute value of nominal force should be chosen depending on the elastic compliance of the object. In case of softer objects, a lower absolute value can be chosen. Surface structures will deform and cannot be detected anymore. To be able to measure equally good at soft and rigid objects, the nominal force should take values $\leq 4.5\,\mathrm{N}$. Caldwell [17] for example decided to use $F = 0.3\,\mathrm{N}$.

10.4.5 Interaction and User Movements

As stated earlier, users are interacting with haptic devices based on physical contact or non-physical in case of motion capture. Beside force position, velocity and acceleration are relevant measurands. The kind of interaction with the haptic system determines measuring range as well as dynamics and sensing principle. In case of

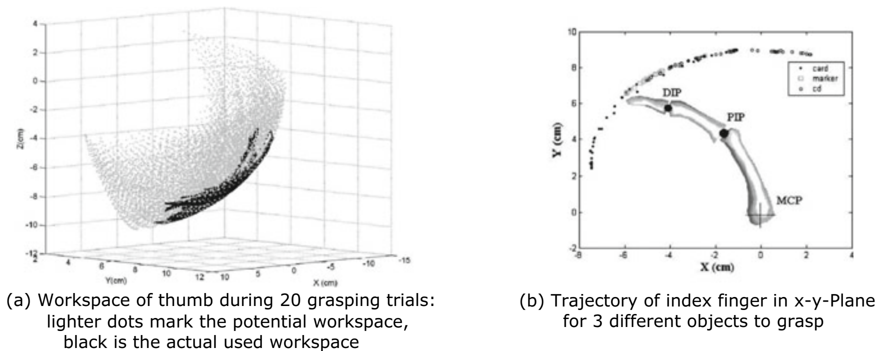

(a) Workspace of thumb during 20 grasping trials: lighter dots mark the potential workspace, black is the actual used workspace

(b) Trajectory of index finger in x-y-Plane for 3 different objects to grasp

Fig. 10.9 Workspace of thumb and index finger and trajectories during grasping tasks [19]

physical contact, nearly every sensing principle is possible; only the task (dynamic exploration of objects, tactile, grasping or other kinesthetic) has to be taken into account concerning measuring range, resolution and bandwidth. In case of non-physical contact, contactless sensing principles like marker-based motion capture (e.g. reflecting or magnetic markers and appropriate detection system as well as inertial measurement units) or camera-based systems and rarely found acoustic sensors (e.g. ultra-sound or near-field RADAR sensors) are in use [6]; motion range and distance between display and user give a limit to sensor specifications.

Let us have a closer look on patterns of movement and trajectories of fingers, hands and limbs. Concerning fingers and hands, we distinguish three different grasps: Finger touch, precision grasp and power grasp (Chap. 2). Depending on the users' grasping strategy, one up to five digits are involved in the reach-to-grasp-task [18]. Kamper et al. found out that no matter of grasping strategy or object property fingertip followed a stereotypical trajectory, which can be modelled by a logarithmic spiral [19]. The spiral is scaling with object size and shape. Working space of fingers were analyzed as well as velocity of finger movement. Grasping a soft ball a speed of fingertip (ring finger) $\leq 40\, rmcm/s$ was detected. Grasping a mug, fist moved with a speed of up to 60 cm/s. They found out that just a percentage of maximum workspace of fingers is used during grasping, in case of the thumb just 4.2%. Figure 10.9 shows typical workspace of thumb and index finger measured in the mentioned study.

In 2009, unconstrained three-dimensional hand and arm movement has been analyzed [20, 21]. Movement speed of up to 1.5 m/s for arms [20] and up to 1 m/s for hands [21] depending on the movement trajectory occurred. Maximum speed of hand and influence of age on it was studied in 2001, where 20 men (age in between 25 and 70) have been tested [22]. An average speed of maximal 3 m/s was observed. In 1996, dynamic movement of elbow, wrist and forearm was modelled for simulation purposes based on measurements [23]. Peak velocity of wrist action was $45°/s$ (deviation of ±20%). Acceleration was not observed.

Another source of information for working space, speed and acceleration is the field of biomechanics; there are plenty of studies analyzing movement of limbs and

hands while sportive disciplines like boxing, swimming etc. (e.g. [24]). Movement capabilities of fingers, wrist and forearm are focused in rehabilitation. The progress of patients' flexibility is of interest [25, 26]. Sensorized gloves (e.g. *SenseGlove* combined with VR headsets are used for movement analysis during grasping- and positioning-tasks; e.g. Ay [25] provides an overview of actual measurement and trainings systems for movement analysis in rehabilitation. In 2021, a study was performed at Hamburg University of Technology (TUHH) to observe the progress in flexibility of forearm, wrist and fingers of 24 hemiparetic patients [27]. Beside the displacement of fingertips, also hand and forearm movement was tracked. The maximum flexion angles for the index finger, corresponding to the fist configuration on each cycle, have been statically measured on the subjects as 85° for the MCP joint, 105° for the PIP joint, and 70° for the DIP one. In addition, the average of whole joints for a healthy person highly depends on both time of exercise and motivation of person. An average nominal angular velocity of $25\,\mathrm{rad/s}$ and an average nominal acceleration of $38\,\mathrm{rad/s^2}$ was derived from position measurement. Frequency rage of all analyzed movements was within a few hundred Hertz.

10.4.5.1 Selection of Design Criteria

Following the description of the most relevant constraints, limiting factors for sensor design in haptic applications can be found in physiological values. Nominal load, resolution, covered frequency range and measurement uncertainty can be derived from humans' haptic perception. For a quantitative analysis of these requirements, the contact between measuring object and sensor is to bring into focus. Measurement range and number of detectable vector components are defined by intended application and the structure of the device. The geometrical dimensions and other mechanical requirements are given depending on the point of integration into the haptic system. The diagram displayed in Fig. 10.10 visualizes the procedure of how to identify most important requirements for sensor design.

10.5 Force Sensor Design

This section deals with selection and design of force sensors, which are implemented in haptic systems. Approaches like measuring current in actuators to derive occurring force are not part of the chapter. In Sect. 10.4 fundamental problems have been re discussed, which are the basis of every sensor design process. A selection of factors to be taken in account is made in Sect. 10.4.5.1 and will help us during the development or selection process. After a short introduction in basic transfer properties, sensor characteristics are analyzed according to haptic aspects and complemented by application examples.

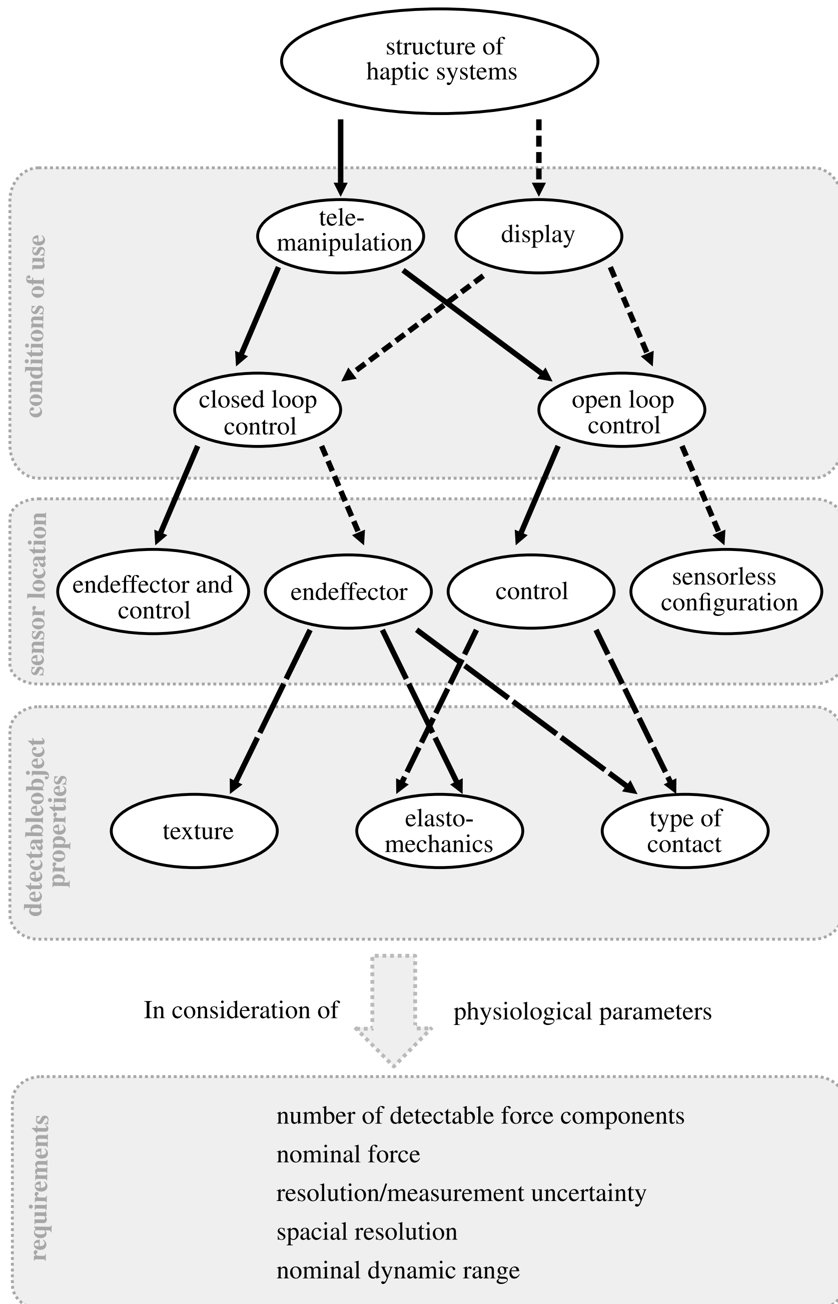

Fig. 10.10 Tree diagram to identify the principle requirements on haptic sensors, representatively listed for force sensors. Beside mechanical characteristics of the object, also physiological parameters of human haptic perception have to be considered

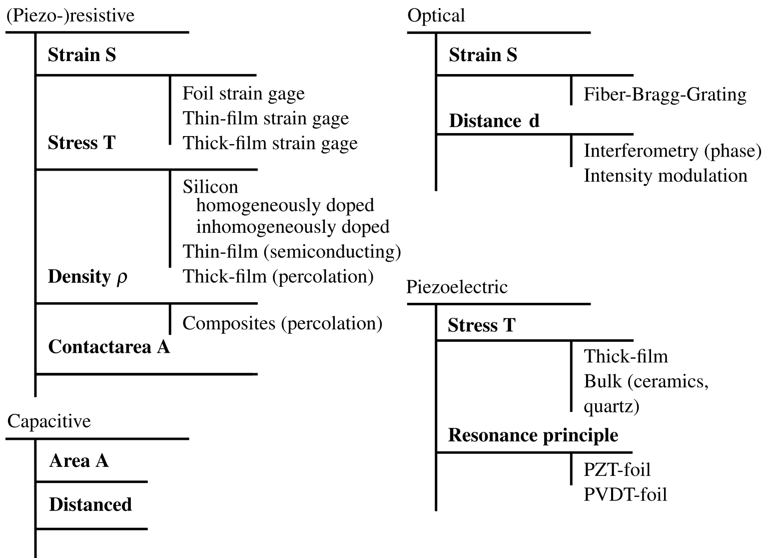

Fig. 10.11 Overview of established measurement principles for detecting forces in haptic systems. Furthermore, active sensor systems are also discussed in the following section

10.5.1 Sensing Principles

Within the previous section, the most important criteria for the design and development of a haptic sensor were named and introduced. Sect. 10.5.2 summarizes major requirements once again in tabular form. In order to help choosing a suitable sensor principle, variants according to Fig. 10.11 are presented in this section. Beside established measurement elements, such as resistive, capacitive, optic or piezoelectric ones, other less common sensor designs based on electro-luminescence or active moving coils are discussed too.

Most sensor principles are active transformers using the deflection method for force measurement, which means that elasto-mechanic values such as stress or strain are detected and the corresponding force is calculated. Sensors belonging to the group of active transducers are resistive, capacitive, optic and magnetic ones, working according to the displacement-principle too. Piezoelectric, electro-dynamic or electrostatic sensors are part of the group passive transducers. After a short introduction in elasto-mechanics each sensing principle will be discussed according to its operating mode and several applications will be presented. All sensor principles will be estimated concerning their applicability for kinesthetic and tactile force measurement, and put into relation to requirements known from Chap. 5. At the end of this chapter a ranking method for the selection of suitable sensor principles is be given.

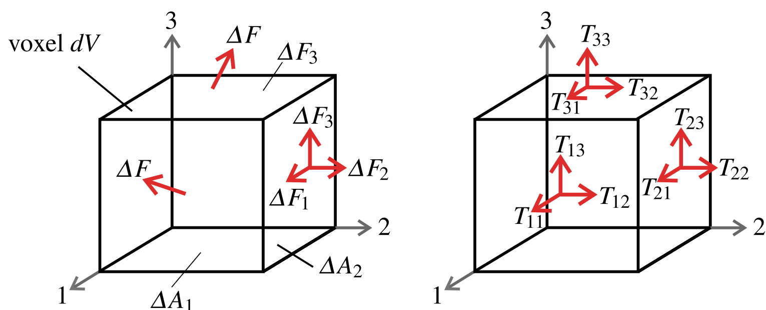

Fig. 10.12 Voxel dV of an elastic object. Due to external deformation internal stress occurs which can be described by the component T_{ij} of the stress tensor [28] © Springer Nature, all rights reserved

10.5.1.1 Basics of Elasto-Mechanics

As mentioned before, a large number of sensor principles base upon elasto-mechanics. This section will summarize fundamental knowledge that is necessary for sensor design. If force is exerted to an elastic body, it deforms elastically depending on the amount of force. Internal stress T occurs resulting in a shape change–the strain S. Stress and strain are correlated by specific material parameters, the so called elastic moduli s_{ij}.

For a better comprehension a short *gedankenexperiment* will be performed [28]. If a volume element ΔV is cut from an object under load (Fig. 10.12), substitute forces ΔF will act upon the surfaces of the cuboid to keep the state of deformation. Due to the required state of equilibrium the sum of all forces and torques acting upon ΔV must equal zero.

Subdividing the force ΔF in its three components ΔF_1, ΔF_2 and ΔF_3, just those components remain orthogonal to the surface elements ΔA_j. The quotient of the acting force component ΔF_i and the corresponding surface element ΔA_j results in a mechanical stress T_{ij}. Following the equilibrium condition $T_{ij} = T_{ji}$ six independent tension components remain, resulting in the stress tensor. Tensor elements can be factorized into normal (stress parallel to surface normal) and shear stress components (stress orthogonal to surface normal). Analyzing the volume element ΔV before and after load, a displacement of the element ΔV with relation to the coordinate system $\langle 123 \rangle$ such as a deformation happens. The sides of the cube change their lengths and are not orthogonal to each other anymore (Fig. 10.13).

To describe that shape change, strain S_{ij} is introduced. The quantity strain is a tensor too, consisting of nine elements (Eq. 10.1)

$$\begin{pmatrix} d\xi_1 \\ d\xi_2 \\ d\xi_3 \end{pmatrix} = \begin{pmatrix} S_{11} & S_{12} & S_{13} \\ S_{21} & S_{22} & S_{23} \\ S_{31} & S_{32} & S_{33} \end{pmatrix} \cdot \begin{pmatrix} \Delta x_1 \\ \Delta x_2 \\ \Delta x_3 \end{pmatrix} \tag{10.1}$$

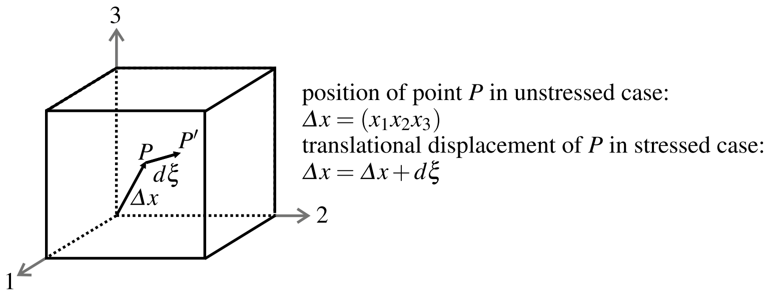

Fig. 10.13 Displacement of point P to P' due to application of force visualizes the state of strain [28] © Springer Nature, all rights reserved

Due to volume constancy the following correlation can be defined as

$$S_{ij} = S_{ji} = \frac{1}{2} \cdot \left(\frac{\delta \xi_i}{\delta x_j} + \frac{\delta \xi_j}{\delta x_i} \right) \tag{10.2}$$

and thus, the matrix can be reduced to six linear independent elements. Normal strain components act parallel to the corresponding normal to the surface, which results in volume change. Shear components, acting normal to the surface, describe the change of the angle between the borders of the volume element. In case of isotropic materials, such as e.g. metals or Al_2O_3 ceramics, the correlation between shape change mentioned before and mechanical strains can be formulated as follows:

$$\begin{pmatrix} S_1 \\ S_2 \\ S_3 \\ S_4 \\ S_5 \\ S_6 \end{pmatrix} = \begin{pmatrix} s_{11} & s_{12} & s_{12} & 0 & 0 & 0 \\ s_{12} & s_{11} & s_{12} & 0 & 0 & 0 \\ s_{12} & s_{12} & s_{11} & 0 & 0 & 0 \\ 0 & 0 & 0 & 2(s_{11} - s_{12}) & 0 & 0 \\ 0 & 0 & 0 & 0 & 2(s_{11} - s_{12}) & 0 \\ 0 & 0 & 0 & 0 & 0 & 2(s_{11} - s_{12}) \end{pmatrix} \cdot \begin{pmatrix} T_1 \\ T_2 \\ T_3 \\ T_4 \\ T_5 \\ T_6 \end{pmatrix} \tag{10.3}$$

For simplification, six independent strain resp. stress components are summarized in a vector. Components with index 1, 2 and 3 mark normal components, those with indices 4, 5 and 6 shear components [28]. Parameters s_{ij} are regardless of direction. Taking YOUNGs modulus E and shear modulus G into account, parameters can be derived:

$$s_{11} = \frac{1}{E}, s_{12} = \frac{\nu}{E}, \frac{1}{G} = 2(s_{11} - s_{12}) = \frac{2}{E}(1 + 2\nu) \tag{10.4}$$

ν marks the so-called POISSON ratio, which is material dependent. Using metal ν values between 0.25 and 0.35 can be achieved. In case of homogeneous materials Eq. (10.3) can be reduced to a linear correlation $T = E \cdot S$. For anisotropic materials such as silicon or quartz elasto-mechanic properties are depending on the orientation of the coordinate system (comp. Sect. 10.5.1.3), resulting in a matrix of elastic coef-

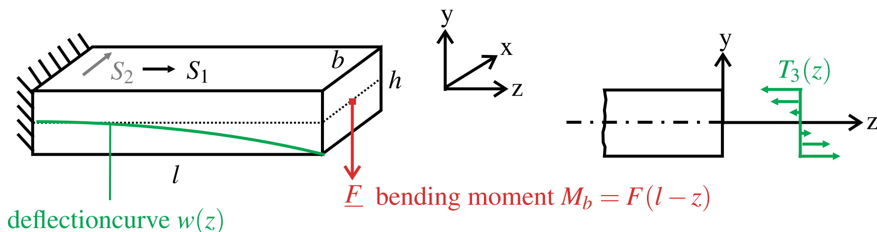

Fig. 10.14 Behavior of a bending beam, the right-hand detail shows stress distribution along the profile

ficients with up to 21 elements. For further reading on elasto-mechanics e.g. [28, 29] are recommended.

Example "Beam Bending"

If a force vector is exerted to the tip of a beam bender made of isotropic materials and clamped on one side (Fig. 10.14), a bending moment M_B occurs.

Mechanical stress components $T(y)$ are linear distributed on the cross section and take values of $T(y) = c \cdot y$, whereas c is a proportional factor. Bending moment equals the integral of the stress $T_3(y)$ distributed on the cross section.

$$M_B = \int_A y \cdot T_3(y) dA = c \cdot \int_A y^2 dA \tag{10.5}$$

As the integral $\int_A y^2 dA$ equals the axial moment of inertia I, c is calculated as

$$c = \frac{M_B}{I}. \tag{10.6}$$

The resulting strain components S_1 and S_2 act transversal to the beam's surface. For elastic deformation strain component S_1 and stress component T_2 are correlated via theYOUNGs modulus E

$$S_2 = \frac{T_2}{E} = \frac{M_B}{I \cdot E} = \frac{F \cdot (l - z)}{I \cdot E} \tag{10.7}$$

and therefore depending on the geometry of the cross section A of the beam, position z at the beam's surface and acting force F. For calculations of strain component S_1 transversal contraction has to be considered as follows

$$S_1 = -\nu \cdot S_2. \tag{10.8}$$

Further readings of elasto-mechanics, for example the calculations of deformation of fiber-reinforced composites, the works of GROSS [28], WERTHSCHÜTZKY [29] and BALLAS [30] are recommended.

10.5.1.2 Detection of Force

According to Fig. 10.14 acting forces can be measured evaluating both resulting strain distribution on the surface and displacement of beam. According to the example above, detection of strain S_2 can be derived using BERNOULLIs theory. Thus, strain components acting transversal to the surface can be neglected for slender and long beam-geometries. Stress or strain sensitive elements should be placed in such a way, that a maximum surface strain change can be detected.

Correlations described above, are examples for a cantilever beam. Being able to measure more than just one force component, a suitable deformation element has to be designed considering the elasto-mechanic correlations. For example works of BRAY [31] and RAUSCH [32] can help designing such an element. Primary objective is to generate a strain distribution in loading case, which enables to deduce the force components.

The correlation of force F_i and electric signal v_i of the sensor element usually is given by a linear system of equations (e.g. [33]). Equation (10.9) shows an example for a three-axial sensor:

$$\begin{pmatrix} v_1 \\ v_2 \\ v_3 \end{pmatrix} = \begin{pmatrix} a_{11} & a_{12} & a_{13} \\ a_{21} & a_{22} & a_{23} \\ a_{31} & a_{32} & a_{33} \end{pmatrix} \cdot \begin{pmatrix} F_1 \\ F_2 \\ F_3 \end{pmatrix} \quad (10.9)$$

It can be assumed that all force components contribute to each individual voltage signal v_i. The elements a_i of the matrix can be found by calibrating the sensor. During the calibration process, only one independent force component for each direction is applied to the sensor and the resulting voltage components are measured. After inverting the matrix $\mathbf{A}$ to $\mathbf{A}^{-1}$ the force vector can be calculated easily.

A lot of research is done in reducing the number of measuring cycles for calibration of multi-axial force sensors. Most common methods are:

- Least squares method [34]: Most accurate method. Execution of load cycle with n load steps for each direction. For a tri-axial force sensor $6n$ measuring cycles are necessary.
- Shape from motion method [33, 35]: Application of a force vector with known absolute value, which is randomly rotating in space. Accuracy comparable to the first method, but less time consuming. Only valid, if all components have the same amount of nominal load. If not so, then the third method is advisable.
- Hyperplane calibration method [36]: Accuracy and time consumption comparable to the second method. Three quasi-orthogonal load vectors must be applied to the sensor.

For further information on calibration check above mentioned literature.

10.5.1.3 Resistive Strain Measurement

One of the most commonly used sensing principles for force sensing is based on resistive detection of strain or rather stress components occurring in a (measuring) object. With resistive strain measurement, a resistor pattern is applied on the bending elements surface. Resistors must be located in areas of maximum strain. As a quick reminder: Electrical resistance is defined via

$$R_0 = \rho \cdot \frac{l}{A} = \rho \cdot \frac{l}{b \cdot h}, \tag{10.10}$$

ρ marks specific resistance, l, b, h (length, width, height) define volume of the resistor itself. The total differential shown in Eq. (10.11) gives relative resistivity change resulting from the deformation:

$$\frac{dR}{R_0} = \underbrace{\frac{dl}{l} - \frac{db}{b} - \frac{dh}{h}}_{rel.\,volume\,changing} + \underbrace{\frac{d\rho}{\rho}}_{piezoresistive\ part}. \tag{10.11}$$

Deformation causes on the one hand the change of the geometrical part $\frac{l}{A}$. Taking YOUNGs modulus E and POISSONs ratio ν account, plain stress for isotropic material can be derived [28]:

$$\frac{dl}{l} = S_1 = \frac{1}{E} \cdot T_1 - \frac{\nu}{E} \cdot T_2, \tag{10.12}$$

$$\frac{db}{b} = S_2 = -\frac{\nu}{E} \cdot T_1 + \frac{1}{E} \cdot T_2, \tag{10.13}$$

$$\frac{dh}{h} = S_3 = -\frac{\nu}{E} \cdot T_1 - \frac{\nu}{E} \cdot T_2. \tag{10.14}$$

Indices 1, 2 and 3 mark the direction components. Concerning the geometrical change, the resulting gage factor k describing the sensitivity of the material takes a value of about two (Eq. 10.15). On the other hand plane stress provokes a chance of specific resistivity ρ.

Material specific changes will be discussed within paragraph Sect. 10.5.1.3. Using Eq. (10.15) the correlation between strain and relative resistivity change is formulated:

$$\frac{dR}{R_0} = \underbrace{\left(2 - \frac{d\,(N \cdot \mu)}{S \cdot N \cdot \mu}\right)}_{:=k,\,gagefactor} \cdot S \tag{10.15}$$

whereas μ represents the electron mobility and N the number density of molecules. The change of the resistivity can be measured using a so called WHEATSTONE bridge circuit. This circuit is built of one up to four active resistors connected in a bridge circuit and fed by a constant voltage or constant current (Fig. 10.15). Eq. (10.16)

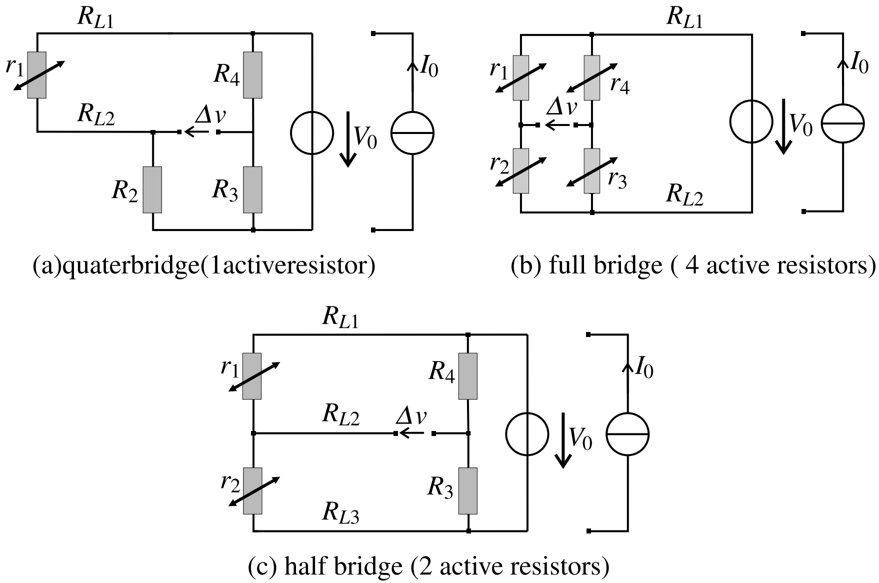

Fig. 10.15 WHEATSTONE bridge configurations for evaluating one up to four resistors

calculates the bridge Fig. 10.15c with the assumption, that the basic resistances R_{0i} equal the resistance R_0. The values of R_0 such as gage factors are specific to material and listed in Table 10.5 (further Informations e.g. [32, 37]).

$$\Delta v = \frac{V_{cc}}{R_0 \cdot I_0} = \frac{1}{4} \cdot \left\{ \frac{r_1}{R_{01}} - \frac{r_2}{R_{02}} + \frac{r_3}{R_{03}} - \frac{r_4}{R_{04}} \right\} \tag{10.16}$$

The supply with constant current I_0 has the great advantage that a temperature dependent drift of the measurement signal will be compensated. More advanced information can be found in [38, 39].

In case of metallic resistors a gage factor of approximately two occurs. The material specific component of metals is less important and affects the first decimal place only. In case of semiconductors and ceramic materials, the material specific component is dominant. In case of semiconductor-strain gages, the gage factor takes values up to 150. Using resistor pastes, applied in thick film technology on substrates,[1] and poly-silicon layers, sputtered in thin film technology the material specific component is dominant. On this, gage factors achieve values of up to 18 in case of thick-film resistors and up to approximately 30 for thin-film resistors. Table 10.5 lists the gage factor for several materials usually used in strain measurement. As mentioned earlier, strain gages are manufactured in different technologies. The most commonly used

[1] For substrate material mainly (layer-) ceramics are used. Less frequent is the use of metals, as isolating layers have to be provided then.

Table 10.5 Gage factor, strain resolution and nominal strain of important resistive materials according to [32]

Technology	Material	Gage factor	R_0 in Ω	S_{min}	S_N	References
Foil strain gage	$CuNi$	About 2	120, 350, 700	$\pm 10^{-7}$	±0.1%	[47–49]
Thick-film	$Bi_2Ru_2O_7$	12.1 ... 18.3	1,000	$\pm 10^{-6}$	±0.1%	[40, 50]
	PEDOT:PSS	0.48 ... 17.8	–	≥ 10%	–	[42, 51]
Thin-film	$TiON$	About 1k	4 ...5	$\pm 10^{-7}$	±0.1%	[29, 50, 52]
	Poly-Si	20 ... 30	About 1k	$\pm 10^{-7}$	±0.1%	[29, 50]
Si-technology	Homogeneous	100 ... 255	120 ... 1k	$\pm 10^{-6}$	±0.2%	[53]
	Inhomogeneous	80 ... 255	1k ... 5k	$\pm 10^{-7}$	±0.05%	[29, 45, 54]
Fiber-sensors	Carbon	1.3 ... 31	About 10k	–	0.2 ... 15%	[55, 56]

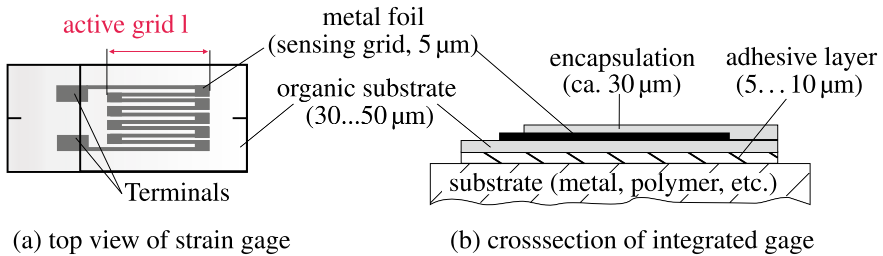

Fig. 10.16 Assembly of conventional strain gages: measuring grid is usually made of a patterned metal foil. In case of special applications metal wires are applied

types are foil-strain gages; thick- and thin-film manufactured measurement elements are found mainly in OEM-sensors and for specific solutions in automation industry due to the necessary periphery and the manufacturing process. Relevant literature can be found in the publications of PARTSCH [40] and CRANNY [41].

To deposit thin-film sensing layers, other technologies like inkjet or aerosol jet printing can be used. The inks are suspension containing electrically conducting particles made of carbon, copper, gold, silver or even conducting polymers like PEDOT:PSS. One advantage is that compared to conventional thick-film pastes the finishing temperature is below 300 °C and thus various substrates can be functionalized. For further information, see [32, 42, 43].

Foil strain gages are multilayer systems made of metallic measurement grids and organic substrates. It is applied (Fig. 10.16) and fixated on bending elements via cold hardening cyano-acrylate adhesive (strain analysis) or via hot hardening adhesives such as epoxy resin (transducer manufacture). These gages are long-term stable, robust, and especially used for high-precision tasks in wind-tunnel-scales and balance sensors. Achievable dynamics, resolution and measurement range are solely depending on the deformation element. The minimum size of the individual strain

two-element strain rosettes for detecting plain strain
(unknown principle directions)

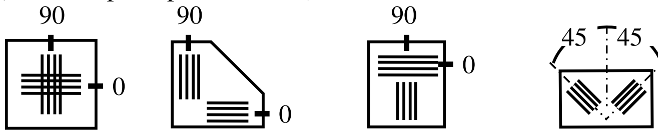

three-element strain rosettes for detecting plain strain
(unknown principle directions)

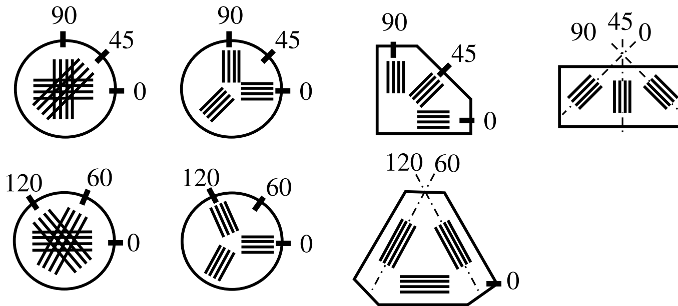

Fig. 10.17 Compilation of possible grid configurations of strain gages. See also

gages taken of the shelf is in the area of 3 mm width and 6 mm length. The measurement pattern itself is smaller in its dimensions. On this, it is possible to shorten the organic substrate to finally achieve 1.5 mm width and 5 mm length as a typical minimum size. If foil strain gages are considered, the surface strains resulting from the nominal load should be 1,000 μm/m for an optimum usage of the strain gage. Many measurement patterns are applied for force and torque sensors. Fig. 10.17 shows a selection of commercialized measuring grids ready for application on deformation elements.

Beside resistive foil strain gages, semiconductor strain gages are available. Their general design is comparable to conventional strain gages, as the semiconducting elements are assembled with organic substrates.[2] Measurement elements are used identical to foil strain gages and are available in different geometrical configurations such as T-rosettes.

Using measuring elements with a higher gage factor (Table 10.5) deformation elements can be designed stiffer, allowing smaller nominal strains. Such elements are especially relevant for the design of miniaturized sensors for haptic systems, as small dimensions and high cut-off frequencies have to be achieved. A commercially available example is the OEM-sensor *nano 17* from ATI (Fig. 10.18). Strain elements are piezoresistive ones and their gage factor takes values of approximately 150. Due to high potential for miniaturization and manifold application in haptic systems,

[2] Also single semiconducting elements without organic substrate are available. They are highly miniaturized (width of about 230 μm, length of about 400 μm), but has to be insulated from the deformation element.

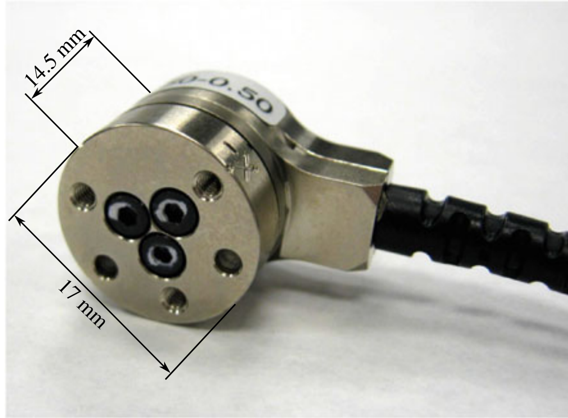

Fig. 10.18 Miniaturized force/torque sensor nano17. Resonance frequency of the sensor takes a value of about 7.2 kHz. © 2022 *ATI Industrial Automation, Inc.*, Apex, NC, USA, all rights reserved

piezoresistive sensors–especially silicon sensors–will be discussed in an independent subsection.

Piezoresistive Silicon Sensors

Published by CHARLES S. SMITH in 1954 for the first time [44], semiconducting materials with a symmetric crystal structure such as silicon or germanium possess a change in their conductivity σ due to an applied force or pressure. In the following paragraphs, this effect is discussed more deeply for mono-crystalline silicon.

The Piezoresistive Effect

If a semiconducting material is deformed due to a load, stress components T_i are generated inside the material. For your information: Due to the anisotropic properties of the material the elasto-mechanic properties are depending on the position of the coordinate system, and consequently on the orientation of the crystal lattice. These stress components affect the electron mobility μ and–as a consequence–the specific resistivity ρ. ρ is a material specific value, characterized via the parameters electron mobility μ and number of charge carriers N (comp. Sect. 10.5.1.1). Considering these parameters, correlation between relative resistivity change and the resulting strain tensor can be expressed to:

$$\frac{d\rho}{\rho} = \frac{dV}{V} - \frac{d(N \cdot \mu)}{N \cdot \mu}, \text{ with } \rho = \frac{V}{N \cdot \mu \cdot |q|}, \tag{10.17}$$

whereas V is the volume of the resistive area and $|q|$ is the charge of the particles.

Following the OHM's law the specific resistance ρ is connected by the vector $\mathbf{E} = (E_1; E_2; E_3)^T$ of the electrical field and the current density $\mathbf{J} = (J_1; J_2; J_3)^T$:

$$\begin{pmatrix} E_1 \\ E_2 \\ E_3 \end{pmatrix} = \begin{pmatrix} \rho_{11} & \rho_{12} & \rho_{13} \\ \rho_{21} & \rho_{22} & \rho_{23} \\ \rho_{31} & \rho_{32} & \rho_{33} \end{pmatrix} \cdot \begin{pmatrix} J_1 \\ J_2 \\ J_3 \end{pmatrix} = \begin{pmatrix} \rho_1 & \rho_6 & \rho_5 \\ \rho_6 & \rho_2 & \rho_4 \\ \rho_5 & \rho_4 & \rho_3 \end{pmatrix} \cdot \begin{pmatrix} J_1 \\ J_2 \\ J_3 \end{pmatrix} \tag{10.18}$$

Table 10.6 Piezoresistive coefficients of homogeneously doped silicon [45]

Doping	N in $\frac{1}{cm^{-3}}$	ρ in Ωcm	π_{11} in $\frac{mm^2}{N}$	π_{12} in $\frac{mm^2}{N}$	π_{44} in $\frac{mm^2}{N}$
n-Si	$6 \cdot 10^{14}$	11.7	$-102.2 \cdot 10^{-5}$	$+53.4 \cdot 10^{-5}$	$-13.6 \cdot 10^{-5}$
p-Si	$1.8 \cdot 10^{14}$	7.8	$+6.6 \cdot 10^{-5}$	$-1.1 \cdot 10^{-5}$	$+138.1 \cdot 10^{-5}$

Due to the symmetric crystalline structure of silicon[3] six independent resistive components ρ_i result, which are symmetrical to the diagonal of tensor ρ. Taking the matrix of piezoresistive coefficients π into account the influence of the six acting stress components T_i can be formulated. The cubic symmetry results in a reduction of the number of piezoresistive and direction dependent coefficients to three. By doping silicon with impurity atoms such as boron or phosphor areas of higher resistivity are generated. By influencing the type and the concentration of dopant the three π-coefficients can be influenced. Further information on doping can be found e.g. in [45, 46].

$$\begin{pmatrix} \rho_1 \\ \rho_2 \\ \rho_3 \\ \rho_4 \\ \rho_5 \\ \rho_6 \end{pmatrix} = \begin{pmatrix} \rho_0 \\ \rho_0 \\ \rho_0 \\ 0 \\ 0 \\ 0 \end{pmatrix} + \begin{pmatrix} \pi_{11} & \pi_{12} & \pi_{12} & 0 & 0 & 0 \\ \pi_{12} & \pi_{11} & \pi_{12} & 0 & 0 & 0 \\ \pi_{12} & \pi_{12} & \pi_{11} & 0 & 0 & 0 \\ 0 & 0 & 0 & \pi_{44} & 0 & 0 \\ 0 & 0 & 0 & 0 & \pi_{44} & 0 \\ 0 & 0 & 0 & 0 & 0 & \pi_{44} \end{pmatrix} \cdot \begin{pmatrix} T_1 \\ T_2 \\ T_3 \\ T_4 \\ T_5 \\ T_6 \end{pmatrix} \cdot \rho_0 \tag{10.19}$$

For homogenous silicon with a small concentration of dopants the values in Table 10.6 can be used.

Depending on angle between current density vector **J** and stress component T_i three effects can be distinguished. Within the so-called longitudinal effect current i is guided parallel to the normal component of stress, within transversal effect i is guided normal to the normal component of stress, and thus shear effect i is guided parallel or normal to the shear component of stress. Figure 10.19 visualizes the mentioned correlations.

For the resistivity change, depending on the orientation of the resistive area from Fig. 10.19, the following equation becomes valid:

$$\frac{dR}{R} \approx \frac{d\rho}{\rho} = \pi_{\mathrm{L}} \cdot T_{\mathrm{L}} + \pi_{\mathrm{Q}} \cdot T_{\mathrm{Q}} \tag{10.20}$$

As a consequence longitudinal and transversal stress components are influencing the calculation of the resistivity change. Depending on the crystallographic orientation of the resistive areas the π-coefficient is formed by longitudinal- and transversal coefficient (Table 10.7). For homogeneous Boron concentration of $N_{\mathrm{R}} \approx 3 \cdot 10^{18}\,\mathrm{cm}^{-3}$ the following values are achieved [45]:

[3] Face centered cubic.

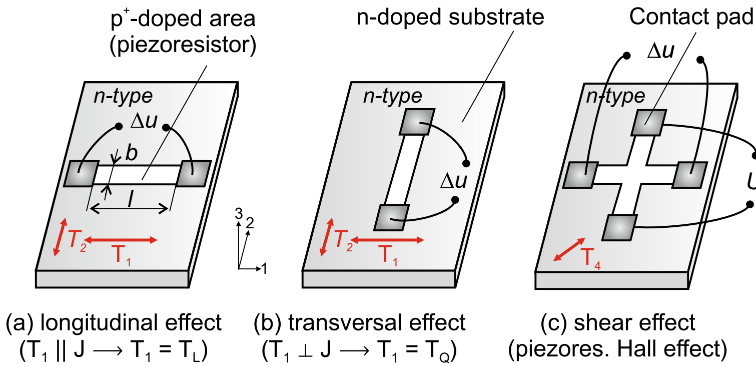

Fig. 10.19 Visualization of the the piezoresistive effects: longitudinal, transversal and shear effect in silicon [32]. Transversal and longitudinal effect is normally used for commercial silicon sensors

Table 10.7 Compilation of π_l- und π_q-coefficients for selected resistor assemblies dependent on the crystallographic orientation [59]

Surface orientation	Longitudinal	π_l	Transversal	π_q
(100)	[100]	π_{11}	[010]	π_{12}
	[110]	$\frac{\pi_{11}+\pi_{12}+\pi_{44}}{2}$	[$\bar{1}$10]	$\frac{\pi_{11}+\pi_{12}-\pi_{44}}{2}$
(110)	[111]	$\frac{\pi_{11}+2\pi_{12}+2\pi_{44}}{3}$	[$\bar{1}$12]	$\frac{\pi_{11}+2\pi_{12}-\pi_{44}}{3}$
	[110]	$\frac{\pi_{11}+\pi_{12}+\pi_{44}}{2}$	[001]	$\frac{\pi_{11}+5\pi_{12}-\pi_{44}}{6}$

$$\pi_{\mathrm{L}} = 71.8 \cdot 10^{-5}\,\mathrm{MPa}^{-1},$$

$$\pi_{\mathrm{Q}} = -65.1 \cdot 10^{-5}\,\mathrm{MPa}^{-1}.$$

More advanced information for the design of piezoresistive silicon-sensors can be found in the publications of BAO [45], BARLIAN [46], MEISS [57], RAUSCH [32] and WERTHSCHÜTZKY [58].

Examples of Piezoresistive Silicon Sensors

Piezoresistive silicon sensors for physical quantities like pressure and force are commonly integrated in silicon deformation elements. In case of pressure transducers, this kind of manufacture is state of the art. For all pressure ranges, sensor elements can be purchased. For example the company Silicon Microstructures Inc. (SMI) sells chips with glass-counter body for absolute pressure measurement with an edge length of 650 µm (Fig. 10.20a). In case of a suitable packaging, these sensors could be arranged in an array to measure the uni-axial force- or pressure-distribution on a surface.

In case of force sensors, realization of miniaturized multi-component force sensors is current issue in research. Dimensions of single sensor elements range from 200 µm to 2 mm. Nominal force covers a range of 300 mN to 2 N. Due to batch-manufacture of

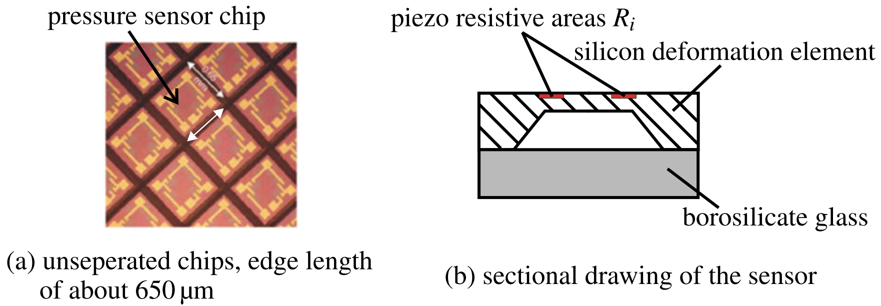

(a) unseperated chips, edge length of about 650 μm

(b) sectional drawing of the sensor

Fig. 10.20 Example of piezoresistive silicon pressure sensors [60]

measurement elements, realization of both single sensor elements and array-design[4] is possible. Sensitivity of sensors takes values of 2% relative resistivity change in loading case. Figure 10.21 shows four examples of current topics in research. Variants (a) [61], (b) [62] and (d) [63] were designed for force measurement in haptic systems. Variant (c) [64] was built for tactile, dimensional measurement technology. Force transmission is always realized by beam- or rod-like structures.

Since year 2007 a Hungarian manufacturer is selling the *Tactologic* system. Up to 64 miniaturized sensor elements are connected in an array of $3 \times 3\,\text{mm}^2$. Sensor elements have a size of $0.3 \times 0.3\,\text{mm}^2$ and are able to measure shear forces up to 1 N and normal force up to 2.5 N at nominal load. The force transmission is realized by soft silicone dots, applied to every individual sensor element (Fig. 10.22a and b). Using this array, static and dynamic loads in the range of kilohertz are measurable. But the viscoelastic material properties of the force transmission influence the dynamics due to creeping, especially the measurement of the normal forces [65, 66]. Another approach is to use piezoresistivity of silicon micro-machined transistors using the above mentioned shear effect (especially MOSFET, [67–69]). As well as strain measurement, these sensors are used to monitor the state of stress occurring in packaging process [67, 69]. Polyimide foil containing sensor elements (strain sensitive transistors) with a thickness of about 10 μm are available since at least around year 2000 [68].

Further Resistive Sensors

Besides resistive transducers presented until now, other more "exotic" realizations exist, which will be introduced within three examples. All sensors are suitable for array assembly to measure position-dependent pressure and a single force component. The used measurement principles are based on the change of geometrical parameters of the force elements. The examples shown in Fig. 10.24 (a) [70] and (b) [71] use the load-dependency of the constriction resistance. With increased pressure[5] the electrical contact area A increases and the resistance decreases.

[4] By isolating arrays instead of single sensors in the last processing step.

[5] The force can be calculated taking the contact area into account.

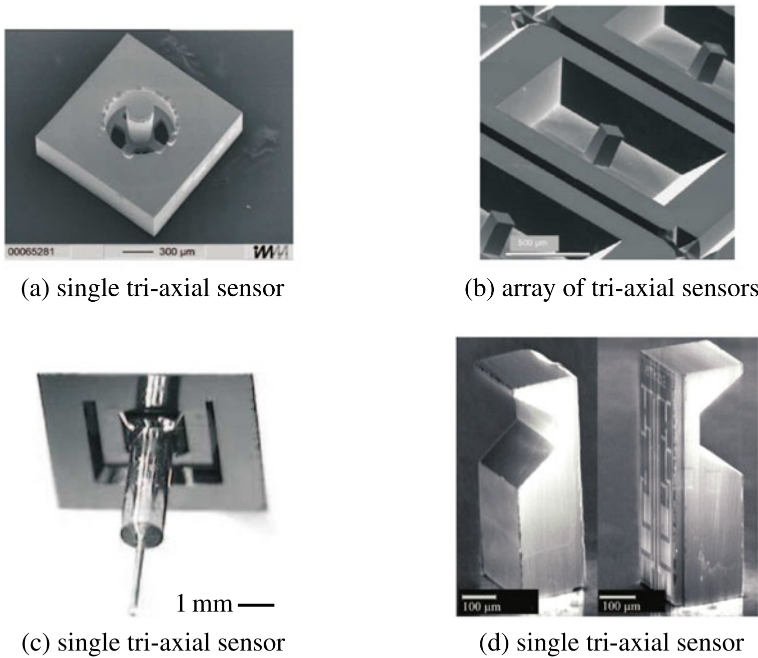

(a) single tri-axial sensor (b) array of tri-axial sensors

(c) single tri-axial sensor (d) single tri-axial sensor

Fig. 10.21 Different realizations of piezoresistive silicon force sensors: **a** [61] © Elsevier, all rights reserved, **b** [62] © Elsevier, all rights reserved, **c** [64], **d** [63]

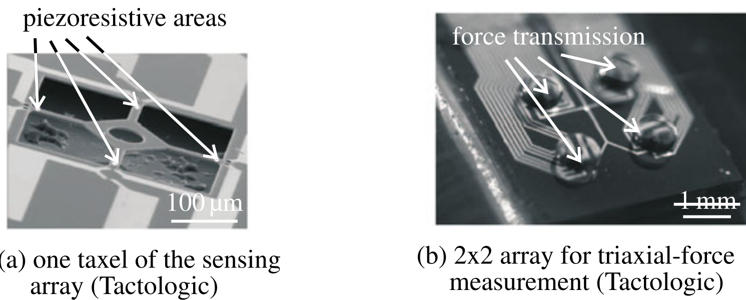

(a) one taxel of the sensing array (Tactologic)

(b) 2x2 array for triaxial-force measurement (Tactologic)

Fig. 10.22 Tactile multi-component force sensor [65] © Elsevier, all rights reserved

The companies *Interlink Electronic* and *TekScan* use this effect for their sensor arrays (also called *Force Sensing Resistors–FSR*). Interlink distributes polymer-foils printed with resistor pastes in thick-film technology. Their basic resistance takes values in the region of $M\Omega$. The sensor foils have a height of 0.25 mm and a working range of zero to one Newton respectively 100 N. Beside the sensitivity to force or pressure, the sensors show a temperature dependency of $0.5\%\ K$.

The sensor foils from *TekScan* are located in the range of 4.4 N up to 440 N, the spatial distribution reaches up to 27.6 elements per centimeter. The available

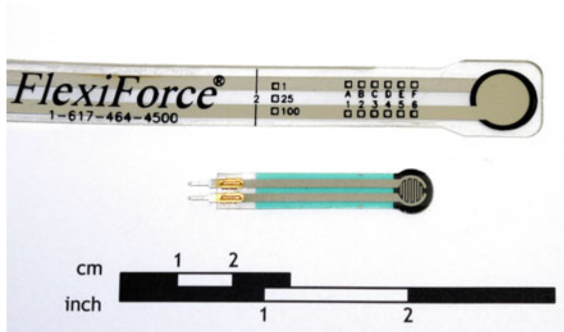

Fig. 10.23 Foil-sensors for compressive force detection, top: FLEXIFORCE by *TekScan Inc.*, South Boston, MA, USA , bottom: FSR by *Interlink Electronics*, Camarillo, CA, USA. These sensors are often used to detect grasp forces. © 2022 *TekScan Inc.*, used with permission

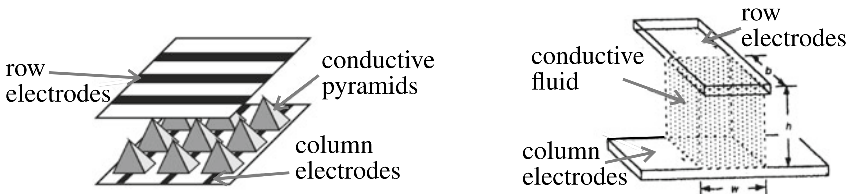

(a) micro machined tactile array developed by Fraunhofer Institute IBMT (b) variation of the electrodes distance

Fig. 10.24 Selected examples of foil sensors using the effect of a load-dependent constriction resistance [70, 71], own illustrations

array size reach from approximately $13 \times 13\,\text{mm}^2$ up to $0.5 \times 0.5\,\text{m}^2$. The height of the foils is around 0.1 mm. The measurement inaccuracy takes a value of 10%. The frequency range reaches from static up to 100 Hz. Beside the application in data gloves, as described by BURDEA [8], the foil sensors are used in orthopedics to detect the pressure distribution in shoes and prosthesis and within automotive industry for ergonomic studies (Fig. 10.23).

Another approach is the variation of the distance between two electrodes (Variant (b) in Fig. 10.24). The sensing element is made of flexible substrates. The electrodes are arranged in rows and columns. The gaps in between are filled with an electrically conductive fluid. In loading case the fluid is squeezed out and the distance of the electrodes varies. A disadvantage of this principle is given by the necessity for very large distance variations up to 10 mm to achieve usable output signals. Until today, this principle is still a topic of research.

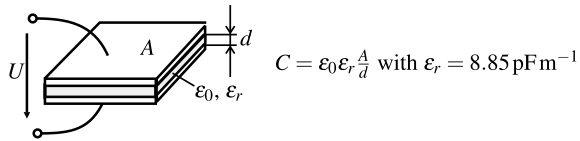

Fig. 10.25 Assembly of a single capacitance

10.5.1.4 Capacitive Sensors

Within every capacitive sensor at least two electrodes are parallel located to each other. Figure 10.25 shows a design based on a single measurement capacity. In contrast to the resistive principle–measuring the mechanical variables stress and strain–the capacitive principle measures the integral values displacement (or elongation) directly.

Concerning the working principle, three classes can be identified, which shows some similarities to electrostatic actuators discussed in Sect. 9.5. The first class uses the displacement principle. On this, the mechanical load changes the electrode distance d or the active electrode area A. In the third class the relative dielectric ε_r is influenced. The change of electrode distance is usually used for measuring force, pressure, displacement, and acceleration. In these cases, the mechanical load is directly applied to the electrode and displaces it relatively to the other one. The resulting capacitance change can be calculated:

$$\frac{\Delta C}{C_0} = \frac{1}{1 \pm \xi/d} \approx \pm\frac{\xi}{d}. \tag{10.21}$$

ξ marks the change of distance. Additionally, the electrode distance can be kept constant, and only one electrode can be parallel displaced (Fig. 10.26). The active electrode area varies accordingly and the resulting capacitance change can be used to measure angle, filling level, or displacement. It is calculated according to:

$$\frac{\Delta C}{C_0} = 1 \pm \frac{\Delta A}{A_0}. \tag{10.22}$$

The third option for a capacitance change is the variation of the relative dielectric. This principal is often used for measuring a filling level e.g. of liquids, or as a proximity switch for layer thickness. This capacitance change is calculated according to

$$\frac{\Delta C}{C_0} = 1 \pm \frac{\Delta \varepsilon_r}{\varepsilon_{r0}}. \tag{10.23}$$

Characteristics of Capacitive Pressure and Force Sensors

The main principle used for capacitive force- respectively pressure transducers is measuring displacements. Consequently, the following paragraph will concentrate on this principle. As stated within Eq. (10.21) for the change of distance, the interconnection between capacitance change and mechanical load is nonlinear for single

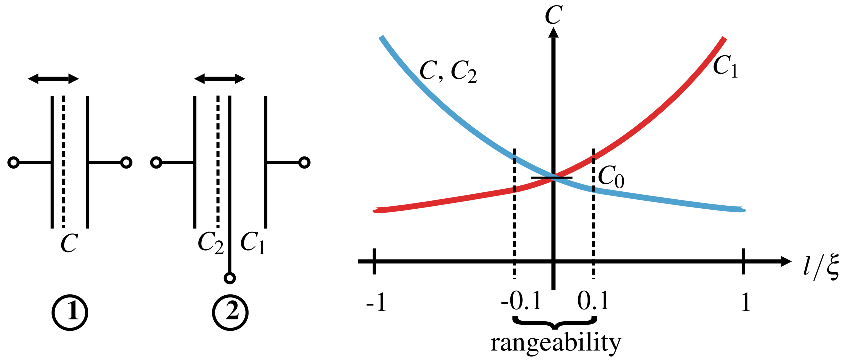

(a) variation of electrode distance in case of single (1) and differential setup (2)

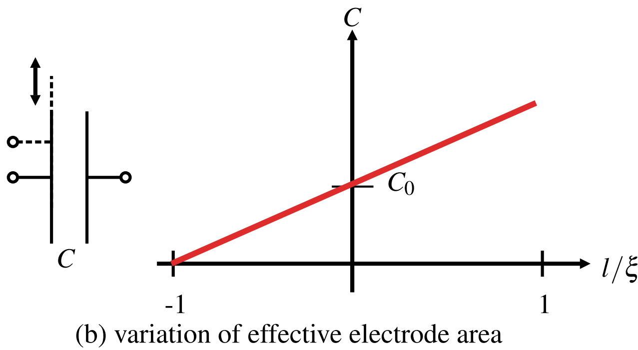

(b) variation of effective electrode area

Fig. 10.26 Schematic view of capacitive sensing principle and characteristic curve of capacitance

capacities. The displacement ξ lies in the range of 10 nm–50 µm [29]. For linearization of the characteristic curves, an operating point has to be found, e.g. by arranging three electrodes as a differential capacitor. The displacements ξ typical for the working range are $\leq 10\%$ than the absolute electrode distance d. In this range the characteristic curve can be approximated as linear (Fig. 10.26a). With the principle varying the electrode's surface the capacitance changes proportional to it, resulting in a linear capacitance change (Fig. 10.26b).

The evaluation of the capacitance change can be made by an open- or closed-loop measuring method. Either concerning open-loop method, the sensor is integrated in a capacitive bridge circuit, or it is put into a passive oscillating circuit with coil and resistor. Alternatively, the impedance can be measured at a constant measurement frequency. An alternative could be the application of a pulse-width-modulation (also called: re-charging method). A closed-loop approach is characterized by the compensation of the displacement by an additional energy. The main advantage of the closed-loop signal conditioning is the high linearity achieved by very small displacements. Additional information can be found in [39, 58].

The advantage of capacitive sensor in contrast to resistive sensors lies in the effect of little power consumption and high sensitivity. Additionally, the simple structure enables a low-cost realization of miniaturized structures in surface micro-machining (Fig. 10.27). In contrast to the resistive sensors–where positions and dimensions of the resistive areas have a direct influence on transfer characteristics–the manufacture tolerances for capacitive sensors are quite high. Mechanically induced stress due to packaging and temperature influence has almost no influence on their performance. Even miss-positioning of electrodes next to each other do not change the transfer characteristics, only the basic capacitance. The manufacturing steps with silicon capacitive sensors are compatible to CMOS-technology. This allows a direct integration of the sensor electronics on the chip, to minimize parasitic capacities. Especially with miniaturized sensors[6] a good signal-to-noise ration can be achieved [72]. The problem of parasitic capacities or leakage fields is one of the major challenges for the design of capacitive actuators, as it achieves easily a level comparable to the capacitance used for measurement. An additional challenge can be found in the constancy of the dielectric value, which is subject to changes in open air-gap actuators due to humidity or other external influence factors.

Examples of Capacitive Sensors

Concerning the manufacturing technology capacitive sensors integrated in haptic systems can be distinguished in three classes. Miniaturized pressure sensors, being realized using silicon microtechnology, represent the first class. Due to their small size of few millimeters, the moving masses of the sensor are low and thus cover a wide dynamic range (frequencies from static to several kilohertz). As shown before, the micro-machined capacitive sensors may be combined to arrays for measuring spatially distributed load. As an example Sergio [75] reports the realization of a capacitive array in CMOS-technology. A challenge is given by the capacity changes in the range of femto-Farad, which is similar to the capacity of the wiring. A relief is given by a parallel circuit of several capacities to a sensor element [29]. The frequency range of the shown examples range from static measurement up to several MHz upper cut-off frequency. Consequently, it is suitable for haptic related measurements of tactile information. Another example is given by an array made of poly-silicon. It has an upper cut-off frequency of 1,000 Hz and a spatial resolution of 0.01 mm^2 suitable for tactile measurements. It was originally designed for acquisitions of finger-prints. Rey [76] reports of the use of such an array for intracorporal pressure measurement at the tip of a gripper. Once again, the leakage capacities are a problem, as they are within the range of the measured capacity changes.

Two examples of multi-component force sensors built in surface micro-machining are shown in Fig. 10.27 (a) [73] and (b) [74]. The two-axial sensor[7] is designed for atomic force microscopy. The nominal load of this application lie in a range of μN. The three-axial sensor was designed for micro-manipulation, e.g. in molecular

[6] Due to the small electrodes a small basic capacitance is achieved, comp. equation in Fig. 10.25.

[7] With respect to "force" component.

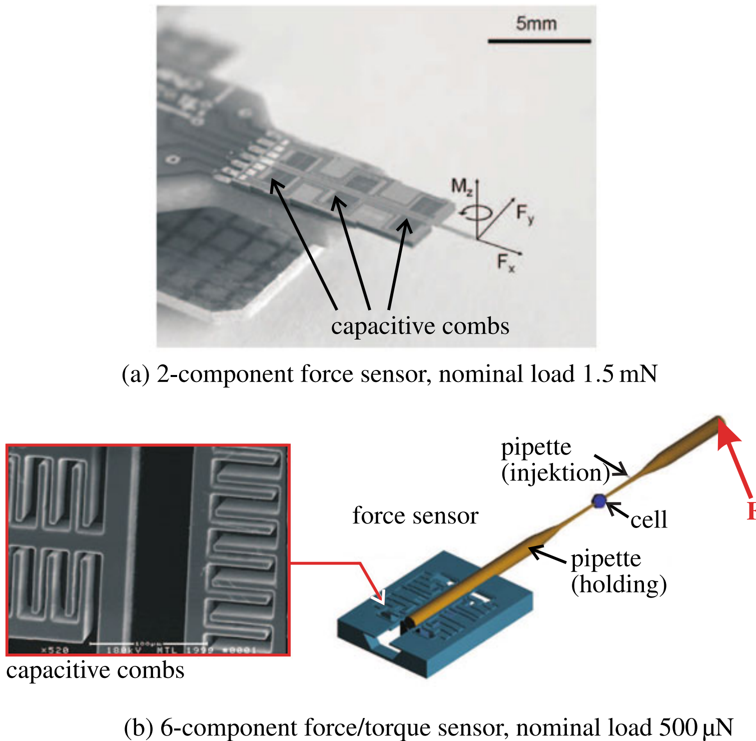

(a) 2-component force sensor, nominal load 1.5 mN

(b) 6-component force/torque sensor, nominal load 500 µN

Fig. 10.27 Examples of capacitive silicon multi-component force sensors [73, 74] © IOP Publishing, all rights reserved

biology, with similar nominal values of several μN. Both sensors are using the displacement change for measurement.

The second class is represented by ceramic pressure load cells. They are widely used in automotive industry and industrial process measurement technology. Substrate and measurement diaphragm are typically made of Al_2O_3 ceramics. The electrodes are sputtered on ceramic substrates. Substrate and measurement diaphragm are connected via solder applied in thick-film technology. In contrast to silicon sensors, ceramic sensors are macroscopic and have dimensions in the range of several centimeters. Based on the technology sensors in differential-, relative-, and absolute-designs with nominal pressures in the range of zero to 200 mbar such as in zero to 60 bar are available (e.g. Fig. 10.28, Fa. Endress + Hauser). The frequency range of these sensors is low, upper cut-off frequencies of approximately 10 Hz are achieved.

The third class is built from foil sensors, distributed e.g. by the company *Althen GmbH*, Kelkheim, Germany. These capacitive sensor elements are arranged in a matrix with a spacial resolution of $\leq 2 \times 2\,\text{mm}^2$. As substrate a flexible polymer foil is used. The height of such an array is 1 mm. The frequency range ranges from static to approx. 1,000 Hz. Nominal loads up to 200 kPa can be acquired with a

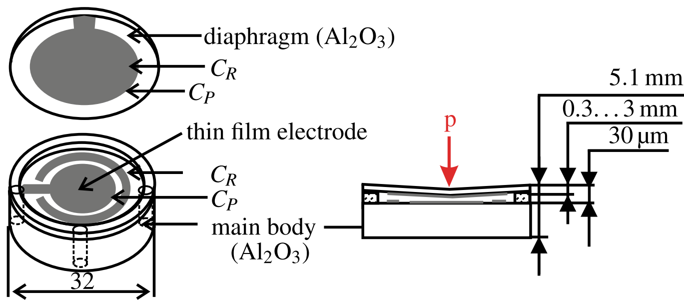

Fig. 10.28 Schematic view of a ceramic pressure sensor fabricated by *Endress + Hauser*, Weil am Rhein, Germany, used with permission

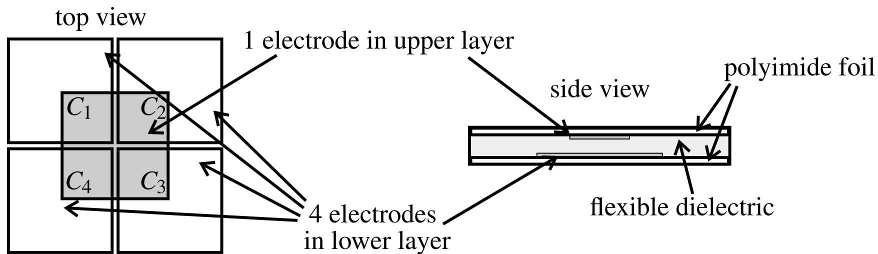

Fig. 10.29 Schematic view of capacitive shear force sensors as presented in [77], own visualization

resolution of 0.07 kPa. Due to creeping (comp. Sect. 10.4.3) of the substrate and parasitic capacities a high measurement inaccuracy exists.

Another polymeric foil sensor in the field of investigation is that one shown in Fig. 10.29 [77]. In contrast to prior examples, this array is used for direct force measurement. Normal forces are detected measuring the change of electrode distance, shear forces by detecting the change of active electrode surface. Similar to the sensor of the company *Althen* static and dynamic changes up to 1,000 Hz can be measured. The spatial resolution is given with $1 \times 1\,\text{mm}^2$. A disadvantage of the design is the high measurement inaccuracy through creeping of the polymer and leakage capacities.

10.5.1.5 Optical Sensors

In the area of optical measurement technology sensors based on freely propagating beams and fiber-optics are available. For force and pressure sensing mainly fiber-optic sensors are used, which will be introduced further within this subsection. All fiber-optic sensors have in common, that mechanical load influences transmission characteristics of the optical transmission network, resulting in an influence of parameters of a reflected or simply transmitted electromagnetic wave. The electromagnetic

wave is defined by its wave equation [78].

$$\nabla^2 \Psi = \frac{\delta^2 \Psi}{\delta x^2} + \frac{\delta^2 \Psi}{\delta y^2} + \frac{\delta^2 \Psi}{\delta z^2} \tag{10.24}$$

Ψ represents an arbitrary wave. A possible solution for this differential equation is the propagation of a plane wave in open space. In this case, electrical field E and magnetic field B oscillate orthogonal to each other. Electrical field propagating in z-direction is described by Eq. (10.25).

$$E(z,t) = \frac{1}{2} A(z,t) \cdot e^{j\omega_0 t - \beta_0 z} \tag{10.25}$$

A marks the amplitude of the envelope, ω_0 is the optical carrier frequency and the propagation constant β_0. With the propagation group velocity $v_g(\lambda)$[8] the E- and B-field are connected. Depending on the transmitting medium group velocity can be calculated via refraction index n_g [79].

$$v_g(\lambda) = \frac{c_0}{n(\lambda)} \tag{10.26}$$

According to wavelength λ, n different values result. Waves are propagating differently depending on their frequency and wavelength. A pulse "spread out". For further information sources [78–82] are recommended. If only mechanical load such as force or pressure influences the transmission network, the resulting deformation can influence the transmission in two different ways:

1. Material specific: Change of the refraction index n (photoelastic effect)
2. Geometric: Change of beam guidance.

The photo-elastic effect describes the anisotropy of the refraction index influenced by mechanical stress. Figure 10.30 visualizes this effect. Resulting refraction index change is dependent on applied stress T and is given by the following equation [83]:

$$\Delta n = (n_1 - n_2) = C_0 \cdot (T_1 - T_2) \tag{10.27}$$

C_0 is a material specific, so-called photo-elastic coefficient. T_i marks the resulting internal stress. Depending on refraction index polarization, wavelength and phase of beam are changing. In the geometric case, mechanical load changes the conditions of the beam guidance. Using geometrical optics influences of mechanical loads on intensity and phase of radiation can be characterized.

A disturbing source for all fiber-optical sensors cannot be neglected: the temperature. Refraction index is depending on temperature changes, and consequently influences the properties of the guided wave. Beside thermal-elastic coefficients

[8] In vacuum it is equal to speed of light $c_0 = 2.99792458 \cdot 10^8$ m/s.

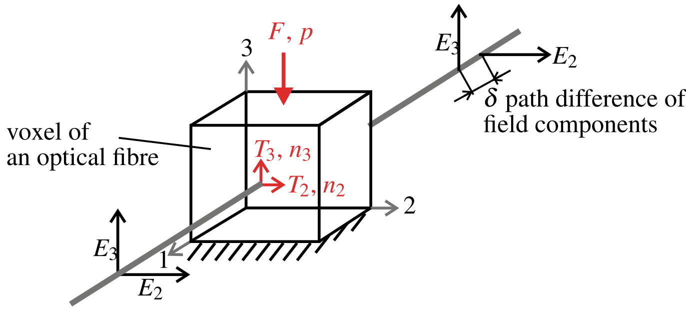

Fig. 10.30 Visualization of photoelastic effect [83]. Due to different refraction indices perpendicularly to the propagation direction propagation velocity of each field component is different and an optical path difference δ occurs. Polarization is changing

describing the strain resulting from temperature changes within any material, temperature directly influences the refraction index itself (paragraph Sect. 10.5.1.5). For temperature compensation a reference fiber has to be used, un-loaded and only influenced by temperature change. An advantage of all fiber-optical sensors is given by their immunity to electromagnetic radiation. The following paragraphs introduce the most important principles for optical force- and pressure measurement.

Change of Intensity

In principal, two transducer types varying the intensity can be distinguished. Both have in common, that mechanical load varies the condition of total reflection (Fig. 10.31). The angle α_c is defined as the critical angle for total reflexion and defined by SNELLIUS' law:

$$sin(\alpha_c) = \frac{n_2}{n_1} \tag{10.28}$$

The numerical aperture NA gives the appropriate critical angle θ_c for coupling radiation into a multimode fiber:

$$sin(\theta_c) = \sqrt{n_1^2 - n_2^2} \tag{10.29}$$

If the angle varies due to mechanical load and takes values larger than θ_c resp. smaller values than α_c, conditions for total reflections are violated. The beam will not be guided within the core of the fiber. Total intensity of the transmitted radiation will become less. Figure 10.32 show a schematic sketch of the design of the very first variant. The sensor element is attached to the end of a multimode fiber.

In a first variant the light (e.g. emitted by a laser-diode $\lambda = 1550$ nm) is coupled into a multimode fiber. A reflective element is attached to the end of the transmission line. The element can be designed as a deformable object or a rigid one mounted on a deformable substrate. Mechanical load acts on this object. Due to the load the reflective element will be deformed (in case of a flexible surface) or displaced (in case

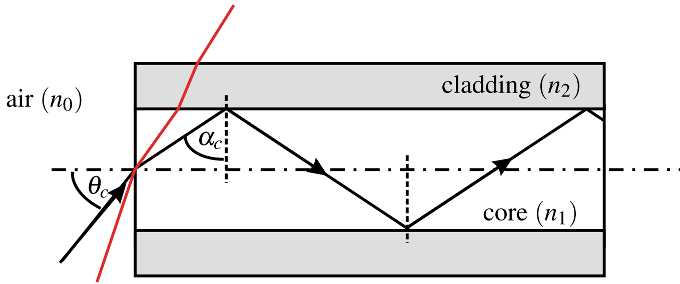

Fig. 10.31 Guidance of multimode fibers. Beams injected with angles above θ_c are not guided in the core

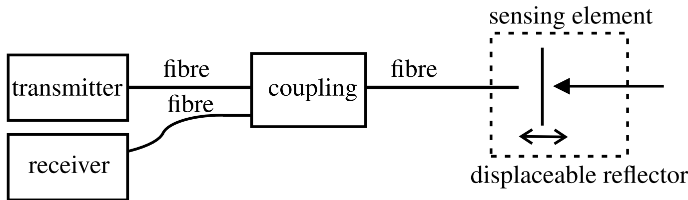

Fig. 10.32 Schematic view of a fiber optic sensor with intensity modulation

of a rigid surface). Varying the displacement the mode of operation is comparable to a displacement sensor. The intensity is directly proportional to the displacement (Fig. 10.33). The load itself is a function of displacement and directly proportional to the elastic compliance n of the sensor element:

$$F(z) = n \cdot z. \tag{10.30}$$

If the geometry of the area changes, a part of the beam–according to the laws of geometrical optics–is decoupled into the cladding (dispersion) and an intensity loss can be measured at the detector (Fig. 10.33).

In academic publications from Peirs [84] and Kern [85] such a mode of operation is suggested for multi-component force measurement. In this case, the measurement range is directly proportional to the mechanical properties of fixation of the reflective body. Using the calculation method known from Sect. 10.5.1.1 this fixation can be designed. A disadvantage of this principal is the use of polymers for the coupling of the reflective object. This leads to creeping of the sensor signal. The measurement inaccuracy of these sensors lies in a range of 10% [85]. Their diameter takes a value of few millimeters. The length depends the application. Another source of noise is the temperature. A temperature change leads to a dilatation (or shrinkage) of the polymer itself and displaces the reflective element. The displacement change results in a defective measurement signal. Due to the small size, an array assembly is possible.

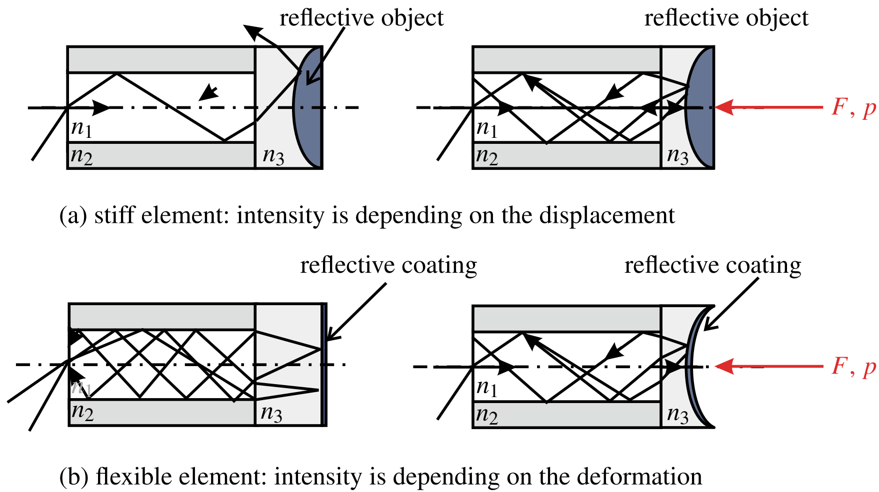

Fig. 10.33 Variation of intensity due to displacement of rigid and flexible elements

The second variant is a so-called "micro-bending sensor". Its fundamental design is schematically given in Fig. 10.34. As stated before, a beam is coupled into a multimode fiber. Force, pressure or strain is applied by a comb-like structure results in micro-bending of the fiber (Fig. 10.34b).

In case of deformation–similar to the first variant–a part of the light is decoupled into the cladding. The intensity of the measured light diminishes.[9] The gaps between the comb-like structures for micro-bending sensors are in the range of one millimeter. The height of the structure is in the same dimension [86]. To apply mechanical loads an area of $\cong 1$ cm length and a width of ≥ 5 mm is used. Measurement range depends on displacement of the bending structure and diameter of the fiber itself. PANDEY [87] describes the realization of a pressure sensor for loads up to 30 bar. If the bending diameter becomes smaller, lower nominal pressures and forces are possible. Concerning the detection of force components, only one-component sensors can be realized using this principle.

If spatially distributed mechanical load has to be measured, multiple micro-bending structures can be located along one fiber. To evaluate the several measuring points, for instance optical time domain reflectometry (ODTR) can be used. This device sends a pulsed signal (light pulses of around 10 μs length) guided in a fiber, and measures the reflexion depending on time. Based on the propagation velocity of the beam inside the fiber v, the time delay for each measuring point can be calculated by relating them. Additional information can be found in [86, 88] or [87]. The dynamics of these sensors is only limited by sensor electronics and could theoretically be applied to the whole range of haptic applications.

[9] Both versions are possible: Measuring the transmitted and the reflected radiation.

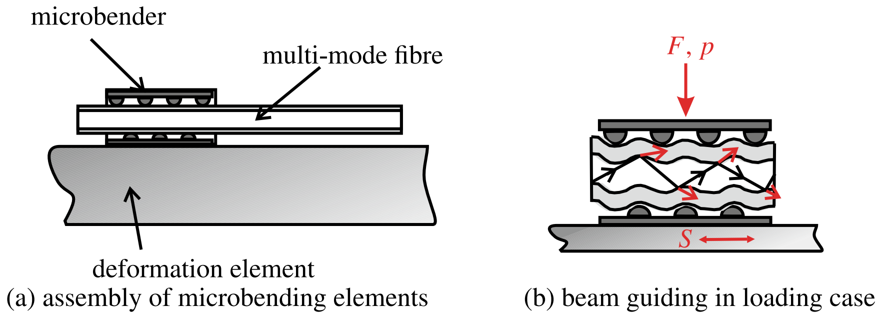

Fig. 10.34 Variation of beam guidance in case of microbending

Change of Phase

The variation of the phase of light by mechanical load is used for interferometric sensors. The most commonly used type is based on the Fabry-Pérot-interferometer, discussed in the following paragraph. Other variants are Michelson- and Mach-Zehnder-interferometers. The assembly is made of two plane-parallel, reflective and semi-transparent objects e.g. at the end of a fiber, building an optical resonator (Fig. 10.35). The beam is reflected several times within the resonator and interferes with each reflection. The resonance condition of this assembly is given by the distance d of the reflective elements and the refraction index n within the resonator. The so-called "free spectral range" marks the phase difference δ, generating a constructive superposition of beams:

$$\delta = \frac{2\pi}{\lambda} \cdot 2 \cdot n \cdot d \cdot cos(\alpha) \tag{10.31}$$

Figure 10.35b shows the typical characteristics of the transmission spectrum of a Fabry-Pérot interferometer. According to the formula shown above the corresponding wavelength yields a transmission peak; all other wavelengths are damped and annihilated. Due to the mechanical load the distance d of the surfaces is varied, changing the conditions for constructive interference. Sensors using this principle are e.g. used by the company *LaserComponents Gmbh*, Olching, Germany, for uniaxial force- or pressure measurement, and can be bought for nominal pressures up to 69 bar [89]. The influence of temperature would also appear to be problematic too and has to be compensated by a reference configuration parallel working.

Beside pressure transducers, single component forces and strains can be measured (Fig. 10.36). The design equals a Michelson-Interferometer. The sensor element is made of two multimode fibers, whereas the strain acts upon only one fiber. Identical to the Fabry-Pérot-configuration the sensor element is made of two plane-parallel reflective surfaces, whose distance varies according to varying strain. Inside the measuring electronics a reference design is included. To measure the mechanical load the phase of reference and measuring assembly is compared. This measurement principle enables to measure frequencies in the range of several kilohertz. The geometrical

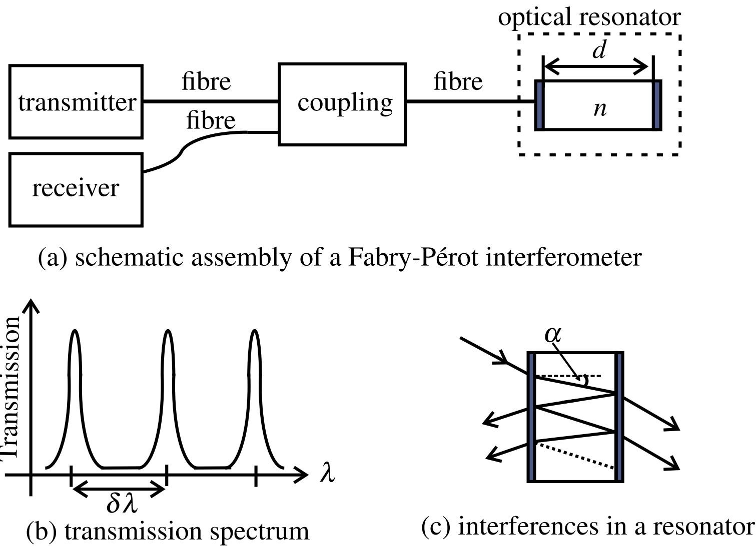

Fig. 10.35 Assembly and operating mode of a Fabry-Pérot interferometer

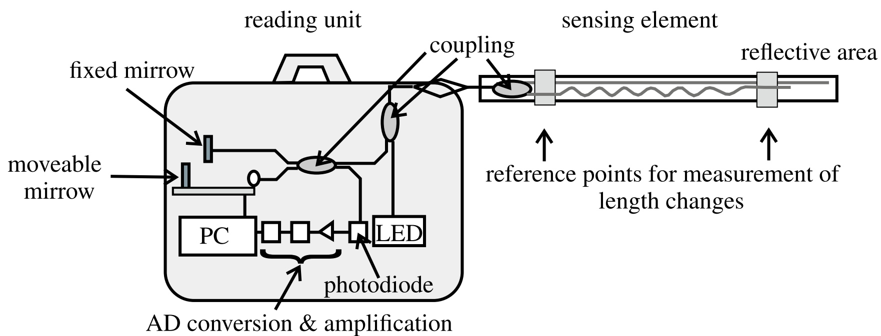

Fig. 10.36 Temperature compensation in interferometric strain sensing elements

dimension is given by the diameter of the fiber including some protective coating $\leq$ 1 mm, and the length of 2–20 mm depending on the application itself. For pressure sensors the measuring error with respect to nominal load takes a value of about 0.5%, with strain gages at a factor of $15 \cdot 10^{-6}$.

Change of Wavelength

For optical detection of strain so called fiber BRAGG grating sensors (FBG sensor) are widely used. To realize the sensing element the refractive index of the core in a single mode fiber is varied due to the position (Fig. 10.37) and a grating arise [90]. The refractive index modulation can be described by

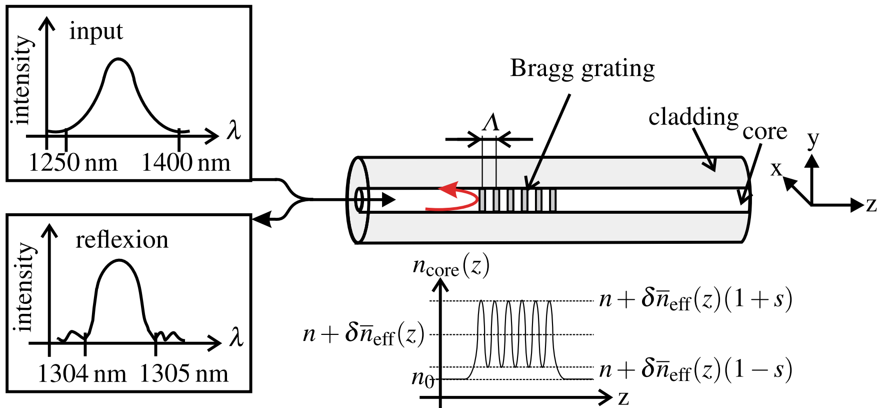

Fig. 10.37 Operational mode of fbg sensors [90]

$$n(z) = n_0 + \delta n_{effective}(z) = n_0 + \delta \overline{n}_{effective} \cdot \left(1 + s \cdot cos\left(\frac{2\pi}{\Lambda} z + \phi(z)\right)\right) \tag{10.32}$$

whereas n_0 is the refractive index within the core, $\delta\overline{n}_{effective}$ is the average of the index's modulation and s a measure of the intensity of the index's modulation. Λ marks the grating period and the phase shift $\phi(z)$ resulting from the measured value. In idle situation results $\phi(z) = 0$. Figure 10.37 gives a schematic drawing of the assembly.

If light is coupled into the fiber, only parts of it are reflected according to the law of Bragg. The reflective spectrum shows a peak at the so called Bragg-wavelength λ_b. This wavelength depends on the refractive index $n(z)$ and the grating period Λ:

$$\lambda_b = 2n\Lambda. \tag{10.33}$$

In loading case both grating distance and refractive index varies. The maximum of the spectrum is shifting from λ_0 to another wavelength. According to the wavelength shift mechanical load can be determined. This leads us to thee following condition:

$$\frac{\Delta\lambda}{\lambda_0} = \underbrace{(1 - C_0)}_{gagefactor} \cdot (S + \alpha_{VK} \cdot \Delta\vartheta) + \frac{\delta n/n}{\delta\vartheta} \cdot \Delta\vartheta, \tag{10.34}$$

whereas α_{VK} is the coefficient of thermal expansion of the deformation body, and C_0 the photoelastic coefficient. Beside the change induced by mechanical strain S the change of temperature ϑ influences the wavelength shift in the same dimension. Compensating the influence of temperature another FBG sensor has to be installed as reference at an un-loaded area. The temperature compensation is afterwards achieved by comparison between both signals. Analogous to resistive strain sensors a gage fac-

tor of $k \approx 0.78$ can be achieved with constant measurement temperature. Extensions up to 10.000 µm/m can be achieved.

The width of the sensor lies in the area of single mode fibers. The sensors length is defined by the grating, which has to be three milimetres at least to provide a usable reflective spectrum ([91–93]). Resolution takes a value of 0.1 µm/m and is–such as its dynamics–defined by the sensor electronics. Similar to strain gages these sensors can be mechanically applied on deformation elements, whose dimensions and shapes define the measurement range. A challenge with the application of fiber-sensors in this context is the differing coefficients of thermal expansion between deformable element, adhesive and fiber. Additionally, reproducibility of the adhesive-process for fibers is not as high as typically required. Especially creeping of glue results in large measurement errors. Comparable to the micro-bending principle, fbg sensors are applicable to several spatially distributed measurement points. To distinguish the several positions gratings with different periods Λ_i and thus different BRAGG-wavelengths λ_b are used. The company *Hottinger Baldwin Messtechnik GmbH*, Darmstadt, Germany, distributes several designs containing a application area around the grid for strain measurement.

Besides monitoring of structures or strain analysis, fbg sensors can be used for realizing force sensors too. MUELLER describes the use of fbg sensors in a tri-axial force sensor for medical application [94]. Further information on the application of fbgs can be found in [90–93].

10.5.1.6 Piezoelectric Sensors

Piezoelectric sensors are widely used, especially for measurement of highly dynamic activities. The measurement principle is based on a measure induced charge displacement within the piezoelectric material, the so called reciprocal piezoelectric effect (Sect. 9.3). Charge displacement leads to an additional polarization of the material resulting in a change of charge on the materials surface. This can be detected using electrodes (Fig. 10.38). Beside the measurement of force, it is for pressure- and acceleration measurement in particular. For force measurement, the longitudinal effect is primarily used. Detailed information about the piezoelectric effect and possible designs are found in Sect. 9.3. Materials used for sensing elements will be introduced in the following paragraph.

The general equation of state states for operation in sensor mode:

$$D_i = \underbrace{\varepsilon_{ij}^T \cdot E_j}_{\to 0} + d_{im} \cdot T_m, \tag{10.35}$$

$$D_3 = d_{31} \cdot T_1. \tag{10.36}$$

A stress contribution in the sensing material leads to a change of charge density D_i, whereas ε_{ij}^T marks relative permittivity and d_{im} piezoelectric charge constant. Taking geometric parameters of the sensor, eletrode area $A = l_1 \cdot l_2$ and thickness l_3

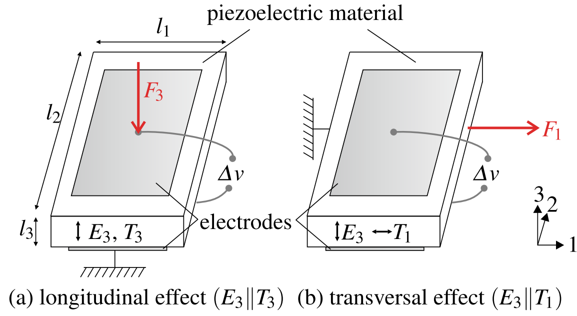

(a) longitudinal effect $(E_3 \| T_3)$ (b) transversal effect $(E_3 \| T_1)$

Fig. 10.38 Visualization of piezoelectricity

of dielectric, the resulting charge q can be derived. Taking electric parameters into account, sensor output voltage Δu can be calculated [15, 29, 95]:

$$q = D_3 \cdot A_3, \tag{10.37}$$

$$\Delta v = q \cdot \frac{1}{C_\mathrm{p}}, \text{ with } C_\mathrm{p} = \frac{e_{33}^T \cdot l_2 \cdot l_1}{l_3}, \tag{10.38}$$

C_p marks capacitance and e_{33}^T piezoelectric force constant.

Technically relevant materials can be distinguished into three groups. The first group is built of mono-crystals such as quartz, gallium-, and orthophosphate.[10] Polarization change in case of mechanical load is direct proportional to the stress. Its transfer characteristic is highly linear and does not have any relevant hysteresis. Piezoelectric coefficients are long-term stable. One disadvantage is the small coupling factor k of about 0.1. For remembrance: k is defined as the quotient of the transformed to the absorbed energy.

The second group is formed by polycrystalline piezo-ceramics, such as barium titanate ($BaTiO_3$) or lead zirconate titanate (PZT, $Pb(ZiTi)O_3$), being manufactured in a sintering process. The polarization is artificially generated during the manufacturing process (Sect. 9.3). An advantage of this material is the coupling factor, which is seven times higher than that one of quartz. A disadvantage is the nonlinear transfer characteristics with a noticeable hysteresis, and a reduced long-term stability. The materials tend to depolarize.

The last group is build from partial crystalline plastic foils made of polyvinylidene fluoride (PVDF). Its coupling factor lies with 0.1 to 0.2 in the area of quartz. Advantageous are the limit size (foil thickness of a few μm) and the high elasticity of the material.

The first two sensor materials are used in conventional force sensors, as e.g. distributed by the company Kistler. Nominal forces take values of 50 N to 1.2 MN. The sensor typically has a diameter of 16 mm and a height of 8 mm. Alternations of load up to 100 kHz are measurable. Single- as well as multiple-component sensors

[10] This crystal is especially applicable for high temperature requirements.

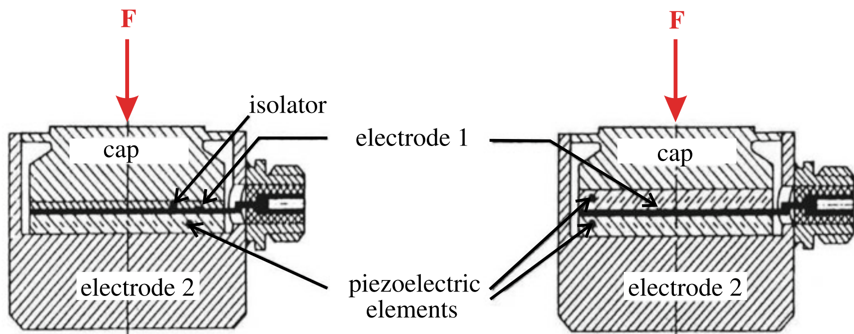

(a) possible assemblies for piezoelectric force sensors

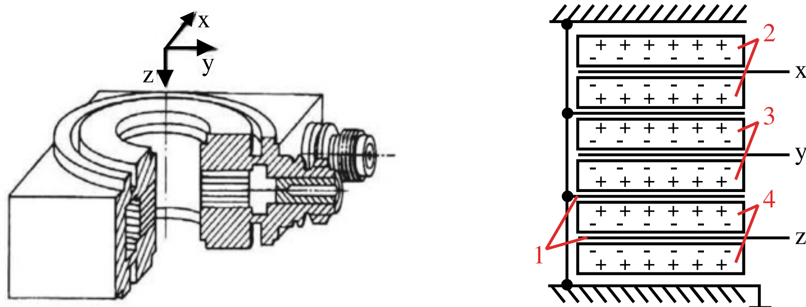

(b) assembly of a 3-component sensor: 1 electrodes, 2 quartz plates shear effect - F_x, 3 quartz plates longitudinal effect - F_z, 4 quartz plates schear effect - F_y

Fig. 10.39 Possible assemblies of piezoelectric force sensors

are state of the art. Figure 10.39 shows the general design of a three-component-force-sensor from Kistler.

Piezoelectric force sensors are typically used for the analysis of the dynamic forces occurring during drilling and milling or for stress analysis in automotive industry. In haptic systems, these sensor variants can hardly be found. Not exclusively but mostly because they are not suitable to measure static loads. Sensors based on PVDF-foils as piezoelectric material are increasingly used for the measurement of tactile actions. The piezoelectric effect however is used for the generation of a displacement and not for its measurement, making this variant being described in paragraph Sect. 10.5.1.7.

10.5.1.7 Less Common Sensing Principles

Sensor designs shown in this subsection are not force or pressure sensors for conventional purposes. All of them have been designed for different research projects in the context of haptic systems. Focus of these developments lies in the spatially distributed measurement of tactile information.

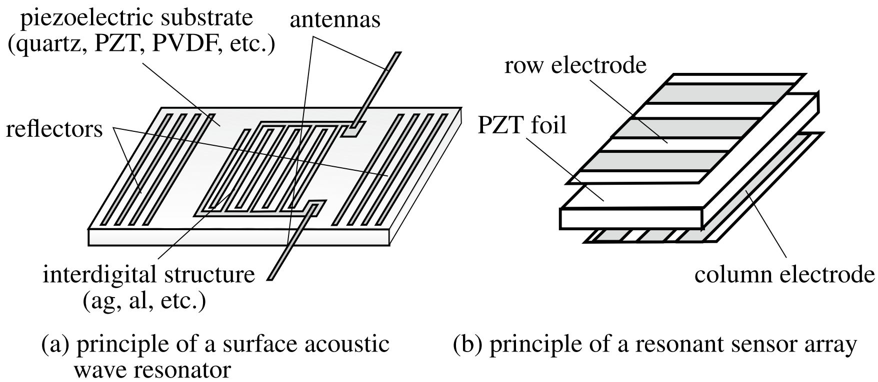

Fig. 10.40 Schematic view of resonance sensors, own illustrations following **a** [32], **b** [96]

Resonance Sensors

For measurement of vibrotactile information e.g. the so called resonance principle could be used. Figure 10.40a shows the principal design of such a sensor. A piezoelectric foil (PZT or even PVDF) is used as an actuator. Electrodes on both sides of the foil apply an electrical oscillating signal, resulting in mechanical oscillations of the material due to the direct piezoelectric effect. The structure oscillates at its resonance frequency f_0 calculated by the following formula

$$f_0 = \frac{1}{2d} \cdot \sqrt{\frac{n}{\rho}} \tag{10.39}$$

whereas d is the thickness, n the elasticity and ρ the density of the used material. The load, responsible for the deformation, is proportional to the frequency change [96]. For spatially distributed measurement, the sensors are connected as arrays of elements with 3x3 and 15x15 sensors. The dimensions of the sensing arrays takes values of 8x8 mm^2 resp. 14x14 mm^2. The thickness of the foil is $\ll$ 1 mm. A huge disadvantage of this principle is the high temperature dependency of the resonance frequency from the piezoelectric material used. The coefficient lies at 11.5 Hz per 1 °C within a temperature range between 20 and 30 °C [70, 97].

So called surface acoustic wave resonators, SAW sensors, make use of the change of their resonance frequency too. The excitation occurs via an emitter called "Interdigital structure" (Fig. 10.40b). The mechanical oscillations with frequencies in the range of MHz distribute along the surface of the material. They are reflected on parallel metal structures and detected by the receiving structure. Due to mechanical values applied the material is deformed, the runtime of the mechanical wave changes, and consequently the sensor's resonance frequency. With this design, the temperature is one of the major disturbing values. SAW sensors are used for measurement of force, torques, pressure and strain. The dynamic range reaches from static to highly dynamic loads.

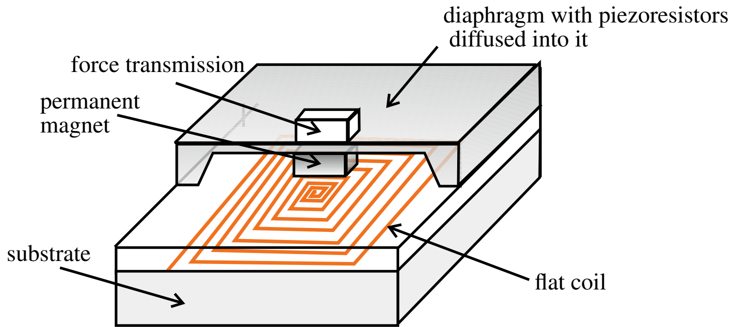

Fig. 10.41 Schematic view of an active element [99]. The dimensions are $6 \times 6 \times 1\,\mathrm{mm}^3$

Electrodynamic Sensor Systems

Within the research project *TAMIC* an active sensor system for the analysis of organic tissue in minimally invasive surgery was developed [216]. The underlying principle is based on an electrodynamic actuated plunger excited to oscillations (Sect. 9.1). The plunger is magnetized in axial direction. The movements of the plunger induce voltages within an additional coil included in the system. The material to be measured is damping the movement, which can be detected and quantified by the induced voltage. The maximum displacement of the plunger is set to one millimeter. The system is able to measure dynamically from 10 to 60 Hz. The nominal force lies in the range of 200 mN. The geometrical dimensions of the system are a diameter of $\leq$15 mm, and a length of $\leq$400 mm, which is near to typical minimally invasive instruments. Detailed information can be found in [98].

Another example for a miniaturized sensor for the measurement of spatially distributed tactile information is presented by Hasegawa in [99]. Figure 10.41 shows the schematic design of one element.

The elements are arranged in an array structure. In quasi-static operation mode the system is able to measure contact force and the measurement object's elasticity. The upper surface is made of a silicon-diaphragm with a small cubical for force-application to the center of the plane. The displacement of the plate is measured identical to a silicon-pressure or -force sensor with piezoresistive areas on the substrate. By the displacement the applied contact force can be derived. For measuring the elastic compliance of the object, a current is applied to the flat coil (Fig. 10.41). In the center of the diaphragm's lower side a permanent magnet is mounted. The electrically generated magnetic field is oriented in the opposite direction of the permanent magnet. The plate is displaced by this electromagnetic actuator and the cube is pressed back into the object. The force necessary to deform the object is used in combination with the piezoresistive sensors signal for calculation of the object's elastic compliance. In the dynamic operation mode the coil is supplied with an oscillating signal, operating the diaphragm in resonance. Due to interaction with the measured object the resonance condition changes. By the changing parameters, such as phase

rotation, resonance frequency, and amplitude, elastic coefficients such as damping coefficients of the material can be identified. Due to the high degree of miniaturization highly dynamic actions up to several kilohertz are possible to be measured. The nominal force lies in the area of 2 N, the resolution of the system is unknown.

Electro-Luminescence Sensors

A high resolution touch-sensors is presented by SARAF [100]. It is thought to be used for the analysis of texture on organ surfaces. On a transparent glass substrate a layer-compound of 10 μm height made of gold- and cadmium sulfite particles[11] is applied. The single layers are separated by dielectric barriers. The mechanical load is applied on the upper gold layer, resulting in a break-through of the dielectric layer and a current flow. Additionally, energy is released in form of small flashes. This optical signal is detected using a CCD-camera. The signal is directly proportional to the strain distribution generated by the load. The resulting current density is measured and interpreted.

The spatial resolution of the design is given with 50 μm. Nominal pressures of around 0.8 bar can be detected. The sensor area has a size of $2.5 \times 2.5\,\text{mm}^2$, the thickness of the sensor is $\leq$1 mm and thus very thin. Additional information can be found in [100].

10.5.2 Selection of a Suitable Sensor

In earlier sections sources for the requirements identification have been presented. Afterward, presentation and discussion of the most relevant sensor principles to measure forces were made. This section is intended to help engineers to select or even develop an appropriate force sensor. Depending on the identified requirements found using Sect. 10.4, a suitable sensor principle can be chosen.

To get a better overview, the basic requirements described in Sect. 10.4.5.1 are collected in Table 10.8. The requirements are distinguished concerning human perception in kinesthetic and tactile information. More detailed information concerning force- and spatial-resolution can of course be found in Sect. 10.4. The properties of active and passive transformers–force measurement is done via a mechanical variable such as strain or stress detected via elasto-mechanics–are strongly dependent on the design of the deformation element. Especially the nominal force, number of components to be measured and the dynamics are directly influenced by the deformation element's design.

A comparison of all sensor principles can hardly be done. Consequently, the methods will be compared separately from each other. As an evaluation criterion transfer characteristics and geometrical dimensions are chosen. Figure 10.42 classifies the principles according to gage factor and geometry. According to the increasing size of the strain sensing element, the whole force sensor can be designed at a higher level

[11] A semi-conducting material.

Table 10.8 Compilation of main requirements on haptic sensors. Depending on system topology and measurement task further requirements have to be considered

Type of information	Requirements	Values
Kinaesthetic	Nominal load F_N	(5 ... 100) N
	Resolution ΔF	5% F_N
	Frequency range	(0 ... 10) Hz
Tactile	Nominal load F_N	≤ 0.3 N or ≤ 4.5 N
	Resolution ΔF	5% F_N
	Frequency range	(0 ... 1,000) Hz
	Spatial resolution Δx	Structural dependent, ≥ 0.5 mm

of miniaturization. A direct result of smaller size is the minimized mass, providing an increased upper cut-off frequency. If the gage factor of the sensing element is higher, lower absolute value of strain is necessary to get a high output signal. Additionally, the over-all design can be designed stiffer. This enables to detect smaller nominal forces and thus higher cut-off frequencies. Concerning the lower cut-off frequency strain sensing elements are suitable for measuring static loads. Using piezoresistive and capacitive silicon-sensor an upper cut-off frequency of 10 kHz or more can be measured with high resolution.

The other sensor principles can be compared contingent on nominal load and dimensions. Figure 10.43 classifies the presented principals according to their nominal load and corresponding construction space.

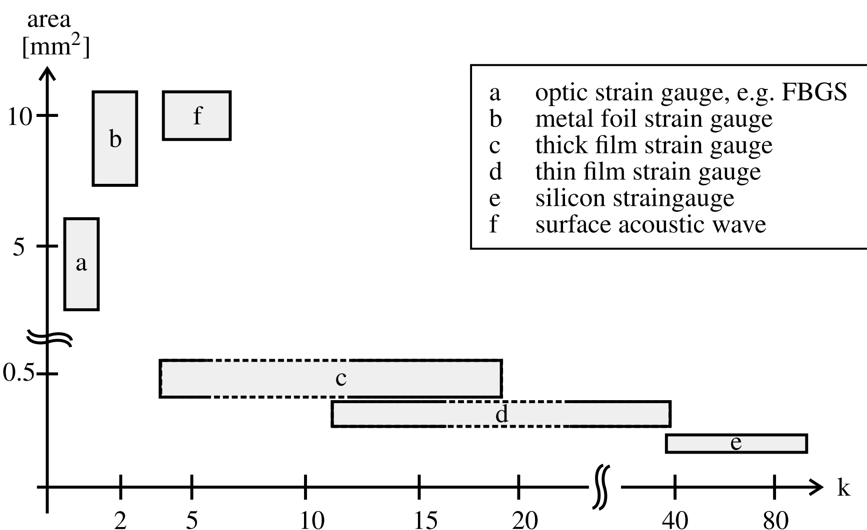

Fig. 10.42 Comparison of different strain measurement technologies due to dimensions and gage factor

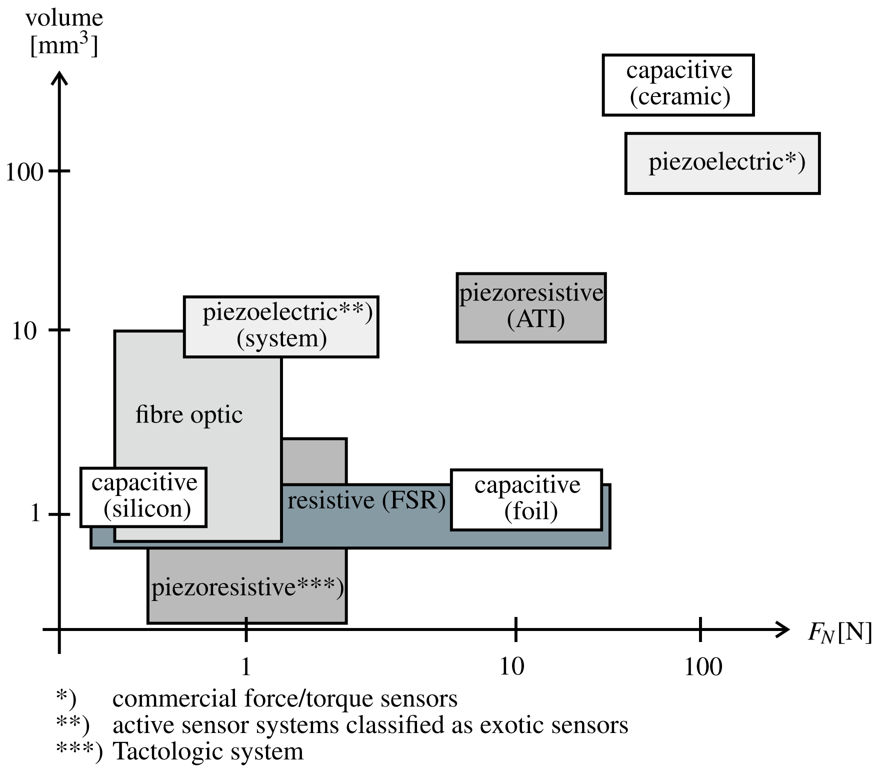

Fig. 10.43 Comparison of different measurement technologies due to dimensions and nominal load

Except the piezoelectric sensors, all sensor principles can be used for measuring static and dynamic loads. The upper cut-off frequency mainly depends on the mass of the sensor which has to be moved. Consequently, the more miniaturized the sensor the higher the upper cut-off frequency becomes. Figure 10.44 compares the presented sensor principles according to the detectable nominal load and the corresponding dynamic range.

By means of the shown diagrams a pre-selection of suitable sensor principles for the intended application can be done. Additional sensor properties such as resolution, energy consumption, costs or impact of noise are strongly depending on the individual realization and will not be taken into account here. Advanced descriptions of sensor properties can be found in literature highlighted in the corresponding subsections for the individual principle.

To give an example how to select a suitable force sensor, the task *laparoscopic palpation of tissue* is chosen. Figure 10.45 shows the tree diagram which can be used for analyzing the task and deriving requirements. Laparoscopic palpation is a telemanipulation tasks for characterizing texture. It is done via closed-loop control.

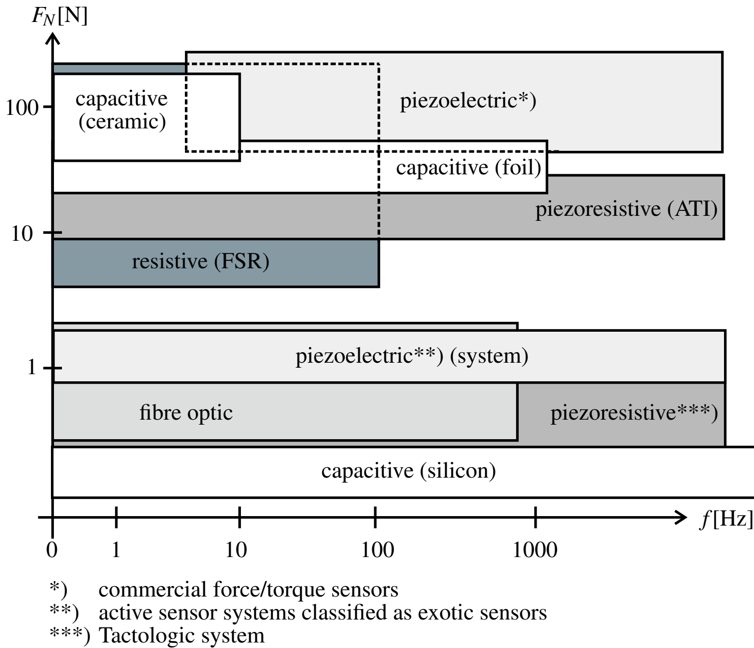

Fig. 10.44 Comparison of different measurement technologies due to nominal load and frequency range

To avoid undesired influences of the laparoscopic instrument itself onto the sensing signal (e.g. friction between instrument and abdominal wall), the sensor should be integrated into the tip. The laparoscope is used to scan the tissues surface. Detecting three directions of contact force, texture and even compliance of tissue can be analyzed.

Taking contact information and into account (Table 10.8) cut-off frequency, resolution and nominal force can be derived. The dimensions of the laparoscope limit the construction space. Also static information has to be measured, thus an active sensing principle like (piezo-)resistive, capacitive, inductive or optic should be considered. Due to limited space, piezoresistive sensing is recommendable.

Is no force sensor with the determined requirements available, a deformation element has to be designed separately taking load condition and elasto-mechanics into account. For example [31, 32] are helpful references for designing deformation elements. The strain sensing element can be chosen depending on the aimed resolution and construction space. Table 10.9 gives an overview of common strain sensing technologies.

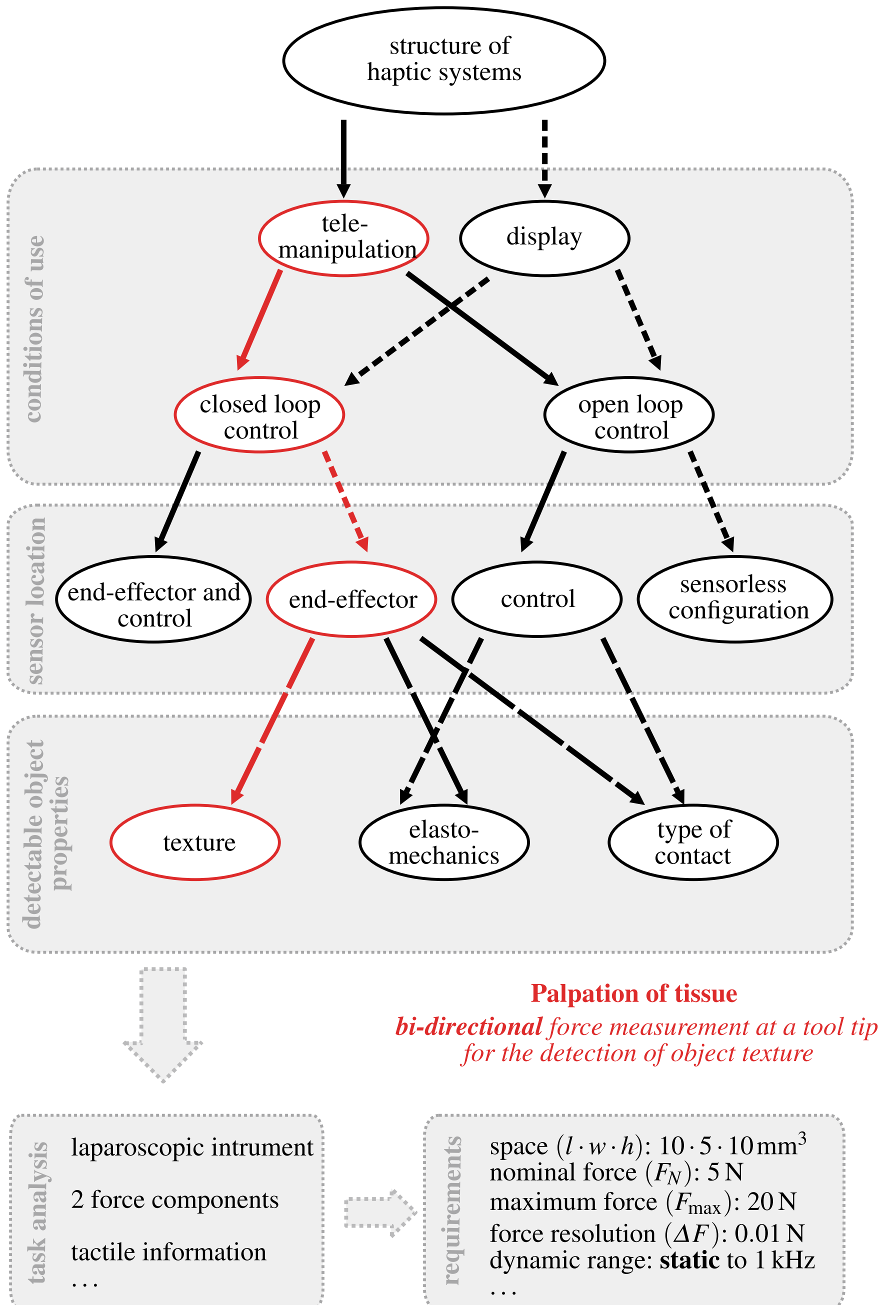

Fig. 10.45 Tree diagram for selecting a force sensor. Exemplarily, the task *laparoscopic palpation of tissue* is chosen

Table 10.9 Comparison of common sensing principles for strain measurement [32]

Principle	Material	Gage factor	S_{min}	S_N	S_{max}	Thickness h_M	References
Foil-strain gage	Constantan	2.0	$\pm 10^{-7}$	±0.1%	±2%	80 ... 100 μm	[47–49]
Thick-film	$Bi_2Ru_2O_7$	12.1 ... 18.3	$\pm 10^{-6}$	±0.1%	±0.2%	≤50 μm	[40, 50]
	PEDOT:PSS	0.48 ... 17.8	–	≥ 10%[a]	–	1 ... 10 μm	[42, 51]
Thin-film[b]	$TiON$	4 ...5	$\pm 10^{-7}$	±0.1%	±2%	≤1 μm	[29, 50, 52]
	Poly-Si	20 ... 30	$\pm 10^{-7}$	±0,1%	±2%	≤1 μm	[29, 50]
Si-Technology	Homogeneous	100 ... 255	$\pm 10^{-6}$	±0.2%	±0.3%	10 ... 15 μm	[53]
	Inhomogeneous	80 ... 255	$\pm 10^{-7}$	±0.05%	±0.1%[c]	17 ... 100 μm	[45, 54]
Capacitive	PVDF[d]	≤ 83	–	±0.3%	±1%	About 150 μm	[101]
	Inter-digital	1 ... 5	$\pm 10^{-7}$	±0.1%	±5%	≤ 500 μm	[50, 102, 103]
FBGS	–	0.78	$\pm 10^{-7}$	±0.2%	±1%	150 ... 250 μm	[104, 105]
Piezoelectric	PZT[e]	$\leq 2{\cdot}10^6$	$\pm 10^{-10}$	–	±0.1%	200 μm	[106, 107]
SAW	Quartz	1.28 ... 20	$\pm 10^{-7}$	±1%	±2%	About 600 μm	[29, 108–111]
Magneto-elastic	NiFe45/55	About 1,500	$\pm 10^{-8}$	±0.2%	–	About ≤80 μm	[15, 112, 113]
Fibers	Carbon	1.3 ... 31	–	–	0.2 ... 15%	12 μm	[55, 56]

[a] Depending on substrate, in [114] polymeric fibers with a maximum strain of 10% are used
[b] Maximum strain depends on elasticity of deformation element
[c] According to [115] elongation of break takes a value of ±0.2%
[d] $d\varepsilon/\varepsilon$, sandwich-topology
[e] patch transducer, PI

10.6 Tactile Sensing and Touch Sensors

With the increasing number of systems using touch-sensitive surfaces for ↪ HCI, touch sensors have become more prevalent. They detect, whether a human user touches a sensitive two- or three-dimensional surface of an object or system. It is a special kind of force sensors (so-called tactile sensors) and requirements as well as constraints were already mentioned in Section Sect. 10.5. One can differentiate between sensors that detect the contact position and ones that detect different types of touch or contact pose.

When analyzing this kind of systems, one can identify several functional principles. Because of robustness, low costs and high sensitivity, resistive and capacitive principles are among the most used in ↪ HCI. DAHIYA AND VALLE provide a thorough analysis of different measurement principles in [116] for the usage in robotic applications. In the following, the function of resistive and capacitive systems is described in more detail.

10.6.1 Resistive Touch Sensors

Resistive touch sensors to detect contact positions are based on two flexible, conductive layers that are normally separated from each other. If a user touches one of the layers, a connection is made between both layers and the position of the connection point can be calculated from the different resistances as shown in Fig. 10.46 based on Eqs. (10.40) and (10.41).

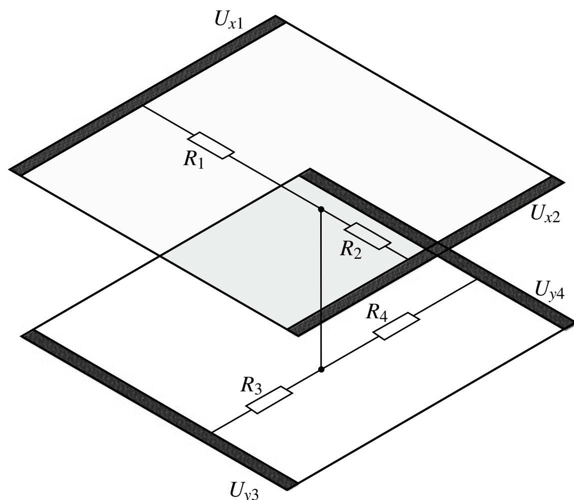

Fig. 10.46 Principle of resistive touch sensors

$$u_{\mathrm{x,out}} = \left. \frac{R_2}{R_1 + R_2} U_{x1} \right|_{U_{x2}=0\,\mathrm{V}, \quad U_{y3}, U_{y4} \text{ in Hi-Z state}} \tag{10.40}$$

$$u_{\mathrm{y,out}} = \left. \frac{R_4}{R_3 + R_4} U_{y3} \right|_{U_{y4}=0\,\mathrm{V}, \quad U_{x1}, U_{x2} \text{ in Hi-Z state}} \tag{10.41}$$

Resistive touch sensors exhibit a high resolution of up to 4096 dpi in both dimensions and a high response speed (<10 ms). With additional wiring, also the pressure on the screen can be recorded. This principle does not support multi-touch detection, i.e. the simultaneously contact in more than one position, with the setup shown in Fig. 10.46. A simple mean to measure multi-touch interactions, too, is the segmentation of one of the conductive layers in several (n) conductive strips called *hybrid analog resistive touch sensing*. This increases the number of calculations to obtain a position reading from 2 to $2n$, but this is still less than the calculation of a whole matrix with at least n^2 calculations.

For the usage of resistive touch sensors, there are a couple of commercially available integrated circuits (as for example MAX 11800 with a footprint as low as $1.6 \cdot 2.1\,\mathrm{mm}^2$) that will alleviate the integration of such a sensor in a new system.

10.6.2 Capacitive Touch Sensors

For capacitive touch sensors detecting positions, two general approaches are known. *Self-capacitance* or *surface-capacitance* sensors are built up from a single electrode. The system measures the capacitance to the environment, that is altered when a user touches the surface. Based on the measurement of the current that is used to load the changed capacitance, a position measure can be deducted similar to the calculation in the case of resistive sensors. This sensor type is prone to errors from parasitic capacitive coupling, the calculation of multiple touch positions is possible but requires some effort.

When more than one capacitor is integrated in a surface, one can use the mutual capacitance type sensor. In that case, the capacitors are arranged in a matrix and the capacitance of each capacitor is changed by approaching conductive materials like fingers or special styluses. This matrix is read out consecutively by the sensor controller. Because of the matrix arrangement, the detection of multi-point touch is possible. As with resistive sensor systems, there are several commercially available integrated circuits for the readout of such capacitive matrices.

For the identification of contact poses, like for example the touch with a single finger or a whole hand, the self-capacitance approach can be used as well. In that case, the changed capacitance is considered as an indicator for the touch pose with regard to an arbitrary shaped electrode. Since the realization of such a function is quite simple in terms of the required electronics, this procedure is incorporated in standard components under several brand names, like for example ATMEL QTOUCH.

Sometimes, capacitive sensor systems are combined with inductive sensor systems that track the position of a coil with respect to the reference surface. This is for example used to make use of stylus' on touchscreens and graphic tablets. Because of the different sensor principles, one can weigh the tool equipped with the coil more and avoid misreadings by the capacitive effect of the user's hand.

10.6.3 Other Principles

However, a lot of other principles are known as well, that are often based on the change of a position and a detection of this change with different sensing principles. Examples include optical and magnetic measuring principles as described above in Sect. 10.7. They are often investigated in the context of robot tactile sensing, where not only touch, but also pose, handling and collision are of interest [116]. In these cases, the use of flexible materials and microtechnology is of interest, which makes this kind of sensor to most welcome examples for microsystem engineers.

A recent example for such a sensing system is a sensorized multicurved robot finger, which was published by researchers at Columbia Engineering in 2020 [117]. It is an optic-based sensing system of phototransistors and diods encapsulated by a transparent elastomer: Depending on contact situation and amount of force the elastomer is deforming, intensity of light is modulated, and thus force is evaluated.

A comparable topology provides the BIOTAC TOCCARE sensing system by *SynTouch Inc*. It mimics the interactions of human hand exploring material and identify different materials. The system contains biomimetic sensors evaluating 15 dimensions of touch evaluation information about texture, adhesive and thermal properties as well as compliance and friction.

Another commercially available tactile sensing systems is USKIN developed by *XELA Robotics* for measuring grip forces in three directions of space. Available are arrays of 3-axis tactile sensors in different sizes. Beside 3-axis force measurement, displacement in 3-axis is measured and evaluated too.

For the use in haptic systems, the current state of development of such systems as for example shown in [116–119] has to be critically checked. As a general classification Table 10.10 gives some advantages and disadvantages for possible sensing principles.

A quite fancy example for advanced touch sensors is based on an impedance spectroscopy measurement, the TOUCHÉ-system by SATO ET AL. allows to differentiate different grips and body poses from an impedance measurement. Examples include the identification of the finger positions on a door knob, the discrimination of arm poses when sitting on a table or even the detection of someone touching a water surface. Applications include gesture interfaces for worn and integrated computers as well as the possibility of touch passwords, which consist out of a predefined sequence of touch poses. [120].

Table 10.10 Advantages and disadvantages of different touch sensing principles according to [116]

Sensing principle	Advantages	Disadvantages
Capacitive	Sensitive, low cost, commercial readout circuits available	Cross-talk, hysteresis, complex electronic
Conductive composites	Mechanically flexible, easy fabrication, low cost	Hysteresis, non-linear response, slow reaction time
Magnetic	High sensitivity, good dynamic range, no mechanical hysteresis, robust	Restricted to non-magnetic medium, complex readout, size, high power consumption
Optical	Sensitive, immune to electromagnetical interference, no electrically conductive parts, flexible, fast response	Bulky, sensitive to bending, power consumption, complex readout
Piezoelectric	High sensitivity, good dynamic response, high bandwidth	Temperature sensitive, difficult electrical connection, no static measurement
Piezoresistive	High sensitivity, low cost, low noise, simple electronics	Mechanically stiff, non-linear, hysteresis, signal drift
Resistive	High sensitivity, low cost, commercial readout circuits available	Power consumption, no multi-touch, no contact-force measurement
Ultrasonic	Fast dynamic response, good force resolution	Limited utility at low frequency, temperature sensitive, complex electronics

10.7 Positioning and Displacement Sensors

To acquire the user's reaction in haptic systems, a measurement of positions respectively their time derivatives (velocities, accelerations) is necessary. Several measurement principles are available to achieve this. A mechanical influence of the sensor on the system has to be avoided for haptic applications, especially kinaesthetic ones. Consequently, this discussion focuses on principles, which do not affect the mechanical properties significantly. Beside the common optical measurement principles, the use of inductive or capacitive sensors is promising especially in combination with actuator design. This chapter gives an overview about the most frequently used principles, amended by hints for their advantages and disadvantages when applied to haptic systems.

10.7.1 Basic Principles of Position Measurement

For position measurement two principle approaches can be distinguished: differential and absolute measuring systems.

10.7.1.1 Incremental Principle

Differential systems acquire the change in discrete steps together with the direction of change, and protocol (typically: count) these events. This protocol has to be set back to a reference position by an external signal. If no step loss happens during movement, a prior initialized differential system is able to provide the absolute position as output. If this initializing reference position is set in point which is passed often, a differential system will be referenced frequently during normal operation. Potential step losses would then affect the time till the next initializing event only.

Measurement of the steps is done via a discrete periodic event, typically encoded in a code disc with grooves or a magnetic rotor. This event is transformed by the sensor in a digital signal, whose frequency is proportional to the velocity of the movement (Fig. 10.47a). Some additional directional information is required to be able to measure the absolute position. A typical solution for this purpose is the use of two identical event types with a phase shift (between 1 and 179°, typically 90°. By looking at the status (*high/low*) of these incremental signals (Fig. 10.47b) at e.g. the rising edges of the first incremental signal (A), a *low* encodes one movement direction, and a *high* encodes the opposite movement direction. Accordingly the count process either adds or subtracts the pulses generated–in this case–by the second signal (B). State-of-the-art microcontrollers are equipped with counters for incremental measurement already. They provide input pins for count-signal and count-direction. Discrete counters are sold as “Quadrature-Encoder” ICs and frequently include actuator drive electronics, which can be applied for positioning tasks. Latter prevents them from being useful for typical haptic applications.

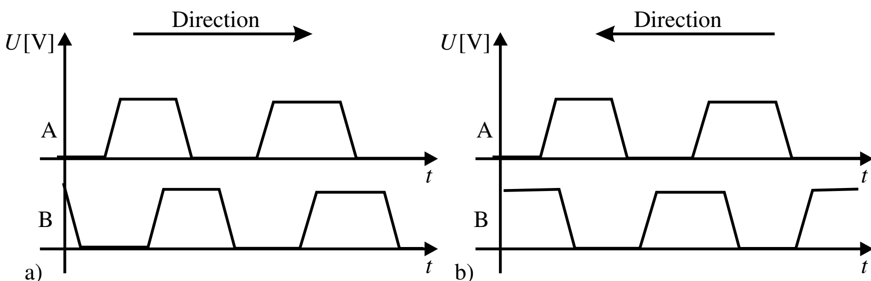

Fig. 10.47 Principle of direction detection with two digital signals with a 90° phase-lag

10.7.1.2 Absolute Measurement Principle

Absolute measurement systems acquire a position- or angle-proportional value directly. They are usually analog. A reference position for these systems is not necessary. They have advantages with reference to their measurement frequency, as they are not required to measure with dynamics defined by the maximum movement velocity. The acquisition dynamics of incremental principles is given by the necessity not to miss any events. In case of absolute measurement principles the measurement frequency can be adjusted to the process-dynamics afterward, which is usually less demanding. However by the analog measurement technology the efforts are quite high for the circuit, the compensation of disturbances, and the almost obligate digitization of the analog signal.

An alternative for the pure absolute measurement with analog technology is given by a discrete absolute measurement of defined states. In Sect. 9.2.2.1, Fig. 9.18, a commutation of EC-drives with a discrete, position coding of magnet-angles with field plates was already shown. This approach is based on the assumption to achieve a discrete resolution of ΔD from m measurement points with n states by

$$n^m = \Delta D. \tag{10.42}$$

In case of the commutated EC-drive $m = 3$ measurement points, which are able to have $n = 2$ states, could encode 8 positions on the circumference, but only six were actually used. But there are other more complex code discs with several lanes for one sensor each. These sensors are usually able to code two states. However e.g. by the use of different colors on the disc many more states would be imaginable. A resolution of e.g. 1 degree (360 discrete steps) would need the number of

$$m = \frac{\log(\Delta D)}{\log(n)} = 8.49 \tag{10.43}$$

at least nine lanes for encoding.

10.7.2 Requirements in the Context of Haptics

Position measurement systems are primarily characterized by their achievable resolution and dynamics. For haptic devices, in dependence on the measurement basis for computer mice and scanners, position resolutions are frequently defined as dots-per-inch ΔR_{inch}. Consequently the resolution ΔR_{mm} in metric millimeters is given as:

$$\Delta R_{\text{mm}} = \frac{25,4\,\text{mm dpi}}{\Delta R_{\text{inch}}}. \tag{10.44}$$

A system with 300 dpi resolution achieves an actual resolution of 84 μm. In dependency on the measurement principle used, different actions have to be taken to achieve this measurement quality. With incremental measurement systems the sensors for the acquisition of single steps (e.g. holes on a mask) are frequently less resolutive, requiring a transformation of the user's movement to larger displacements at the sensor. This is typically achieved by larger diameters of code discs and measurement at their edge. These discs are mounted on an axis, e.g. of an actuator. With analog absolute systems an option for improving the signal is conditioning. It is aimed at reducing the noise component in the signal relative to the wanted signal. This is usually done by a suppression of the noise source (e.g. ambient light), the modulation and filtering of the signal (e.g. lock-in amplifier, compare Sect. 10.7.6.1) or the improvement of secondary electronics of the sensors (high resolution A/D-transformer, constant reference sources).

Beside the position measurement itself, its dynamic has to be considered during the design process. This requirement is relevant for incremental measurement systems only. Absolute measurement systems need a bandwidth equal to the bandwidth provided by the interface and the transmission chain (Chap. 11) for positioning information. Incremental measurement systems however have to be capable of detecting any movement event, independent from the actual movement velocity. The protocol format, usually given by counters part of the microcontrollers, has to be dimensioned to cover the maximum incremental frequency. This requires some assumptions for the maximum movement velocity v_{max}. If e.g. a system with 300 dpi position resolution move at a maximum velocity of 100 mm/s, the dynamic f_{ink} for detecting the increments is given as

$$\frac{1}{f_{\text{ink}}} = \frac{\Delta R_{\text{mm}}}{v_{\text{max}}} \tag{10.45}$$

For the example the necessary measurement frequency is given with $f_{\text{ink}} = 1190\,\text{Hz}$. The effective counting frequency is usually chosen with factor two to four higher than that, to have a security margin for counting errors and direction detection.

10.7.3 Optical Sensors

Optical Sensors for position measuring are gladly and frequently used. They excel by their mechanical robustness and good signal to noise ratios. They are cheap and in case of direct position measurement quite simple to read out.[12]

Code Discs

Code discs represent the most frequently used type of position measurement systems with haptic devices, especially within the class of low-cost devices. They are based

[12] The examples presented here are discussed either for translatory and rotatory applications. But all principles may be applied to both, as a translation is just a rotation on a circle with infinite diameter.

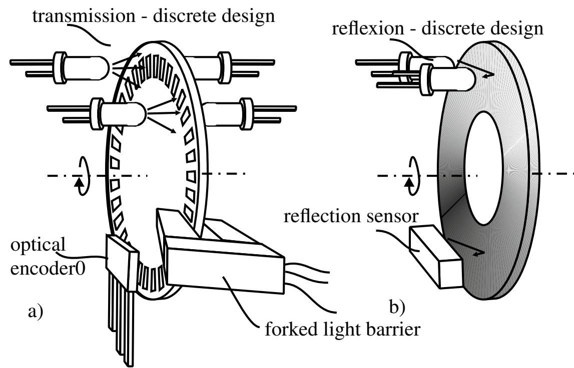

Fig. 10.48 Incremental optical position measurement (**a**), and absolute position measurement via gray-scale values (**b**)

on transmission (Fig. 10.48a) or reflection of an optical radiation, which is interrupted in discrete events. The necessary baffle is located near to the receiver. It is manufactured by stamping, or printed on a transparent substrate (glass, plastic material) via thigh-film technology or laser printers. For high requirements on resolution they are made of metal, either self-supportive or on a substrate again. In theses cases the openings are generated by a photolithographic etching process. The receivers can be realized in different designs. Figure 10.48 shows a discrete design with two senders in form of diodes and two receivers (photodiode, phototransistor). The placement of sender/receiver-units have to allow the phase shift for directional detection (Sect. 10.7.1.1). An alternative is given by a fork light barriers already including a compact sender/receiver unit. Additionally opto-encoders (e.g. HLC2705) exist including the signal conditioning for direction-detection from the two incremental signals. The output pins of these elements provide a frequency and one signal for the direction information.

Gray Scale Values

With similar components, but for absolute measurement a gray scale disc or gray scale sensor can be built. Once again there are transmission and reflection (Fig. 10.48b) variants of this sensor. In any case the reflection/transmission of the radiation varies dependent on the angle or position of a code disc. The amplitude of the reflection gives absolute position information of the disc. For measurement, once again, either a discrete design or the usage of integrated circuits in form of so called reflection sensors is possible. Although such sensors are frequently used as pure distance switches only, they show very interesting proportional characteristics between the received numbers of photons and their output signal. They are composed of a light emitting diode as sender and a phototransistor as receiver. In some limits the output is typically given by a linear proportional photoelectric current.

Reflection Light Switches

Reflection light switches show useful characteristics for a direct position measurement too. In the range of several millimeters they have a piecewise linear dependency

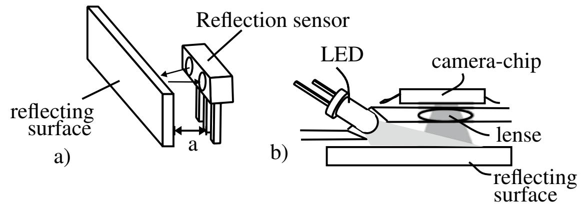

Fig. 10.49 Distance-measurement with reflection light switches (**a**), and via the movement of an reflective surface in two DoFs "mouse-sensor" (**b**)

between photocurrent and the distance from the sensor to the reflecting surface. Consequently they are useful as sensor for absolute position measurement of translatory movements (Fig. 10.49a). By this method e.g. with the SFH900 or its SMD successor SFH3201 within a near field up to $\approx$1 mm measurement inaccuracies of some micrometers can be achieved. In a more distant field up to 5 mm the sensor is suitable for measurement inaccuracies of $\frac{1}{10}$ mm still.

Mice-Sensor

The invention of optical mice without ball resulted in a new sensor-type interesting for other applications too. The optical mice-sensors are based on an IC measuring an illuminated surface through an optic element (Fig. 10.49b). The resolution of the CMOS sensors typically used range from 16 $\times$ 16 to 32 $\times$ 32 pixels. By the image acquired the chip identifies the movement of contrast difference in their direction and velocity. The interface of the calculated values varies from sensor to sensor. The very early types provided an incremental signal for movements in X and Y-direction identical to approaches with code discs described above. They additionally had a serial protocol included to read the complete pixel information. Those sensors (e.g. ADNB-3532 family) provide serial protocols for a direct communication with a microcontroller only. This allowed a further miniaturization of the IC and a minimization of the number of contact pins necessary. The resolution of state-of-the-art sensor is in between 500 and 1000 dpi, and is usually sufficient for haptic applications. Only the velocity of position output varies a lot with the sensor types available at the market, and has to be considered carefully for the individual device design. The frequency is usually below 50 Hz. Additionally early sensor designs had some problems with drift and made counting errors, which could be compensated only by frequent referencing.

The sensors are usually sold for computer-mouse-similar applications and corresponding optics. But beside that it is also possible to make measurements of moving surfaces with an adapted optic design at a distance of several centimeters.

Triangulation Sensors

Optical triangulation is an additional principle for contactless distance measurement; however it is seldom used for haptic devices. A radiation source, usually a laser, illuminates the surface to be measured, and the reflected radiation is directed on different positions along a sensor array (Fig. 10.50). The sensor array may be made of discrete photodiodes. Frequently it is a CCD or CMOS row with the corresponding

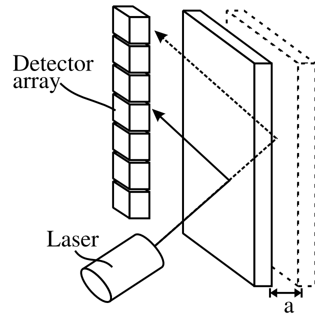

Fig. 10.50 Triangulation of a distance with laser-diode and detector array

high resolution. By focal point identification weighting several detectors a further reduction of measurement inaccuracy can be achieved. Compared to other optical sensors, triangulation sensors are expensive as the detection row with a sufficient resolution is a high cost factor. Their border frequency ≫ 1 kHz) and their measurement inaccuracy (<10 μm) leave nothing to be desired. It is one of the very few principles, which can hardly be used for measuring rotating systems.

10.7.4 Magnetic Sensors

Beside the optical measurement principles, especially the group of magnetic measurement principles is relevant for haptic devices. This is a consequence from the fact that electrodynamic and electromagnetic actuators already require magnetic fields to generate forces. For systematization, sensor for static fields, field plates and hall-sensors, and sensor for induced currents and time dependent fields can be distinguished.

Field Plates or Magnetic Dependent Resistors

Field plates or magnetic dependent resistors (MDR) are two pole elements with a resistance being controlled by the presence of a magnetic field. They make use of the GAUSS-effect, which is based on charge carriers being displaced by the LORENTZ-force when crossing a magnetic field. The resulting increase of the path length [121] requires an increase of the ohmic resistance of the material. The parameter characterizing this dependency is dependent on the electron mobility and the path length in the magnetic field. A frequently used material is InSb with very high electron mobility. For an additional increase of the effect, the conductor is formed like in the shape of a meander similar to strain gauges. MDRs are not sensitive to the polarity of the magnetic field. They are detecting the absolute value only. The increase of resistance is nonlinear and similar to a characteristic curve of a diode or transistor. A magnetic bias is recommended when using the plates to make sure they are in their linear working point.

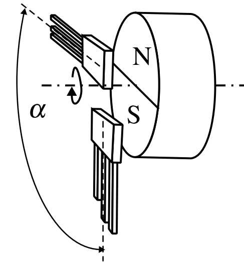

Fig. 10.51 Measurement of the rotation angle of a magnet via field plates or hall-sensors

Hall-Sensors

Hall-sensors are based on the GAUSS-effect too. In contrast to field plates they are not measuring the resistance increase of the current within the semiconductor, but the voltage orthogonal to the current. This voltage is a direct result of the displacement of the electrodes along the path within the material. The resulting signal is linear and bipolar in dependency on the field-direction. ICs with an integrated amplifier electronics and digital or analog output signals can be bought off the shelf. A frequent use can be found with sensors being located at a phase angle α with diametral magnetized rotational magnets (Fig. 10.51). In this application a rotation and rotation-direction is measured.

Inductance Systems

An often forgotten alternative for position measurement is the measurement of changing inductances. The inductance of a system is dependent on many parameters, for example the magnetic permeability of a material in a coil. Using a differential measurement in between two coils (Fig. 10.52b) a displacement measurement can be made, if a ferromagnetic material moves in between both coils as a position-depending core. As alternatives the geometry of the magnetic circuit may be changed, or its saturation may influence the inductance of the coils. Latter approach is used in systems, where grooves on a ferromagnetic material trigger events in a nearby coil (Fig. 10.52a).

A simple electronic for measuring inductance is the use of a LR-serial circuit, which–for example with a microcontroller–is triggered with a voltage step. The measurement value is given by the time the voltage at the resistor needs to trigger a comparator voltage. The duration encodes the inductance, assuming a constant resistance. For the actual design it has to be considered, that the winded coil has an own resistance which cannot be neglected. As an alternative a frequency nearby the resonance $\frac{L}{R}$ of the LR-circuit can be applied. The voltage amplitude measured varies dependent on the inductance's detuned by the movement of the ferromagnetic core.

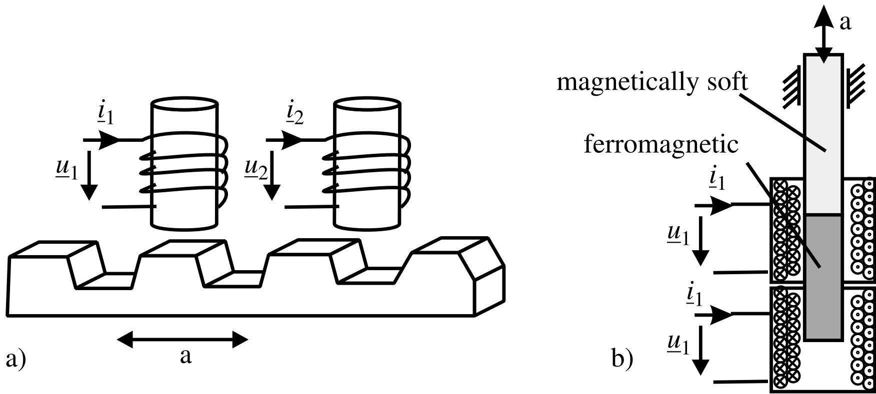

Fig. 10.52 Incremental measurement of a movement via induced currents (**a**) and differential measurement of the position of a ferromagnetic core (**b**)

10.7.5 Other Displacement Sensors

Beside the displacement measurement principles discussed above there are some rarely used principles still worth to be mentioned here.

Ultrasonic Sensors

Ultrasonic sensors (Fig. 10.53) are based on the running time measurement in between the emission of acoustic oscillations and the moment of the acquisition of their reflection. The frequency chosen is dependent on the requirements on measurement accuracy and the medium for propagation of the wave. As a rough rule of thumb, the denser a material is, the less the damping becomes for acoustic waves. For measurement in tissue frequencies between 1 and 40 MHz are applied. In water frequencies between 100 and 500 kHz and in the atmosphere frequencies well below 30 kHz are used.

Whereas with medical applications in tissues the medium shows a damping quite linear in the range of 1dB/Mhz/cm, the measurement within the atmosphere is strongly dependent on the frequency chosen and usually nonlinear. Additionally the acoustic velocity is dependent on the acoustic density of the medium. For the transversal direction—typically used for measurement—velocities between 340 m/s for air and 1500 m/s for water can be achieved. According to the wave theory the minimum measurement accuracy possible in transversal direction is $\frac{\lambda}{2}$, which is coupled to both factors mentioned above. It is a natural border of minimum resolution to be achieved.

The most frequently used source and receiver for the mechanical oscillation are piezoelectric materials (Fig. 10.53b), whose step response oscillations are sharpened by a coupled mass.

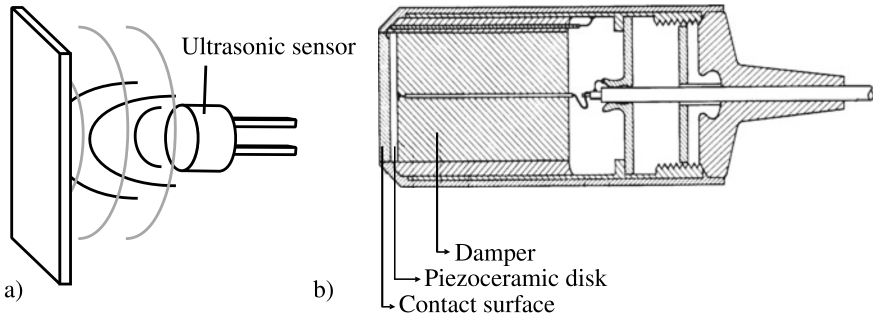

Fig. 10.53 Distance measurement via ultrasonic sensors (**a**) and cross-section through a medical ultrasonic head with fixed focus (**b**)

Capacitive Sensors

In Sect. 9.5 the equations for the calculation of capacities between plates of electrostatic actuators (Eq. 9.75) were introduced. Of course the measurement of a variable capacity, especially with the linear effect of a transversal plate displacement, can be used for position measurement. This is especially interesting if there are conductive components in the mechanical design, which already move relative to each other. As the capacity is very much dependent on the permittivity of the medium between the plates, which can be strongly influenced by oil or humidity, such a measurement can be done on insusceptible or other well housed actuators only. Additionally leakage fields of conductors or geometries nearby are usually of the same size as the capacity to be measured. But capacitive sensors for haptic devices can be found in the context of another interesting application. The measurement of the capacity of the handle, even when isolated by a non conductive layer, allows identifying a human touch very securely.

Proximity Sensors

Proximity sensors are realized using inductance, capacitive or photoelectric systems. In case of inductive or capacitive sensors a measuring object and its material properties (depending whether it is conductive or dielectric) are influencing magnetic or electric field of inductance or capacitor. Is a certain distance (switching theshold) exceeded, the output signal of the sensor is switched from low to high. In nearly every production process proximity sensors are used as contactless switches to control process itself. Inductive proximity sensors are the low-cost option to control state of grippers (closed or open) in industrial processes [4].

10.7.6 Electronics for Absolute Positions Sensors

The absolute measurement of a position requires, as mentioned earlier, some additional effort in the electronic design compared to discrete sensors. Two aspects shall be discussed in the context of this chapter.

Constant-Current Supply and Voltage References

For the generation of a constant radiation or the measurement of a bridge circuit the use of constant currents is necessary. There is always the possibility to wire an operational amplifier as a constant current source, or use transistor circuits. Nevertheless for designs with low quantities there are ICs which can be used as current sources directly. The LM234 for example is a voltage-controlled 3-pin IC, providing a current with a maximum error of 0.1%/V change in the supply voltage. The maximum current provided is 10 mA, which is usually sufficient for the supply of optical or resistive sensors.

The change of the signal is usually measured in relation to a voltage in the system. In this case, it is necessary to provide a voltage which is very well known and independent from temperature effects or changes of the supply voltage. Common voltage regulators as used for electronic supply are not precise enough to fulfill these requirements. An alternative is given by Zener diodes operated in reverse direction. Such diodes however are not applicable to high loads and are of course only available in the steps of Zener voltages. Alternatively, reference voltage sources are available in many voltage steps on the market. The REF02 for example is a six-pin IC, providing a temperature-stable voltage of 5V with an error of 0.3%. The drivable load of such voltage sources is limited, in case of the REF02 it is 10 mA, but this is usually not a relevant limit as they are not thought as a supply to a complex circuit but only as a reference.

10.7.6.1 Compensation of Noise

The obvious solution for the compensation of noise in a measurement signal is given by the usage of a carrier frequency for modulating the signal. The sensor showing no damping at the modulating frequency of course gives a prerequisite. This is usually no problem for optical sensors in the range of several kilohertz. At the receiver, the signal is bandpass-filtered and equalized or otherwise averaged. This suppresses disturbance frequencies or otherwise superimposed offsets.

A simple but very effective circuit for noise compensation is the use of so called "lock-in" amplifiers. On the side of the sender a signal is switched between the states *on* and *off* at a frequency f. In the receiver the wanted signal such as e.g. the offset and other disturbing frequencies are received. A following amplifier is switched with the same frequency between $+1$ and -1 in such a way, that with the receipt of the wanted signal including the disturbance the positive amplification happens. During the period without the wanted signal, when the receiver measures the disturbance

only, the signal is inverted with -1. The resulting signal is low-pass filtered afterward, resulting in a subtraction of the noise signal and providing a voltage proportional to the wanted signal only.

10.7.7 Conclusion on Position Measurement

With haptic devices position measurement is a subordinated problem. In the range of physiological perceived displacements resolutions, there are enough sensor principles, which are sufficiently precise and dynamic for position measurement. We will see in the following Sect. 10.8 that calculation or measurement of accelerations or velocities is easily possible too. Without doubt, the optical measurement technology is the most frequently used technical solution. Nevertheless especially for the design of specific actuators it is indicated to ask the questions, whether there are other sensor principles applicable for a direct integration into the actuator.

If there are specific requirements for measurement in the range of a few μm positioning resolution, the proposed principles should be treated with reserve. Measurements in the range of μm require specific optical or capacitive measurement technology. With the exception of special psychophysical questions it is unlikely that such requirements are formulated for haptic devices.

10.8 Inertial Sensors–Measurement of Velocity and Acceleration

As stated before user's reactions in haptic systems have to be acquired. Beside position measurement first and second derivatives of time (velocities, accelerations) are of interest. Such a necessity may be given with stability issues for closed-loop systems or impedance behavior of users or manipulated objects. Both are vector quantities and especially, velocity is *the* important quantity of kinematics. It represents the time-dependent change of object movement along any curvature. Depending if whether the curvature is linear or not we distinguish translation and rotatory movement and thus, translational speed and acceleration or angular speed and angular acceleration. Velocity and acceleration sensors can be subsummized under the collective term *inertial* sensors.

10.8.1 Measurement of Velocity

Several measurement methods are available to achieve the measurand velocity no matter if translation or rotatory. The acquisition can be done either by direct mea-

surement or by differentiation of the position-signal of a position sensor with digital or analog circuits. Additionally, it can be imagined to e.g. measure a velocity and calculate the position by integration. The capabilities of integration and differentiation and their limits, such as typical direct measurement principles, are sketched in this section.

10.8.1.1 Integration and Differentiation of Signals

The integration and differentiation of signals can either be done analog or digital. Both variants have different advantages and disadvantages.

Analog Differentiation

The basic circuit for an active analog integrator is shown in Fig. 10.54a. It is a high-pass filter, which already gives hints on the challenges connected with differentiation. The high-pass behavior is limited in its bandwidth. The upper border frequency is given by the resonance frequency $f_R = \frac{1}{2\pi RC}$ and by the bandwidth of the operational amplifier. As these components are sufficiently dynamic for haptic applications, this should be no problem in practical realization. Due to the negative feedback however the natural bandwidth limit of the operational amplifier at high frequencies has a phase of 90° adding to the phase of 90° from the differentiation. This makes the circuit sensitive to become electrically instable and oscillate [122].

This effect can be compensated by a serial resistance with a capacity C, which is identical to a linear amplification with the operational amplifier. This diminishes the phase for high frequencies by 45° resulting in a phase margin to the instable border condition. Analog differentiation is an adequate method for the derivation of velocities from positioning signals. A double analog differentiation needs a careful design of the corresponding circuit, as a number of capacitive inputs are placed in series. Additionally it should be considered that the supply voltage limits the amplitude of the operational amplifier. Accordingly, the amplitude's dynamic has to be adjusted to the maximum signal change expected.

Analog Integration

The basic circuit of an active analog integrator is given in Fig. 10.54b. Analog integration is a reliable method from analog calculation technique, but has limited use for haptic applications. The circuit has an upper border frequency given by the resonance $f_R = \frac{1}{2\pi RC}$, and for a non-ideal operational amplifier it has a lower border frequency too. This is a result of the current I_b at the input of the OP-amplifier charging the capacitor with $U_{\text{in}} = 0\text{V}$ continuously. If C=10μF and $I_b = 1\mu\text{A}$, the voltage increases by 0.1 V per second. Whereas in signal processing applications this can be compensated by high-passes in series, for haptic applications covering a bandwidth from several seconds to 10 kHz this behavior is usually not acceptable.

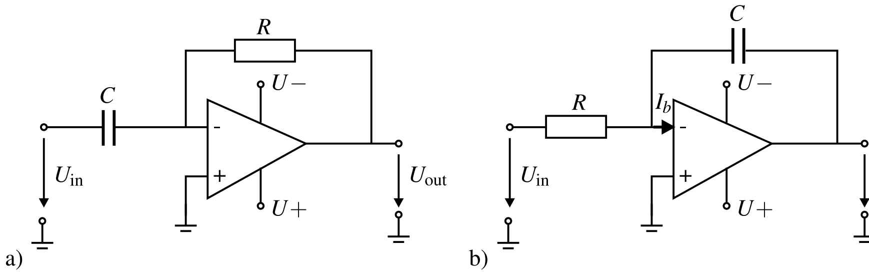

Fig. 10.54 Analog differentiation-(**a**) resp. integration-circuits (**b**) [122] © Springer Nature, all rights reserved

Digital Differentiation

Digital differentiation is realized by a subtraction of two consecutive measurement values. It is very applicable, especially when the signal is measured at high frequencies. The quality of the signal is dependent on the noise on the input. Frequently the least-significant bit of e.g. an AD-conversion is rejected before the differentiation is performed, as it is oscillating with the noise of the AD-conversion (quantization-noise). To derive velocity from position measurements, COLGATE recommends a high position measurement resolution as well as a low-pass filtering of the generated velocity signal to improve the quality [123].

Digital Integration

Digital integration is the summation of continuous measurement values and the division of the sum by the number of values. Alternatively, it can be the sum of discrete changes of a measurement value. The incremental measurement of a digital encoder is also a form of integration based on change information. The procedure is robust at high frequencies beyond the actual upper border frequency of the signal. Beside a sufficient dimension of the register size for the measurement values to prevent an overflow, there is nothing else to worry about.

10.8.1.2 Induction as a Velocity Measure

The most frequent variant to gain information about velocity is given by the digital signal processing of a position-measurement. Nevertheless, to be able to measure velocity directly, the use of a velocity-proportional physical effect is mandatory. Beside Doppler-ultrasonic measurement, which is seldom applicable to haptic systems due to the wavelengths (compare Sect. 10.7.5), the use of electrical induction is the most frequently used direct effect. Accordingly an electrical induced voltage U is generated in a conductor of the length l, moving orthogonal in a magnetic field B with the velocity v:

$$U = v\,B\,l. \tag{10.46}$$

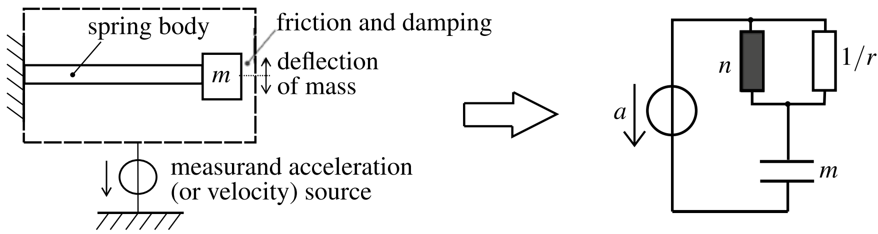

Fig. 10.55 Modelling of acceleration sensors based on force measurement. The differential equation (10.47) gives us the relation of force and equation of motion

Special geometric designs as given with electrodynamic actuators (Sect. 9.2) can be used for velocity measurements with inducing voltages in their coils. In contrast to electrodynamic actuators, the design requires a maximization of conductor length, to generate a pronounced voltage signal. The inductivity of the winding generates a low-pass characteristic in combination with its own resistance. This limits the dynamic of the signal. The biggest error made with these kinds of sensors is given by a bad homogeneity of the winding due to dislocation of single turns. This manufacturing error results in different winding lengths moving in the B-field at different positions of the sensor, which is directly affecting the quality of the measured signal.

10.8.2 Acceleration Measurement

The vector quantity acceleration is the first derivative of velocity and second derivative of position. Depending on the inertial system of measuring object and its movement, up to six or components of motion (linear acceleration and angular rotation rates (role, pitch and yaw) occur. Both, single sensors for acceleration measurement or rotation rates as well as sensors systems measuring all occurring components of motion so called inertial measurement units (IMU) are in use. IMUs consist of both accelerometers and gyroscopes.

A 6-DoF IMU for example consists of an accelerometer for linear quantities and a gyroscope for angular rotation rates. IMUs with nine or 12 DoF are also available that contain accelerometers and gyroscopes for two different measurement ranges, a tri-axis magnetometer (hall sensors), temperature and pressure measurement for example in systems of *Shimmer Sensing* or INVENSENSE technology by *TDK*. Because acceleration due to gravity always affects the measurement, it is crucial to know the orientation of both global reference system (output signal of magnetometer can be used) and local coordinate system of the inertial sensor. Acceleration measurement can be traced back to [4]:

1. Time-dependent measurement of position s: $\mathbf{a} = \frac{\mathbf{dv}(t)}{dt} = \frac{\mathbf{d}^2\mathbf{s}(t)}{dt^2}$, where $\mathbf{s} = [x_1, x_2, x_3]$
2. Force measurement with a known seismic mass m: $\mathbf{F} = m \cdot \mathbf{a}$.

The latter are the most common ones. The topology of that kind of sensors can be modelled with a mass-spring-damper-system: a concentrated seismic mass m is attached at a spring body Fig. 10.55, where damping factor D and spring constant c describing the elasto-mechanic parameters of the spring body.

$$\mathbf{F} = m \cdot \frac{\mathbf{dx^2}}{t^2} + D \cdot \frac{\mathbf{dx}}{dt} + c \cdot \mathbf{x} \qquad (10.47)$$

Depending on acceleration mass is dislocating and spring body is deforming. The deformation can be described using elasto-mechanics, as we learned in the former section about force sensors (Sect. 10.5). In fact, force-measurement principles given in Sect. 10.5 are added by a known mass m only, resulting in a mechanical strain of a bending element or generating another acceleration-proportional signal.

In contrast to velocity measurement, a wide variety of accelerometers exists and most of them are based on force measurement. In professional measurement technology especially piezoelectric sensors for high dynamic measurements, but also piezoresistive sensors for low-frequency accelerations are established. In mechatronic systems with high quantities, MEMS-sensors with comb-like structures in silicon according to the capacitive measurement principle are used. The requirements of automotive industry for airbags and drive stability programs to measure acceleration in many directions made low-price and robust ICs available at the free market, e.g. the ADXL series of Analog Devices. The bandwidth of these sensors ranges from 400 Hz to 2.5 kHz with maximum accelerations >100 g in up to three spatial directions. Only a wide variance of their characteristic values, e.g. the output voltage at 0 g, requires a calibration of the individual sensor.

IMUs with up to 12 DoF are widely used for motion tracking in navigation applications, safety purposes in automotive context or in consumer applications like cellphones, cameras or remote controls for video games. MEMS inertial sensor units are increasingly used where size, weight and cost of sensors are key sides [124]. Both accelerometers and gyroscopes are based on force measurement, where latter ones are using the Coriolis Effect to detect relative angular rotation rates. For example *TDK* is providing 6 DoF ($ICM - 20648$) or 9 DoF ($ICM - 20948$) MEMS-IMUs (packaged ICs and breakout boards), which are integrated in wearables too. With a size of about $3 \times 3 \times 3\,\text{mm}^3$ they do fit in most consumer applications and provide a drift of about 10 °/h. The high gyroscope drift is the main disadvantage of MEMS-IMUs which can be depending on the sensing unit up to 50 °/h in case of XSens MTi system [124]. If higher resolution and accuracy as well as absolute angular velocity has to be measured fiber-gyroscopes using the Sagnac-Effect are integrated. A precise measurement due to drift of 10^{-3} up to 1 °/h is achievable (Xbow IMU 700 CA or 400 CC) [124]. That kind of sensing system is available as a sensing box (e.g. size of XSense MTI $5.8 \times 5.8 \times 2.2\,\text{cm}^3$) and quite spacious compared to the common IC packages like LGA. Inertial sensors as wearables are quite common in rehab and health research. For example *Shimmer Sensing* is purchasing sensing systems including IMUs as well as bioimpedance sensors to provide real-time indication of state of health (SHIMMER3 IMU UNIT, SHIMMER3 EBIO UNIT).

10.9 Imaging Sensors

Within the contents of this book, the focus is laid on device based sensors, like the above described sensors for force, deflection and touch. Pure input sensors, such as the imaging sensors, will be not discussed further as per definition no haptic feedback can be given without a real physical contact. Nevertheless, they can be used to build a complex HMI when combined with body-worn tactile devices and should be kept in mind for such applications. For analyzing gesture and motion of users or interacting objects, imaging sensors play an important role in requirements engineering for quantifying maximum working space, resolution etc. [25]. For that purpose, one can differentiate two general classes of imaging sensors:

1. *Direct Imaging sensors* are usually based on camera systems observing the user or body parts, deriving commands from gestures performed with extremities or facial expressions. Such imaging systems are subject to application in controlled environments (such as inside a car), for direct computer or gameplay interaction (*Microsoft* XBOX KINECT), or even touch interaction on surfaces
2. *Marker based imaging sensors* are again based on camera systems observing special markers worn or held by the user. Such systems can be highly accurate due to the knowledge of relations between markers and their sizes. They are used in professional navigation application such as surgical applications or motion-capture technologies, and can also be found in gameplay situation such as the *Sony* PLAYSTATION MOVE CONTROLLER.

10.10 Temperature Measurement

For temperature measurement two basic strategies are possible [4]:

- Contact-Thermometry: sensor is in contact with measuring object and is brought into a thermodynamically equilibrium with the object. Thermo-resistive and thermo-electric sensors are the most common ones, but also photosensitive semi-conducting sensors, where temperature is influencing the PN-junction are popular.
- Pyrometer: contactless measurement of thermal radiation (Infrared) of objects. Radiation heat is used to heat up a conventional temperature sensor (e.g. thermocouples or semiconductor photosensitive sensors), that is brought into thermodynamically equilibrium with the measuring object air.

Due to the major role of thermoresistive and thermoelectric sensors in technical applications, we want to go in detail. To get an overview about photosensitive semiconducting sensors [125] can be recommended.

10.10.1 Thermoresistors

Thermoresistors detect the temperature of a small area of a measuring object in the range of the sensing element itself. The resistivity of conductive material depends on the concentration of free charge carriers and their mobility [1]. Depending on lattice structure of the material and bonding behavior of valence electrons, both mobility and concentration of free charge carrier are differing. Is a conductive material heated, (thermal) energy is entering the system. The reaction of it differs according to the conductive material. In *metals* we observe a negative temperature coefficient (NTC), what means that with increasing temperature conductivity decreases. Why is that so? We have to look into material modelling: At room temperature, all available charge carriers can more or less freely move through the lattice. Increase of temperature leads to energy entry and lattice vibrations become stronger. Mobility of charge carrier is reduced due to collisions of charge carriers and lattice. In *semiconductors* electrons are bound quite strongly to their atoms [1]. At room temperature only a few charge carriers can move freely. Increasing temperature and thus entry of energy energizes charge carriers, more electrons can overcome the bounding to their atom and concentration of free-charge carriers is increasing. We talk about a positive temperature coefficient (PTC). Commercially available sensors based on thermo resistivity are resistance thermometers (metal-based, e.g. PT100) and thermistors (oxide-based), respectively. Latter ones are beside thermocouples standard in household appliance, less accurate than metal-ones, but a good low cost option. Within metals, a quadratic approximation of resistance change according to temperature usually is sufficient.

$$R(\theta) = R_0 \cdot \left(1 + \alpha \cdot (\theta - \theta_0) + \beta(\theta - \theta_0)^2\right) \tag{10.48}$$

where θ_0 is the reference temperature, R_0 resistance at $\theta = \theta_0$, θ actual temperature and α, β material specific constants of the NTC. Within semiconductors, resistance change according to temperature is highly non-linear and usually exponentially approximated. Sensitivity in comparison to metal-based thermoresistors is up to 40-times higher [4].

$$R(\theta) = R_0 \cdot \exp\left(B \cdot \left(\frac{1}{\theta} - \frac{1}{\theta_0}\right)\right), \tag{10.49}$$

where θ_0 is the reference temperature, R_0 resistance at $\theta = \theta_0$, θ absolute temperature in Kelvin and B a material specific constant of the PTC.

The evaluation and signal processing of thermoresistors does not vary from any other resistive sensor and is done e.g. in a Wheatstone-bridge configuration. Linearization of the transfer function of thermistors cab be achieved using a series resistor. The most accurate sensors for temperature measurement are metal-based ones (Platin-based sensors $PT100$ or $PT1000$), which often are used as reference for temperature measurement.

10.10.2 Thermocouples

Thermoelectric sensors provide a nearly punctiform measurement. Thermocouples consist of two wires of different materials welded together in one point. Is a temperature acting on the interconnection (welded point), an electric potential difference (thermoelectric voltage according to the Seebeck-Effect) occurs at the connecting point (open ends of the wires). The output signal of a thermocouple is proportional to the temperature difference of the measuring point (welded point) and reference point (connection point).

$$v = a_1 \cdot \left(\theta - \theta_{ref}\right) + a_2 \cdot \left(\theta - \theta_{ref}\right)^2, \tag{10.50}$$

where v is the thermoelectric voltage, θ the temperature at the measuring point and θ_{ref} the reference temperature. In comparison to thermoresistors thermocouples provide a higher upper temperature limit (nominal temperature) and do have a very short reaction time, but they lack on accuracy and long-term stability. In terms of accuracy metal-based thermoresistos are the most accurate ones.

10.11 Conclusion

With the exception of force/torque sensors, commercially available sensors for position, velocity, acceleration, touch, images and temperature exhibit sufficient properties for the usage in haptic systems. Within this section, the necessary knowledge of the underlying sensing principles for a sound selection from available sensors is reported. For the use of force/torque sensors, the relevant principle and design steps for the development of a customized sensor are given and can be deepened in the below mentioned background readings.

Recommended Background Reading

[46] Barlian, A. & Park, W. & Mallon, J. & Rastegar, A. & Pruitt, B.: **Review: Semiconductor Piezoresistance for Microsystems.** Proceedings of the IEEE 97, 2009.
Review on piezoresistive silicon sensors. Physics, examples, sensor characteristics.

[31] Bray, A. & Barbato, G. & Levi, R.: **Theory and practice of force measurement**. Monographs in physical measurement, Academic Press Inc., 1990 *Discussion of examples of force sensors. Basic mechanics and hints for designing deformation elements.*

[116] Dahiya, R. S. & Valle, M.: **Robotic Tactile Sensing**, Springer, 2013.
Overview about sensing principles used for robotic applications that are also usable for haptic systems.

[48] Keil, S.: **Beanspruchungsermittlung mit Dehnungsmessstreifen.** Cuneus Verlag, 1995.
All about strain gages. History, materials and technology, selection and application.

[15] Lenk, A. & Ballas, R.G. & Werthschützky, R.& Pfeifer, G.: **Electrical, Mechanical and Acoustic Networks, their Interactions and Applications**. Springer, 2011.
Introduction in modeling dynamics of electromechanical systems using network theory. Contains plenty of useful examples.

[126] Pertijs, M. A. P & Huijsing, J. H.: **Precision Temperature Sensors in CMOS Technology**. Analog Circuits and Signal Processing, Springer, 2006 *Characteristics of temperature dependencies of diode, bipolar and CMOS transistors as well as common realizations. Excellent overview of signal processing and digitalization of sensor outputsignals.*

[32] Rausch, J.: **Entwicklung und Anwendung miniaturisierter piezoresistiver Dehnungsmesselemente.** Dr-Hut-Verlag, München, 2012.
Comparison of sensing principles for strain sensing with focus on piezoresistive silicon elements. Design of a tri-axial force sensor using semiconducting strain gages.

[1] Regtien, P & E.: **Sensors for Mechatronics. Second edition**. Elsevier Inc., 2018 *Good classification of sensors in Mechatronics, common sensing principles and realizations.*

[127] Young, W.C. & Budynas, R.G.: **Roark's formulas for stress and strain. Bd. 6**. McGraw-Hill, New York, 2002.
Mechanics Handbook for calculation of stress and strain fields in complex deformation bodies.

[128] Tränkler, H.R. & Obermeier, E.: **Sensortechnik: Handbuch für Praxis und Wissenschaft**. Springer, 1998.
Extensive overview of sensors and sensor electronics.

References

1. Regtien P, Regtien E (2018) Sensors for mechatronics, 2nd edn. Elsevier Inc
2. van Putten MJ, van Putten MH, van Putten AF (1994) Full additive drift elimination in vector sensors using the alternating direction method (ADM). Sens Actuators A Phys 44(1):13–17
3. Webster JG (1999) The measurement, instrumentation, and sensors: handbook. Springer Science & Business Media
4. Hesse S, Schnell G (2017) Sensoren für die Prozess-und Fabrikautomation, vol 5. Springer
5. Maetzler W et al (2013) Quantitative wearable sensors for objective assessment of Parkinson's disease. Mov Disord 28(12):1628–1637
6. Salah O et al (2011) A systematic approach for design a low-cost mobility assistive device for elderly people. Int J Med Health, Pharm Biomed Eng 5:36–41

7. Michel J (1995) Drehmomentmessung auf Basis funkabfragbarer Oberflächenwellen-Resonatoren. PhD thesis. Technische Universität München. http://www.mst.ei.tum.de/forschung/veroeffentlichungen/abgeschlossene-dissertationen.html
8. Burdea GC (1996) Force and Touch Feedback for Virtual Reality. Wiley- Interscience, New York, NY, USA, pp 978–0471021414
9. Hasser CJ, Daniels MW (1996) Tactile feedback with adaptive controller for a force-reflecting haptic display-part I: design. In: Proceedings of the fifteenth southern biomedical engineering conference, pp 526–529. https://doi.org/10.1109/SBEC.1996.493294
10. Rosen J, Solazzo M, Hannaford M (2002) Task decomposition of laparoscopic surgery for objective evaluation of surgical residents learning curve using hidden Markov model. Comput Aided Surg 7. http://www.ncbi.nlm.nih.gov/pubmed/12173880
11. Kerdok A (2006) Characterizing the nonlinear mechanical response of liver to surgical manipulation. PhD thesis. Harvard University, Cambridge, May 2006. http://biorobotics.harvard.edu/pubs/akthesis.pdf
12. Rausch J et al (2006) INKOMAN-analysis of mechanical behaviour of liver tissue during intracorporal interaction. In: Gemeinsame Jahrestagung der Deutschen, Österreichischen und Schweizerischen Gesellschaften für Biomedizinische Technik 6.9
13. Sirohi J, Chopra I (2000) Fundamental understanding of piezoelectric strain sensors. J Intell Mater Syst Struct 11(4):246–257. https://doi.org/10.1106/8BFBGC8P-XQ47-YCQ0
14. Fung Y-C (1993) Biomechanics: mechanical properties of living tissues, 2nd edn. Springer, New York [u.a.], pp XVIII, 568. ISBN:0-387-97947-6; 3-540-97947-6
15. Lenk A et al (eds) (2011) Electromechanical systems in microtechnology and mechatronics: electrical, mechanical and acoustic networks, their interactions and applications. Springer, Heidelberg. 978-3-642-10806-8
16. Nakatani M, Howe R, Tacji S (2006) The fishbone tactile illusion. In: Eurohaptics. IEEE, Paris. http://lsc.univ-evry.fr/~eurohaptics/upload/cd/papers/f46.pdf
17. Caldwell DG, Lawther S, Wardle A (1996) Multi-modal cutaneous tactile feedback. In: Proceedings of the IEEE international conference on intelligent robots and systems, Diss, pp 465–472. https://doi.org/10.1109/IROS.1996.570820
18. Bullinger EW (1971) Figures of speech used in the Bible. Delmarva Publications, Inc
19. Kamper DG, Cruz EG, Siegel MP (2003) Stereotypical fingertip trajectories during grasp. J Neurophysiol 90(6):3702–3710
20. Maoz U, Berthoz A, Flash T (2009) Complex unconstrained three-dimensional hand movement and constant equi-affine speed. J Neurophysiol 101(2):1002–1015
21. Pollick FE et al (2009) Three-dimensional arm movements at constant equi-affine speed. Cortex 45(3):325–339
22. Kurtz AD (1962) Adjusting crystal characteristics to minimaze temperature dependency. In: Dean M, Douglas RD (eds) Semiconductor and conventional strain gages. Academic Press Inc., New York. ISBN:978-1114789906
23. Lemay MA, Crago PE (1996) A dynamic model for simulating movements of the elbow, forearm, and wrist. J Biomech 29(10):1319–1330
24. Kimm D, Thiel DV (2015) Hand speed measurements in boxing. Proc Eng 112:502–506
25. Aly A (2021) Developing a VR training environment for fingers rehabilitation. Technische Universität Hamburg, Institut für Mechatronik im Maschinenbau, Projektarbeit, Hamburg
26. Pereira MF et al (2020) Application of AR and VR in hand rehabilitation: a systematic review. J Biomed Inf 103584
27. Abbasimoshaei A, Mohammadimoghaddam M, Kern TA (2020) Adaptive fuzzy sliding mode controller design for a new hand rehabilitation robot. In: Nisky I et al (eds) Haptics: science, technology, applications. Springer International Publishing, Cham, pp 506–517. 978-3-030-58147-3
28. Gross D et al (2009) Technische Mechanik: Band 2: Elastostatik. Springer. ISBN:978-3540243120
29. Werthschützky R (2007) Mess-und Sensortechnik-Band II: Sensorprinzipien. Vorlesungsskriptum

30. Ballas R (2007) Piezoelectric multilayer beam bending actuators: static and dynamic behavior and aspects of sensor integration. Springer, Berlin [u.a.], pp XIV, 358. ISBN:978-3-540-32641-0
31. Bray A, Barbato G, Levi R (1990) Theory and practice of force measurement. In: Monographs in physical measurement. Academic Press Inc. ISBN:978-0121284534
32. Rausch J (2012) Entwicklung und Anwendung miniaturisierter piezoresistiver Dehnungsmesselemente. Dissertation. Technische Universität Darmstadt. http://tuprints.ulb.tudarmstadt.de/3003/1/Dissertation-Rausch-online.pdf
33. Voyles R, Morrow J, Khosla P (1997) The shape from motion approach to rapid and precise force/-torque sensor calibration. Trans ASME-G-J Dyn Syst Meas Control 119(2):229–235. https://doi.org/10.1115/1.2801238
34. Berkelman P et al (2003) A miniature microsurgical instrument tip force sensor for enhanced force feedback during robot-assisted manipulation. IEEE Trans Robot Autom 19(5):917–921. https://doi.org/10.1109/TRA.2003.817526
35. Kim K et al (2007) Calibration of multi-axis MEMS force sensors using the shape-from-motion method. Sens J IEEE 7(3):344–351. https://doi.org/10.1109/JSEN.2006.890141
36. Oddo C et al (2007) Investigation on calibration methods for multi-axis, linear and redundant force sensors. Meas Sci Technol 18:623. https://doi.org/10.1088/0957-0233/18/3/011
37. Schaumburg H (1992) Sensoren. Werkstoffe und Bauelemente der Elektrotechnik, vol 3. Teubner Verlag, Stuttgart, p 517. ISBN:3519061252
38. DeGoede KM et al (2001) How quickly can healthy adults move their hands to intercept an approaching object? Age and gender effects. J Gerontol Ser A Biol Sci Med Sci 56(9):M584–M588
39. Werthschützky R, Zahout C (2003) Angepasste Signalverarbeitung für piezoresistive Drucksensoren. In: tm-Technisches Messen/Plattform für Methoden, Systeme und Anwendungen der Messtechnik (Jan 2003), pp 258–264. https://doi.org/10.1524/teme.70.5.258.20043
40. Partsch U (2002) LTCC-kompatible Sensorschichten und deren Applikation in LTCC-Drucksensoren, 1st edn. Elektronik-Technologie in Forschung und Praxis, vol 9. Templin/Uckermark: Detert, pp III, 163. ISBN:3934142117
41. Cranny A et al (2005) Thick-film force, slip and temperature sensors for a prosthetic hand. Measurement science and technology, IOP 16:931–941. https://doi.org/10.1016/j.sna.2005.02.015
42. Lang U et al (2009) Piezoresistive properties of PEDOT: PSS. In: Microelectron Eng 86(3):330–334. https://doi.org/10.1016/j.mee.2008.10.024
43. Maiwald M et al (2010) INKtelligent printed strain gauges. Sens Actuators A Phys 162(2):198–201. https://doi.org/10.1016/j.sna.2010.02.019
44. Smith C (1954) Piezoresistance effect in germanium and silicon. Phys Rev Am Phys Soc 94(1):42–49. https://doi.org/10.1103/PhysRev.94.42
45. Bao M-H (2004) Micro mechanical transducers: pressure sensors, accelerometers and gyroscopes, 2nd edn. Handbook of sensors and actuators, vol 8. Amsterdam [u.a.], Elsevier, pp XIV, 378. ISBN:9780080524030
46. Barlian A et al (2009) Review: semiconductor piezoresistance for microsystems. In: Proc IEEE 97(3):513–552. https://doi.org/10.1109/JPROC.2009.2013612
47. Hoffmann K (1985) Eine Einführung in die Technik des Messens mit Dehnungsmessstreifen. Hottinger Baldwin Messtechnik GmbH (HBM)
48. Keil S (1995) Beanspruchungsermittlung mit Dehnungsmessstreifen. Cuneus Verlag. ISBN:978-3980418805
49. Stockmann M (2000) Mikromechanische Analyse der Wirkungsmechanismen elektrischer Dehnungsmessstreifen. Institut für Mechanik der technischen Universiät Chemnitz. http://www.qucosa.de/recherche/frontdoor/?tx_slubopus4frontend%5C%5bid%5C%5d=urn:nbn:de:bsz:ch1-200000494
50. Arshak K et al (2006) Development of high sensitivity oxide based strain gauges and pressure sensors. J Mater Sci Mater Electron 17(9):767–778. https://doi.org/10.1007/s10854-006-0013-4

51. Latessa G et al (2009) Piezoresistive behaviour of flexible PEDOT.PSS based sensors. Sens Actuators B Chem 139(2):304–309. https://doi.org/10.1016/j.snb.2009.03.063
52. Kon S, Oldham K, Horowitz R (2007) Piezoresistive and piezoelectric MEMS strain sensors for vibration detection. Proceeding of SPIE 6529:65292V–1. https://doi.org/10.1117/12.715814
53. Micron Instruments (2012) U-shaped semiconductor gage. http://www.microninstruments.com/
54. First Sensor Technology GmbH (2009) T-Brücke. Technical Report. First Sensor Technology GmbH. http://www.first-sensor.com/
55. Cochrane C et al (2007) Design and development of a flexible strain sensor for textile structures based on a conductive polymer composite. Sensors 7(4):473–492. https://doi.org/10.3390/s7040473
56. Kunadt A et al (2010) Messtechnische Eigenschaften von Dehnungssensoren aus Kohlenstoff-Filamentgarn in einem Verbundwerkstoff. In: tm-Technisches Messen/Plattform für Methoden, Systeme und Anwendungen der Messtechnik 77(2):113–120. https://doi.org/10.1524/teme.2010.0014
57. Meiss T (2012) Silizium-Mikro-Kraftsensoren für haptische Katheterisierungen: Entwurf, Musterbau und Signalverarbeitung sowie erste Validierung des Assistenzsystems HapCath. PhD thesis. Technische Universität Darmstadt, Institut für Elektromechanische Konstruktionen. http://tuprints.ulb.tu-darmstadt.de/2952/
58. Pfeifer G, Werthschützky R (1989) Drucksensoren. Verlag Technik. ISBN:978-3341006603
59. Stavroulis S (2004) Rechnergestützter Entwurf von piezoresistiven Silizium-Drucksensoren mit realem mechanischem Wandler. Dissertation. Technische Universität Darmstadt, Institut für Elektromechanische Konstruktionen. http://tuprints.ulb.tu-darmstadt.de/473/
60. Simone C (2002) Modelling of neddle insertion forces of percutaneous therapies. Johns Hopkins University, Diplomarbeit Baltimore. https://doi.org/10.1109/ROBOT.2002.1014848. http://ieeexplore.ieee.org/xpls/abs_all.jsp?arnumber=1014848&tag=1
61. Valdastri P et al (2005) Characterization of a novel hybrid silicon three-axial force sensor. Sens Actuators A Phys 123–124 (2005). https://doi.org/10.1016/j.sna.2005.01.006. (Eurosensors XVIII 2004-The 18th European conference on solid-state transducers, pp 249–257)
62. Vazsonyi E et al (2005) Three-dimensional force sensor by novel alkaline etching technique. Sens Actuators A Phys 123–124:620–626. https://doi.org/10.1016/j.sna.2005.04.035
63. Meiss T et al (2007) Fertigung eines Miniaturkraftsensors mit asymmetrischem Grundkörper zur Anwendung bei Katheterisierungen. In: MikroSystemTechnik. https://www.vdeverlag.de/proceedings-de/563061014.html
64. Brand U, Büttgenbach S (2002) Taktile dimensionelle Messtechnik für Komponenten der Mikrosystemtechnik. In: tm-Technisches Messen/Plattform für Methoden, Systeme und Anwendungen der Messtechnik, vol 12. https://doi.org/10.1524/teme.2002.69.12.542
65. Vasarhelyi G, Adama M et al (2006) Effects of the elastic cover on tactile sensor arrays. Sens Actuators A Phys 132:245–251. https://doi.org/10.1016/j.sna.2006.01.009
66. Vasarhelyi G, Fodor B, Roska T (2007) Tactile sensing-processing-interface-cover geometry and the inverse-elastic problem. Sens Actuators A Phys 140:8–18. https://doi.org/10.1016/j.sna.2007.05.028
67. Dölle M (2006) Field effect transistor based CMOS stress sensors. PhD thesis. IMTEK, University of Freiburg. ISBN:978-3899594584
68. Kizilirmak G (2007) Frei applizierbare MOSFET-Sensorfolie zur Dehnungsmessung. PhD thesis. RWTH Aachen. http://darwin.bth.rwth-aachen.de/opus3/volltexte/2007/1973/pdf/Kizilirmak_Goekhan.pdf
69. Unterhofer K et al (2009) CMOS Stressmesssystem zur Charakterisierung von Belastungen auf MEMS Bauteile. In: MikroSystemTechnik KONGRESS 2009. VDE VERLAG GmbH. https://www.vde-verlag.de/proceedings-en/453183009.html
70. Klages S (2004) Neue Sensorkonzepte zur Zungendruckmessung. Diplomarbeit. Technische Universität Darmstadt, Institut für Elektromechanische Konstruktionen, Darmstadt, Aug 2004. http://tubiblio.ulb.tu-darmstadt.de/53658/

71. Russell R (1992) A tactile sensory skin for measuring surface contours. In: Tencon 1992 Region 10 Conference. IEEE. Melbourne, Nov 1992. https://doi.org/10.1109/TENCON.1992.271943
72. Puers R (1993) Capacitive sensors: when and how to use them. Sens Actuators A Phys 37–38:93–105. https://doi.org/10.1016/0924-4247(93)80019-D
73. Beyeler F et al (2007) Design and calibration of a MEMS sensor for measuring the force and torque acting on a magnetic microrobot. J Micromechanics Microengineering, IOP 18(025004). https://doi.org/10.1088/0960-1317/18/2/025004
74. Sun Y et al (2002) A bulkmicrofabricated multi-axis capacitive cellular force sensor using transverse comb drives. J Micromechanics Microengineering, IOP 12:832–840. https://doi.org/10.1088/0960-1317/12/6/314
75. Sergio M et al (2003) A dynamically reconfigurable monolithic CMOS pressure sensor for smart fabric. IEEE J Solid-State Circuits 38(6):966–968. https://doi.org/10.1109/JSSC.2003.811977
76. Rey P, Charvet P et al (1997) A high density capacitive pressure sensor array for fingerprint sensor application. In: International conference on solid-state sensors and actuators. IEEE, Chicago. https://doi.org/10.1109/SENSOR.1997.635738
77. Chase T, Luo R (1995) A thin-film flexible capacitive tactile normal/shear force array sensor. In: Proceedings of the 1995 IEEE IECON 21st international conference on industrial electronics, control, and instrumentation, vol 2. Orlando, FL, pp 1196–1201. https://doi.org/10.1109/IECON.1995.483967
78. Meschede D (2007) Optics, light and lasers: the practical approach to modern aspects of photonics and laser physics, 2nd edn. Optik, Licht und Laser engl.Weinheim:Wiley-VCH-Verlag, pp IX, 560. ISBN:978-3-527-40628-9
79. Meißner P (2006) Seminar zu speziellen Themen der optischen Nachrichtentechnik-Simulatorische und experimentelle Untersuchungen optischer WDM Übertragungssysteme. Skriptum
80. Meißner P (2007) Optische Nachrichtentechnik I-Skriptum zur Vorlesung. Skriptum
81. Palais JC (2005) Fiber optic communications, 5th edn. Pearson Prentice-Hall, Upper Saddle River, NJ, pp XIII, 441. ISBN:0130085103
82. Ziemann, O (2007) POF-Handbuch: optische Kurzstrecken-Übertragungssysteme, 2nd edn. Springer, Berlin [u.a.], pp XXX, 884. ISBN:978-3540490937
83. Hou L (1999) Erfassung und Kompensation von Fehlereffekten bei der statischen Kraftmessung mit monolithischen Nd:YAG-Laserkristallen. PhD thesis. Universität Kassel. https://kobra.bibliothek.uni-kassel.de/handle/urn:nbn:de:hebis:34-159?mode=full
84. Peirs J et al (2004) A micro optical force sensor for force feedback during minimally invasive robotic surgery. Sens Actuators A Phys 115(2–3):447–455. https://doi.org/10.1016/j.sna.2004.04.057
85. Kern T (2006) Haptisches Assistenzsystem für diagnostische und therapeutische Katheterisierungen. PhD thesis. Techische Universität Darmstadt, Institut für Elektromechanische Konstruktionen. http://tuprints.ulb.tu-darmstadt.de/761/
86. Su L, Chiang K, Lu C (2005) Microbend-induced mode coupling in a graded-index multimode fiber. Appl Opt 44(34). https://doi.org/10.1364/AO.44.007394
87. Pandey N, Yadav B (2006) Embedded fibre optic microbend sensor for measurement of high pressure and crack detection. Sens Actuators A Phys 128:33–36. https://doi.org/10.1016/j.sna.2006.01.010
88. Luo F et al (1999) A fiber optic microbend sensor for distributed sensing application in the structural strain monitoring. Sens Actuators A Phys 75:41–44. https://doi.org/10.1016/S0924-4247(99)00043-6
89. LaserComponents Group (2008) Faseroptische Sensoren. http://www.lasercomponents.com/de/1134.html
90. Schreier-Alt T (2006) Polymerverkapselung mechatronischer Systeme-Charakterisierung durch eingebettete Faser Bragg Gitter Sensoren. PhD thesis. Technische Universität Berlin, Fakultät IV-Elektrotechnik und Informatik. http://opus4.kobv.de/opus4-tuberlin/frontdoor/index/index/docId/1494

91. Botsis J et al (2004) Embedded fiber Bragg grating sensor for internal strain measurements in polymeric materials. Opt Lasers Eng 43. https://doi.org/10.1016/j.optlaseng.2004.04.009
92. Ferdinand P et al (1997) Applications of Bragg grating sensors in Europe. In: International conference on optical fiber sensors OFS. Wiliamsburg, Virginia. ISBN:1-55752-485-8
93. Kersey A et al (1997) Fiber grating sensors. J Lightwave Technol 15(8). https://doi.org/10.1109/50.618377
94. Müller M (2009) Untersuchungen zu Kraft-Momenten-Sensoren auf Basis von Faser-Bragg-Gittern. PhD thesis. Technische Universität München. https://mediatum.ub.tum.de/doc/956469/956469.pdf
95. Silicon Microstructures Incooperated (SMI) (2008) Pressure sensors products. http://www.si-micro.com/pressure-sensor-products.html
96. Ping L, Yumei W (1996) An arbitrarily distributed tactile sensor array using piezoelectric resonator. In: Instrumentation and measurement technology conference IMTC-96. IEEE conference proceedings, vol 1. Brussels, pp 502–505. https://doi.org/10.1109/IMTC.1996.507433
97. Gehin C, Barthod C, Teissyre Y (2000) Design and characterization of new force resonant sensor. Sens Actuators A Phys 84:65–69. https://doi.org/10.1016/S0924-4247(99)00359-3
98. Sektion UT (1999) für Minimal Invasive Chirurgie Tübingen. Verbundprojekt TAMIC-Entwicklung eines taktilen Mikrosensors für die Minimal Invasive Chirurgie-Schlussbericht. Technical Report. https://www.yumpu.com/de/document/view/6617211/verbundprojekttamic-entwicklung-eines-taktilen-experimentelle-
99. Hasegawa Y, Shikida M et al (2006) An active tactile sensor for detecting mechanical characteristics of contacted objects. J Micromechanics Microengineering, IOP 16:1625–1632. https://doi.org/10.1088/0960-1317/16/8/026
100. Saraf R, Maheshwari V (2006) High-resolution thin-film device to sense texture by touch. Techncial Report 5779, pp 1501–1504. http://www.sciencemag.org/content/312/5779/1501.full
101. Arshak K, McDonagh D, Durcan M (2000) Development of new capacitive strain sensors based on thick film polymer and cermet technologies. Sens Actuators A Phys 79(2):102–114. https://doi.org/10.1016/S0924-4247(99)00275-7
102. Matsuzaki R, Todoroki A (2007) Wireless flexible capacitive sensor based on ultra-flexible epoxy resin for strain measurement of automobile tires. Sens Actuators A Phys 140(1):32–42. https://doi.org/10.1016/j.sna.2007.06.014
103. Suster M et al (2006) A high-performance MEMS capacitive strain sensing system. J Microelectromechanical Syst 15:1069–1077. https://doi.org/10.1109/JMEMS.2006.881489
104. Roths J, Kratzer P (2008) Vergleich zwischen optischen Faser-Bragg-Gitter-Dehnungssensoren und elektrischen Dehnungsmessstreifen. tm-Technisches Messen 75(12):647–654. https://doi.org/10.1524/teme.2008.0903
105. Schlüter V (2010) Entwicklung eines experimentell gestützten Bewertungsverfahrens zur Optimierung und Charakterisierung der Dehnungsübertragung oberflächenapplizierter Faser-Bragg-Gitter-Sensoren. PhD thesis. Bundesanstalt für Materialforschung und -prüfung-BAM. http://www.bam.de/de/service/publikationen/publikationen_medien/dissertationen/diss_56_vt.pdf
106. Gall M, Thielicke B, Poizat C (2005) Experimentelle Untersuchungen und FE-Simulation zum Sensor-und Aktuatoreinsatz von fl chigen PZT-Funktionsmodulen. In: Deutsche Gesellschaft für Materialkunde e.V. http://publica.fraunhofer.de/dokumente/N-28844.html
107. Physik Instrumente (PI) GmbH (2010) Flächenwandlermodul. http://www.physikinstrumente.de/de/produkte/prdetail.php?sortnr=101790
108. Middelhoek S et al (1995) Silicon sensors. Meas Sci Technol 6(12):1641
109. Reindl L et al (2001) Passive funkauslesbare Sensoren (Wireless Passive Radio Sensors). In: tm-Technisches Messen/Plattform für Methoden, Systeme und Anwendungen der Messtechnik 68.5/2001, p 240. https://doi.org/10.1524/teme.2001.68.5.240
110. Toda K (1994) Characteristics of interdigital transducers for mechanical sensing and non-destructive testing. Sens Actuators A Phys 44(3):241–247. https://doi.org/10.1016/0924-4247(94)00809-4

111. Zwicker TEA (1989) Strain sensor with commercial SAWR. Sens Actuators A Phys 17(1–2):235–239. https://doi.org/10.1016/0250-6874(89)80085-X
112. Amor A, Budde T, Gatzen H (2006) A magnetoelastic microtransformer-based microstrain gauge. Sens Actuators A Phys 129(1–2):41–44. https://doi.org/10.1016/j.sna.2005.09.043
113. Pasquale M (2003) Mechanical sensors and actuators. Sens Actuators A Phys 106(1–3):142–148. https://doi.org/10.1016/S0924-4247(03)00153-5
114. Calvert P et al (2007) Piezoresistive sensors for smart textiles. In: Electroactive Polymer Actuators and Devices (EAPAD), pp 65241i–8. https://doi.org/10.1117/12.715740
115. Mehner J (2000) Entwurf in der Mikrosystemtechnik, vol 9. Dresden Univ, Press, Dresdner Beiträge zur Sensorik, p 9783931828479
116. Dahiya RS, Valle M (2013) Robotic tactile sensing. Springer. https://doi.org/10.1007/978-94-007-0579-1
117. Piacenza P et al (2020) A sensorized multicurved robot finger with data-driven touch sensing via overlapping light signals. IEEE/ASME Trans Mechatron 25(5):2416–2427. https://doi.org/10.1109/TMECH.2020.2975578
118. Goethals P (2008) Tactile feedback for robot assisted minimally invasive surgery: an overview. Technical Report. Workshop, Eurohaptics Conference. Department of Mechanical Engineering, K.U. Leuven
119. Tegin J, Wikander J (2005) Tactile sensing in intelligent robotic manipulation-a review. Ind Robot 32(1):64–70. https://doi.org/10.1108/01439910510573318
120. Sato M, Poupyrev I, Harrison C (2012) Touchä: enhancing touch interaction on humans, screens, liquids, and everyday objects. In: Proceedings of the 2012 ACM annual conference on human factors in computing systems, pp 483–492. https://doi.org/10.1145/2207676.2207743
121. Nührmann D (1998) Das große Werkbuch Elektronik. 7. Franzis' Verlag, Poing. ISBN:3772365477
122. Tietze U, Schenk C (2002) Halbleiter-Schaltungstechnik, 12th edn. Springer, Berlin [u.a.], pp XXV, 1606. ISBN:3-540-42849-6
123. Colgate J, Brown J (1994) Factors affecting the Z-Width of a haptic display. In: 1994 IEEE international conference on robotics and automation, 1994. Proceedings, May 1994, vol. 4, pp 3205–3210. https://doi.org/10.1109/ROBOT.1994.351077
124. De Agostino M, Manzino AM, Piras M (2010) Performances comparison of different MEMS-based IMUs. In: IEEE/ION position, location and navigation symposium. IEEE, pp 187–201
125. Pertijs MA, Huijsing J (2006) Precision temperature sensors in CMOS technology. Springer Science & Business Media
126. Pertijs MAP, Huijsing J (2006) Precision temperature sensors in CMOS technology. In: Analog circuits and signal processing (2006)
127. Young W, Budynas R (2002) Roark's formulas for stress and strain, vol 6. McGraw-Hill New York. ISBN:007072542X
128. Tränkler H, Obermeier E (1998) Sensortechnik: Handbuch für Praxis und Wissenschaft. Springer. ISBN:978-3-642-29941-4

Open Access This chapter is licensed under the terms of the Creative Commons Attribution 4.0 International License (http://creativecommons.org/licenses/by/4.0/), which permits use, sharing, adaptation, distribution and reproduction in any medium or format, as long as you give appropriate credit to the original author(s) and the source, provide a link to the Creative Commons license and indicate if changes were made.

The images or other third party material in this chapter are included in the chapter's Creative Commons license, unless indicated otherwise in a credit line to the material. If material is not included in the chapter's Creative Commons license and your intended use is not permitted by statutory regulation or exceeds the permitted use, you will need to obtain permission directly from the copyright holder.